

TIME, SPACE, AND RHYTHM ACROSS NEURONS IN THE HUMAN MEDIAL
TEMPORAL LOBE AND PREFRONTAL CORTEX

Daniel R. Schonhaut

A DISSERTATION

in

Neuroscience

Presented to the Faculties of the University of Pennsylvania

in

Partial Fulfillment of the Requirements for the

Degree of Doctor of Philosophy

2023

Supervisor of Dissertation

Michael J. Kahana, Edmund J. and Louise W. Kahn Term Professor of Psychology

Graduate Group Chairperson

Joshua I. Gold, Professor of Neuroscience

Dissertation Committee

Michael L. Platt, James S. Riepe University Professor of Psychology

Geoffrey K. Aguirre, Professor of Neurology

Anna C. Schapiro, Assistant Professor of Psychology

Marc W. Howard, Professor of Psychological and Brain Sciences, Boston University

TIME, SPACE, AND RHYTHM ACROSS NEURONS IN THE HUMAN MEDIAL
TEMPORAL LOBE AND PREFRONTAL CORTEX

COPYRIGHT

2023

Daniel R. Schonhaut

To April, Aila, and Martes

ACKNOWLEDGEMENT

The work that went into this dissertation has been, by far, the most difficult that I have ever undertaken. Blood, sweat, and tears. But for the unforeseen challenges, my time in graduate school has also been greatly instructive and at times incredibly rewarding. I owe a huge debt of gratitude to many people without whom I would never have made it this far.

Thank you to my advisor, Mike Kahana, for sticking with me through this journey, and for all the advice along the way. Thank you also to my committee members – Michael Platt, Anna Schapiro, Geoff Aguirre, and Marc Howard – for their support and encouragement when I needed it, and their feedback as the work came together.

To Itzhak Fried, who made all of my graduate research possible, was a gracious host during my visits to LA, and maintained every measure of faith in my scientific ideas. To my labmates in LA, who were not only extremely helpful in teaching me all manner of things single-unit, but who I truly enjoyed getting to visit, talk through experiments with, and spend time with. To Greg Bashaw, who taught me exactly what kind of scientist I wanted to become.

I am thankful to my program director, Josh Gold, for his support. And to the amazing coordinating staff in the neuroscience program – in particular Christine Clay, who helped me through challenges early on in graduate school, and Mariel Featherstone, who helped me through challenges at the end.

At the end of the day, I am most thankful to my friends and labmates in neuroscience, who I learned the most from, struggled the most with, and came to know the best for all the time we spent together, in and out of lab, through the years. You are what made my time in Philly memorable, and what I will miss the most. I can't wait to see where we all go from here.

ABSTRACT

TIME, SPACE, AND RHYTHM ACROSS NEURONS IN THE HUMAN MEDIAL TEMPORAL LOBE AND PREFRONTAL CORTEX

Daniel R. Schonhaut

Michael J. Kahana

Despite their limitations, single- and multi-neuron recordings in humans have incredible potential to reveal how cellular and circuit-level responses give rise to the regional activity patterns found in functional MRI and electroencephalography studies, among other, more widely available techniques in cognitive neuroscience. This research also provides a necessary bridge to discoveries made in animal models, where recent technological advancements have accelerated our understanding of the biological mechanisms that underlie cognition. However, fundamental questions remain about how closely these findings translate to humans. The goal of this dissertation is to further the understanding of how activity patterns at the level of neurons facilitate the complicated processes of human memory. We describe our research on individual neuron correlates of time and place, which together provide a scaffold for organizing events in memory. In a novel experiment involving timed navigation through a virtual environment, we find that neurons in the medial temporal lobe (MTL) and medial prefrontal cortex continually represent time when place is held constant, while neural codes for time and place emerge in parallel when subjects navigate for fixed durations. In a second study, we ask how the timing of neural firing is coordinated across space in the hippocampal-dependent memory system. Combining data from multiple experiments to gather a large sample of neuronal recordings, we find that the answer is partly one of rhythm. Specifically, we show that sporadic bouts of theta frequency (2-10Hz) oscillations in the hippocampus synchronize the timing of neuronal firing not only within the hippocampus, but in connected MTL regions. Collectively, these studies provide answers to long-held questions in memory neuroscience, while opening exciting new avenues for continued research.

TABLE OF CONTENTS

ACKNOWLEDGEMENT	iv
ABSTRACT	v
LIST OF TABLES	viii
LIST OF ILLUSTRATIONS	ix
CHAPTER 1 : INTRODUCTION	1
1.1 Overview	11
CHAPTER 2 : A NEURAL CODE FOR SPATIOTEMPORAL CONTEXT	12
2.1 Abstract	12
2.2 Introduction	13
2.3 Results	13
2.4 Discussion	23
2.5 Methods	26
2.6 Supplementary Material	35
CHAPTER 3 : MTL NEURONS PHASE-LOCK TO HUMAN HIPPOCAMPAL THETA . . .	45
3.1 Abstract	45
3.2 Introduction	46
3.3 Results	47
3.4 Discussion	60
3.5 Methods	64
3.6 Acknowledgments	70
3.7 Author Contributions	70
3.8 Competing Interests	70

3.9 Supplementary Material	71
CHAPTER 4 : GENERAL DISCUSSION	75
4.1 Time cells	75
4.2 Theta phase-locking	80
4.3 Looking ahead	82
BIBLIOGRAPHY	84

LIST OF TABLES

TABLE 1.1 A morning's account.	2
TABLE 2.S1 Neurons by subject and region	43
TABLE 2.S2 Neuron responses by region	44
TABLE 3.1 Neurons by region	48

LIST OF ILLUSTRATIONS

FIGURE 2.1	<i>Goldmine</i> task	14
FIGURE 2.2	Time cells during task-free delays	16
FIGURE 2.3	Time and place cells during navigation	19
FIGURE 2.4	Decoding time across the trial	22
FIGURE 2.S1	Mine regions	35
FIGURE 2.S2	Time spent in each mine region	36
FIGURE 2.S3	Behavioral parameter correlations	37
FIGURE 2.S4	Single-neuron response rates under alternative model specification .	38
FIGURE 2.S5	Delay-to-navigation time decoding	39
FIGURE 2.S6	Firing rate correlations between trial event pairs	40
FIGURE 2.S7	Firing rates over time for all time \times navigation-event cells	41
FIGURE 2.S8	Classifying time during navigation from population neural firing .	42
FIGURE 3.1	Neural oscillations in the hippocampus	50
FIGURE 3.2	Example phase-locking to hippocampal oscillations	52
FIGURE 3.3	Phase-locking to hippocampal oscillations by region and frequency .	55
FIGURE 3.4	Phase-locking to hippocampal oscillations with and without co- occurring local oscillations	58
FIGURE 3.S1	Neural oscillations outside the hippocampus	71
FIGURE 3.S2	Phase-locking to local oscillations	72
FIGURE 3.S3	Two explanations for remote phase-locking to hippocampal theta .	73
FIGURE 3.S4	Phase-locking to local oscillations with and without co-occurring hippocampal oscillations	74

CHAPTER 1

INTRODUCTION

Listen:

Billy Pilgrim has become unstuck in time.

Billy has gone to sleep a senile widower and awakened on his wedding day. He has walked through a door in 1955 and come out another one in 1941. He has gone back through that door to find himself in 1963. He has seen his birth and death many times, he says, and pays random visits to all the events in between.

Kurt Vonnegut, Slaughterhouse-Five

Time and memory are so deeply intertwined that they can seem almost one in the same. Imagining what our memories would be like without a sense of time is not easy—but consider the following scenario describing a series of routine events on a weekday morning, as I might write them in a journal (Table 1.1).

I get to lab at the same time as my labmate, who asks how my morning has gone. “Good,” I say, relaying some of the details. With little effort, I can recall each event in the order it occurred, and how long the event lasted if I care to think about it (“the line moved pretty fast, but the drinks were slow to come out”). I skip over the more boring details to focus on things more interesting or unusual, otherwise narrating events in chronological order—because, well, how much sense would it make to do otherwise?

If time perception was lost but memory for details retained, my morning might have gone differently, and my memory for it would be fragmented and dreamlike. I walked to lab. I fed my cat. I sipped my coffee but burned my tongue (guess I didn’t give the coffee enough time to cool). I brushed my teeth until my girlfriend told me 5 minutes had gone by and

9:00 A.M.	Alarm goes off. Hit snooze and check the news on my phone.
9:10 A.M.	Get out of bed and walk across the hall to the bathroom.
9:10 A.M.	Brush teeth.
9:12 A.M.	Shower.
9:20 A.M.	Cat is waiting impatiently outside the bathroom for breakfast.
9:22 A.M.	Return to the bedroom and get dressed.
9:25 A.M.	Walk to kitchen and feed the cat. ...Also, when did I last change her water? It must have been a couple days ago, so I should refill it.
9:30 A.M.	Return to the bedroom and pack up things for the day.
9:32 A.M.	Walk from my apartment to the coffee shop on the way to lab.
9:40 A.M.	Stand in line at the coffee shop. Three people ahead of me.
9:43 A.M.	My turn to order. That went by pretty fast!
9:45 A.M.	A puppy runs into store, escapes its owner, and darts behind the bar counter. Customers stop what they're doing to watch the scene unfold.
9:48 A.M.	This latte is taking awhile to make..?
9:49 A.M.	Got my latte. It's pretty hot so will give it a few minutes to cool. In the meantime will continue walking to lab.
9:54 A.M.	Reach the start of South St. Bridge, maybe time to check on the latte. Perfect; it's good to drink now.
10:10 A.M.	Arrive at lab.

Table 1.1: A morning's account.

kicked me off the sink. I got dressed and took a shower (or wait, it must have been the other way around..?). My cat yelled at me for breakfast. A puppy ran behind the bar counter. I woke up and read the news.

Given our remarkable ability to remember details of events in our lives, it is perhaps unsurprising that humans have a similarly impressive capacity to track the order and duration of these events [17, 18, 55, 56, 126, 135, 192]. We can answer questions about time in multiple formats – how long ago did event i occur [75]? When did event j occur [94]? Which was more recent, i or j [212]? We retain these abilities across multiple timescales, spanning seconds to years [57, 80]. Some kinds of temporal information are encoded automatically [4], and the timing with which events occur implicitly shapes the order in which they are later recalled [69, 76, 150, 198].

The study of memory therefore demands the study of time, and the challenge for neurosci-

entists is to understand how the brain stores and later integrates the details that comprise events and the times that they occur. A good starting point for these questions comes from studying patients with focal brain lesions, as this approach provides a causal (if coarse) understanding of where in the brain to search for neural processes of interest. In general, lesion studies have found that similar regions are required for remembering event-specific contents and recalling the order and duration of events. These abilities depend on activity within the prefrontal cortex (PFC) [100, 106, 174] and medial temporal lobe (MTL) [36, 139, 142, 143, 170], including the hippocampus [120], as well as thalamic and basal forebrain regions that project to these cortical areas [174, 191].

Along with lesion studies, scientists have taken advantage of the widespread availability of functional magnetic resonance imaging (fMRI) to investigate the neural correlates of time coding in healthy individuals. fMRI is a safe, non-invasive technique with moderate spatial and temporal resolution that provides a proxy for neural activity by measuring magnetic distortions caused by fluctuating blood oxygenation levels. Lesion and fMRI studies have converged around a similar set of regions involved in time coding, with particular emphasis on the hippocampus and surrounding MTL [8, 38, 44, 89, 95, 108, 130, 195]. In contrast to lesion studies, fMRI can reveal how brain activity in specific regions changes between task conditions within-subject. In one study, for example, subjects viewed a feature-length movie before being asked, while in an MRI scanner, to recall the order in which sets of image stills from the movie had appeared (the order of images in each set could not be guessed from logical inference, without reference to memory) [108]. Compared to control conditions in which subjects solved math problems or performed inference-based sequence reconstruction, fMRI activity was selectively increased in the hippocampus and parahippocampal cortices bilaterally, consistent with a role for these regions in supporting temporal order memory. Moreover, subjects who performed this task more accurately also showed proportionally larger increases in hippocampal activity, relative to baseline. In another study, subjects were asked to place image stills from an earlier-viewed television episode on a continuous timeline [130]. When comparing images with low temporal judgment error to images with high error,

the researchers found that fMRI activity was increased in the medial PFC, hippocampus, and a pair of regions upstream of the hippocampus—the anterolateral entorhinal cortex (EC) and perirhinal cortex—that studies in rodents suggest are associated with time coding [194]. In contrast, no activation differences were found in posterior MTL regions that are thought to be more associated with spatial than temporal processing.

In addition to revealing which brain regions exhibit increased activity during time coding tasks, fMRI has been used to examine how neural representations of individual items are shaped by their time and order of occurrence. Several studies describe changes in stimulus-specific, multivoxel activation patterns that accompany temporal learning [8, 32, 37, 46, 82, 171]. For example, Schapiro et al. [171] exposed subjects to a continuous stream of repeated visual stimuli in which some items appeared as sequential pairs while other items were uncorrelated in time. Although subjects did not know about the temporal structure of the task in advance and performed a cover task during stimulus exposure, follow-up testing showed that they implicitly learned which pairs of items occurred sequentially. At the same time, multivoxel representations in the hippocampus and surrounding MTL changed to reflect the temporal relations between items, such that the multivoxel pattern similarity for temporally paired items, but not unpaired items, was increased in post- versus pre-exposure testing. Another study extended this finding to show that stimulus-specific representations in the hippocampus are influenced not only by temporal proximity but by spatial proximity as well [32]. Here, subjects navigated along a predefined route through a virtual environment while encountering objects at specific locations, with teleportation portals serving to partially decorrelate time and space. As in the study by Schapiro et al., hippocampal multivoxel representations of objects encountered nearby in time were more similar in post- versus pre-exposure testing, even after controlling for effects of spatial proximity. Moreover, the degree to which neural representations of objects converged after virtual navigation was correlated with subjects' judgments of temporal proximity. Similar effects were found in the hippocampus for object relations in space, with increased representational similarity between objects reflecting both their actual and remembered spatial proximities. In sum,

fMRI studies indicate that the MTL—and the hippocampus, in particular—is a convergence zone for neural representations of time, space, and environmental stimuli. Neural patterns for specific items change over time to reflect the temporal and spatial contexts in which they are encountered, with time and space possibly playing similar roles as stable contexts to which items can be bound.

Yet for all that can be learned through these described approaches, a critical, unanswered question concerns how neurons in regions that represent time and memory give rise to these abilities. Does a neuron in the hippocampus know how long it takes to make a pot of coffee, or the deadline for this dissertation? How does a code for time emerge from populations of neuronal firing, and how does this time code connect to the behavioral limitations of time perception and temporal memory? Such questions are needed to trace the neurobiological underpinnings of cognitive processes beyond coarse, regional associations. Obtaining answers, however, requires recording activity from sizeable numbers of neurons while subjects perform time-controlled tasks, a prohibitive constraint in most human subjects research due to the risky and invasive nature of such experiments. Where our understanding of these processes in the human brain leaves off, studies in animal models, and particularly in rodents, pick up. Substantial advances in this research over the past two decades has begun to paint a fascinating picture of how memory for time and events is organized in the brain.

A major advance came from a 2008 study from György Buzsáki’s lab that recorded hippocampal area CA1 pyramidal cells while rats ran loops around a T-maze track, alternating between left-turn and right-turn routes for which correct turns led to a water reward [144]. The key manipulation lay in what the rats did in the time between these T-maze trials. Following each run around the track, the rats were trained to run on a stationary wheel for a fixed duration, before being released back onto the track for the next trial. At the time of this study, longstanding dogma in the rodent hippocampal field held that the hippocampus was principally concerned with representing spatial information. This presumption stemmed from the groundbreaking discovery of hippocampal place cells by John O’Keefe and Lynn

Nadel in the 1970’s [133]. Later studies found that, in addition to neurons that responded primarily to place, many neurons in the hippocampus and surrounding MTL represented sensory stimuli and directional signals, firing for example when a rodent was headed in a specific direction, toward a landmark, or in response to a particular smell [41]. While these findings stretched the understanding of what features the hippocampus represents, they did not contradict the view that the hippocampus served to construct cognitive maps for spatial navigation [26, 132]. Adopting this interpretation, Pastalkova et al. suggested that one of two responses should be observed during the wheel-running stages of their T-maze paradigm: Either a small number of hippocampal neurons should act as place cells that selectively represent the rats’ location at the stationary wheel, or hippocampal pyramidal neurons should be silent in the absence of positional updating or navigational demand. Yet the data supported neither hypothesis. Instead, Pastalkova et al. found that about half of all neurons were active during treadmill running, more than at any other position on the T-maze track. Moreover, the large majority of these neurons did not exhibit sustained firing throughout wheel running but instead fired in brief bursts at specific times within the wheel running interval. These preferred firing times were consistent across trials within-neuron but highly variable across neurons. As a result, activity across the population of these neurons comprised a time code for the wheel running interval—a cognitive map of time that challenged the spatial theory of hippocampal function.

In 2011, a second study from Howard Eichenbaum’s lab arrived at similar conclusions as Pastalkova et al. regarding CA1 pyramidal cell activity during delays between tasks. This study coined the term ‘time cells’ to describe these neurons [112]. While these early time cell experiments confounded time and distance elapsed (which was especially problematic for the wheel running paradigm, as rodents run at fairly constant speeds in such a setting), follow-up studies showed that neural codes for time and distance could be disambiguated [103], and time cells were found to activate even in head-fixed and immobilized animals [111]. A study that performed calcium imaging in mice showed that while individual time cells can gain or lose receptive fields over time with a certain probability, the population

time code is stable over several days at a minimum [119]. Finally, in addition to ‘canonical’ time cells in CA1, other studies have identified time cells in hippocampal area CA3, medial EC, and medial PFC [72, 169, 190]. Lesion experiments confirm a role for these regions in temporal memory in rodents, as in humans [7, 33, 47, 73, 84, 123, 187], although it is less clear how or whether time cells in these regions contribute to time perception and memory. It remains possible that alternative time coding mechanisms exist that ensure robustness at the cognitive-behavioral level. Such alternatives could include population neural drift, as shown in Manns et al. [117] and Mankin et al. [114], or a strategy based on one or multiple oscillators, as described for neurons in subcortical and striatal circuits [118, 125, 192].

Additional evidence from animal models highlights several intriguing similarities between time cells and place cells that extend beyond their similarly Gaussian-shaped receptive fields and co-occurrence in the hippocampus. First, it was noted in the earliest time cell studies that many CA1 neurons act as both time cells and place cells, depending on the task context [62, 144]. For example, a neuron might fire 5s into a 10s delay and (separately) at a particular position along a T-maze track. Second, time cell and place cell codes are highly context-dependent, remapping in response to changes in interval length, spatial environment, or other salient cues [14, 62, 109, 112, 144, 189, 208]. Lastly, time cells and place cells are both tuned in part by upstream input from the EC, although differences here are also apparent [40, 186]. In a 2018 study by Tsao et al., recordings from the lateral EC of rats provided clues to the nature of this upstream timing input. As the animals alternated between occupying white- and black-bordered rooms for fixed amounts of time, lateral EC neurons exhibited exponentially increasing or decreasing firing rates with variable time constants, enabling time throughout the experiment to be decoded from population firing patterns with high precision. Additional work from Marc Howard’s lab proposes that these EC responses reflect the Laplace transform of physical time, with the inverse Laplace transform giving rise to Gaussian time cells in the hippocampus [15, 77]. In the experiment by Tsao et al., population decoding of time from neurons in the medial EC—where grid cells are found—was substantially worse than for decoders trained on lateral EC activity. This finding suggests

that while time and space may be similarly represented in the hippocampus, upstream inputs have both regional (lateral versus medial EC) and functional dissociations (exponential ramping versus grid-like firing).

Time cells are also found in the monkey hippocampus, where they exhibit remarkably similar properties to time cells in rodents [28, 136, 167]. However, research in animals alone cannot reveal how neuronal computations contribute to human cognition and behavior. Additionally, even animals as intelligent as monkeys require intensive training and artificial incentives to perform many tasks that are trivial for humans to learn. On the whole, the animal data suggest that time is implicitly tracked in the hippocampus and some surrounding MTL regions, and that similar hippocampal representations of time and place might shape our perception and memory for when and where events occur. But to understand how these neural processes connect to such intricate cognitive processes as perception and memory, animal models alone can take us only so far.

These thoughts motivated the principal undertaking of my graduate work: to design an experiment that would bridge research on time and place coding in animals and humans, and to run this experiment in a setting where it would be possible to record neurons in the human brain. The only ethical grounds for pursuing this research are when it is secondary to clinical demands, as for cases in which hospital patients voluntarily undergoing surgical implantation of intracranial depth electrodes on the advice of their physicians. This happens in some cases of pharmacologically resistant epilepsy, for which a patient is deemed a potential candidate for surgery to remove seizure-generating brain regions or for long-term implantation of a neurostimulating device. In these instances, surgeons will implant electrodes in a number of regions to monitor epileptic activity. These regions commonly include the suspected seizure onset zones, their bilateral counterparts, and adjacent or structurally connected regions. Patients who undergo these electrode implantation procedures must remain in the hospital under close supervision until undergoing a second surgery to remove the electrodes, usually one to two weeks later. It is during these periods in the hospital between electrode

implantation and removal when, in the time between physician rounds, nurse check-ins, visits from family, meals, sleep, and other events, research studies in consenting patients can be conducted. That so many patients find the energy to participate in these studies despite facing intermittent seizures, exhaustion, headaches, and other discomforts is a testament to their remarkable dedication to this field of study and the stake they share in its successes.

Previous research in our lab revealed neurons in the human MTL that encode space similarly to neurons in rodents and other animals. Specifically, while research participants freely navigate through a virtual environment within a computer game, some neurons exhibit place, grid, and head direction-specific responses, while other neurons encode environmental landmarks [42, 92, 93, 127]. However, all of these experiments involved navigating for varying amounts of time on each trial, precluding an analysis of whether neurons fire at specific times within a stable temporal context. Therefore I designed and built a computer game experiment to answer two questions about the neural coding of time. First, during fixed delays when place, view, and other external variables are held constant, do neurons in humans act like time cells in rodents—constructing a continuous, internal representation of time? Second, how do neurons represent time and place within a stable spatiotemporal context in which people navigate through a fixed environment for a controlled duration? After building this experiment, Mike and I began a collaboration with Itzhak Fried, a UCLA neurosurgeon whose lab specializes in human neuron recordings and who worked with us in past studies on place cells and grid cells.

I turn now to a second question that motivated my interest during my graduate studies. This question, too, stemmed from a desire to understand how neurons in the human hippocampus and other memory-related brain regions operate, and how much carry-over exists between human neurophysiology and that of rodents, from which a vast amount of neuroscientific knowledge is based. The question concerns time and space of a different nature, pertaining to relations between neurons themselves.

For neurons to communicate effectively, they must fire precisely. In the rodent hippocampus,

for example, the line between long-term potentiation (0-20ms) and long-term depression (20-100ms) of synapses is razor thin [48]. Understanding how neurons time their firing is therefore critical to understand how they coalesce to form meaningful ensembles. This process is sufficiently challenging to resolve when the neurons in question reside in the same region, but a still greater challenge lies in understanding how neurons communicate effectively between regions. Nonetheless, we know that such inter-regional communication must occur, and it stands to reason that functional connections between regions must be flexible for the brain to move fluidly between different cognitive states. In the memory system, fMRI connectivity between the hippocampus and other regions has been found to correlate with successful memory formation in healthy adults [158, 188], tracks with age-related memory decline [64, 168, 211], and is altered in memory-related disorders including Alzheimer’s disease, mood and anxiety disorders, and schizophrenia [24, 30, 124, 134, 215]. Yet the neural mechanisms that govern these connectivity changes remain a mystery.

In my second study, I sought to test whether the timing of neuronal firing in memory-related regions outside the hippocampus is associated with rhythmic activity, or oscillations, within the hippocampus. Neural oscillations are a promising candidate mechanism for routing information flow in the brain. Oscillations are characterized by rhythmic fluctuations in local field potentials (LFPs) that reflect shifting excitatory and inhibitory synaptic currents, summed over a population of neurons whose size depends on the surface area of the electrodes used for measurement [21, 23]. Neurons recorded in both animals and humans have been found to intermittently synchronize their firing with specific phases of ongoing oscillations [91, 165], and by targeting phases of greater excitability, neurons can more effectively discharge their downstream targets [22, 58, 59].

These concepts extend beyond local circuit operations, with applications to inter-regional communication. For example, recent evidence from intracranial electroencephalography (EEG) recordings in epilepsy patients indicates that increased oscillatory synchronization in the MTL correlates with encoding and retrieval success during verbal learning tasks

[6, 50, 51, 180, 181, 206]. Cortico-hippocampal interactions have been studied at a finer scale in rodents, where cortical neurons phase-lock to hippocampal theta oscillations during goal-directed spatial navigation [9, 60, 96, 175, 178]. Furthermore, experimental manipulations that disrupt this phase-locking are associated with reduced information transfer from cortex to hippocampus along with spatial working memory deficits [90, 141, 177]. However, direct evidence for a relation between extrahippocampal firing and hippocampal oscillations at any frequency in humans has been lacking.

1.1. Overview

In **Chapter 2**, I report my findings on time and space coding among individual neurons in the human MTL and medial PFC, from data collected in collaboration with UCLA over the past three years.

Chapter 3 provides new insights into fundamental relations between hippocampal oscillatory activity and neuronal firing in multiple regions of the memory system.

Chapter 4 discusses future directions and new experiments that stem from these discoveries.

CHAPTER 2

A NEURAL CODE FOR SPATIOTEMPORAL CONTEXT

This chapter has been adapted from Schonhaut DR, Aghajan ZM, Kahana MJ, Fried I (2022) A neural code for spatiotemporal context. *bioRxiv*, 2022. doi: <https://doi.org/10.1101/2022.05.10.491339>

2.1. Abstract

Time and space are primary dimensions of human experience. Whereas separate lines of study have identified neural correlates of time and space, little is known about how these representations converge during self-guided experience. Here we asked how neurons in the human brain represent time and space concurrently. Subjects fitted with intracranial microelectrodes played a timed navigation game where they alternated between searching for and retrieving objects in a virtual environment. Significant proportions of both time- and place-selective neurons were present during navigation, and distinct time-selective neurons appeared during task-free delays absent movement. We find that temporal and spatial codes are dissociable, with time cells remapping between search and retrieval tasks while place cells maintained stable firing fields. Other neurons tracked the context unique to each task phase, independent of time or space. Together these neuronal classes comprise a biological basis for the cognitive map of spatiotemporal context.

2.2. Introduction

Time and space help to organize our experiences, allowing us to reconstruct the past and envision the future. Lesions to the medial temporal lobe (MTL) and prefrontal cortex (PFC) disrupt associations between events and their temporal [106, 139] and spatial [3, 12, 149] contexts. Parallel lines of research have uncovered neurons in these regions that fire at specific locations within a given environment ('place cells' [132]) or specific moments within a stable interval ('time cells' [40, 112, 144]), providing a candidate biological basis for a cognitive map of time and space. Our understanding of these neurons, however, stems largely from studying them in isolation: place cells are usually recorded during exploratory or goal-directed navigation absent time constraints, while time cells are recorded at fixed locations under timed conditions [40]. Thus, despite the longstanding assumption that the brain encodes experiences within their spatiotemporal contexts [81, 196, 197], we lack an understanding of how neuronal representations of time and space converge during experience.

Recordings of neuronal responses in the human brain have now established the existence of place-responsive cells that appear analogous in many ways to place cells in the rodent hippocampus [42, 92, 93, 127]. Recent studies also suggest the existence of neurons that appear selective to time in both verbal list learning [199] and image sequence learning [161] tasks. Yet it remains unclear if neurons in humans encode time during task-free conditions analogous to those studied in animals, or if time cells only appear in tasks requiring explicit attention to time or sequentially-presented stimuli. To address these questions, we recorded single- and multi-neuron activity while subjects played a virtual navigation game under strict time constraints.

2.3. Results

We recruited 10 neurosurgical patients with intracranially-implanted depth electrodes to play a time-constrained, spatial navigation computer game called *Goldmine*, in which they earned points by collecting gold in a visually sparse, underground mine (Figure 2.1). Each trial consisted of four, timed events: First, subjects waited passively for 10s at a fixed

location, the mine base (Delay_1). Next, they had 30s to search for gold that appeared throughout the mine in randomized locations on every trial (Gold Search). Subjects then waited an additional 10s in the mine base under identical conditions to the first delay (Delay_2). Finally, they had 30s to return to remembered gold locations and dig for gold, now invisible (Gold Dig). This sequence repeated for 36 trials per session, and all subjects performed well, collecting 54% (range 35-73%) of golds that were found during Gold Search while maintaining 47% (range 19-71%) digging accuracy (see Methods).

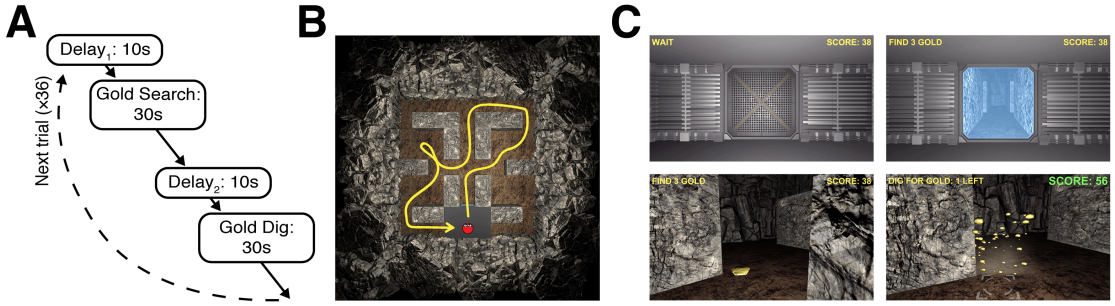


Figure 2.1: Goldmine task. (A) Trial structure and timing. (B) Top-down view of the mine layout. The yellow line shows an example route by a subject (red circle). (C) Gameplay screenshots during Delay (top-left), Gold Search (top-right, bottom-left), and Gold Dig (bottom-right) events.

Using microwires that extended from implanted electrode tips, we recorded extracellular action potentials from 457 single- and multi-units (13-73 units per session, hereafter called ‘neurons’) that were primarily located in the MTL and medial PFC (mPFC; Table 2.S1). Here we investigated associations between these neurons’ firing rates and the spatiotemporal structure of the task.

2.3.1. Time during task-free delays

We first analyzed neural activity during delay events (Figure 2.1A), which replicated conditions in which time cells are found in the rodent hippocampus [40]. To prevent time from being confounded with other behavioral variables, we teleported subjects to the exact same location at the start of every delay, they viewed a static image of a door to the mine that was identical across trials (Figure 2.1C), and – as in animal time cell studies – subjects

were neither instructed nor incentivized to explicitly attend to time. The delays therefore provided a strict test of the hypothesis that neurons encode time within clearly-defined, repeating intervals with fixed external context.

Figure 2.2A shows a selection of neurons that fired in a time-constrained manner consistently across trials, illustrating the range of typical responses. Among the 457 recorded neurons, 99 neurons (22%) exhibited a significant main effect of time (10 discrete, 1s bins), independent of delay-event (Delay_1 or Delay_2) and its interactions with time (permutation test against circularly-shifted spikes; see Methods; Figure 2.2, A and C). These ‘delay time cells’ were present at rates well above chance in the hippocampus and other recorded regions, with no difference in the proportion of significantly-responding neurons between the hippocampus, surrounding MTL (combining amygdala, entorhinal cortex, and parahippocampal/fusiform gyrus), and mPFC ($p > 0.05$, permutation test controlling for differences in neurons recorded per region, between subjects; Table 2.S2). In contrast, only 26 neurons (6%) exhibited a significant time \times delay-event interaction, not exceeding chance (Figure 2.2C). A majority of time-coding neurons during delays therefore did not distinguish between Delay_1 and Delay_2 .

Next we examined the distribution of mean firing rates over time for all main-effect time cells, sorted by their maximal firing time (Figure 2.2D). Individual neurons had highly variable firing rate peaks, and the number of neurons that peaked in each third of the delay was significantly above chance ($p < 0.05$, binomial tests with Bonferroni-Holm correction). Thus, time cells were not restricted to one portion of the delay but instead spanned the entire 10s duration. However, similarly to time cells in animals [62, 112, 144], more time cells peaked near delay onset than at later times (Figure 2.2D), and time cells with earlier peaks also showed larger magnitude responses above their baseline activity ($r = -0.47$, $p < 0.0001$; peak firing time versus maximum z -scored firing rate).

While time cells did not distinguish between Delay_1 and Delay_2 , a distinct group of neurons ($n = 70$, 15%) responded to delay-event as a main effect, independent of time (Figure 2.2, B and C). Some of these ‘event-specific cells’ had dramatically different firing rates between

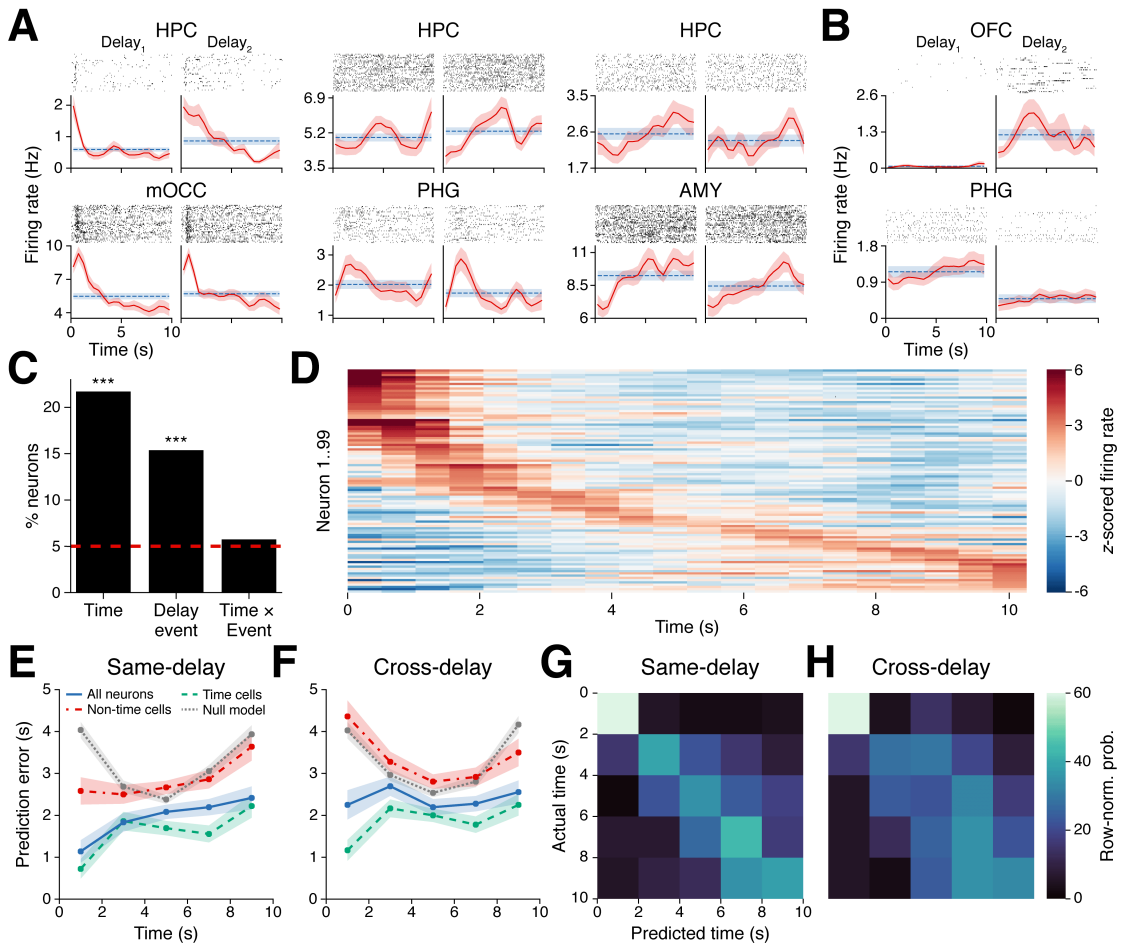


Figure 2.2: Time cells during task-free delays. (A) Subpanels show trial-wise spike rasters and firing rates (mean \pm SEM; solid-red line: 500ms moving average; dashed-blue line: grand average) for six time cells in the hippocampus (top row), medial occipital cortex, parahippocampal gyrus, and amygdala (bottom row, L to R). The left subpanel for each neuron shows Delay₁ activity, and the right subpanel shows Delay₂ activity. (B) Event-specific cells in orbitofrontal cortex (top) and parahippocampal gyrus. (C) Percent of neurons with significant responses to each main effect and interaction (red line: Type 1 error rate). *** $p < 0.0001$, binomial test with Bonferroni-Holm correction. (D) z -scored firing rates for all main effect time cells (each row = one neuron), sorted by time of maximum z -scored firing. (E) Mean \pm SEM prediction errors, across trials, for classifiers that were trained and tested on the same delay event (e.g. both Delay₁) to decode time from firing rates of all neurons (solid, blue line), the 115 neurons that responded to time as a main effect or interaction with delay-event (dashed, green line), 342 neurons that did not respond significantly to time (dash-dot, red line), and chance-level results from null model classifiers (dotted, gray line). (F) Same as (E), but for classifiers that were trained and tested on different delay events (e.g. Delay₁ \rightarrow Delay₂). (G and H) Confusion matrices for same-delay (G) and cross-delay (H) time cell classifiers. Matrix rows sum to 1, with each value indicating the mean probability across held-out test trials.

the two delays, as shown for an orbitofrontal cortex neuron that almost never fired during the 36 Delay₁ trials yet was active in sustained bursts throughout Delay₂ (Figure 2.2B, top). A similar number of event-specific cells fired more during Delay₁ than Delay₂ ($n = 39$, 56%) as showed the opposite response, and like time cells, these neurons appeared throughout the regions we recorded but did not differ significantly between regions (Table 2.S2).

Given the prevalence of time cells at the single-neuron level, we next asked if time could be decoded from neural activity patterns at the population level. Indeed, support vector machines trained on firing rates of all recorded neurons decoded time within 1.9 ± 0.1 s on held-out test trials, significantly outperforming the 3.2 ± 0.1 s error expected by chance ($p < 0.0001$, paired *t*-test versus null model classifiers; see Methods). Mirroring the clustering of time cell peaks near delay onset, classifier error was lowest at delay onset and increased steadily over time, while still remaining better than chance in every time bin (Figure 2.2E).

In spatial navigation studies, place decoding is informed both by place cells and ‘non-place’ cells that lack individually-interpretable responses, indicating that spatial location is represented by a distributed neural code [184]. We compared classifiers that were trained to decode time from all neuron firing rates against classifiers trained only on time cells ($n = 115$, including time as a main effect or interaction) or only on non-time cells ($n = 342$), respectively. Whereas time-cell-only classifiers performed significantly better than all-neuron classifiers ($p = 0.0070$, paired *t*-test; Figure 2.2, E and G), non-time cell classifier predictions were no better than chance ($p > 0.05$, paired *t*-test). Thus, the population code for time during delays depended on the activity of bona fide time cells, and without these neurons there was no delay time code.

Finally, we considered whether time could be decoded from cross-classifiers that were trained and tested on different delay-events (i.e. Delay₁ → Delay₂, or vice versa), as suggested by the prevalence of main-effect time cells over time × delay-event interaction cells. Consistent with this observation, we found that cross-classifiers performed comparably to classifiers that were trained and tested on the same delay event (Figure 2.2, F and H). In summary,

population neural activity was sufficient to decode time, and the two delays shared an overlapping neural time code.

2.3.2. Time and place during navigation

Having observed time-coding neurons during delays, we next asked if similar time coding appeared during virtual navigation, when subjects alternated between searching and digging for gold in the mine (Figure 2.1A). To identify neural responses to time independent of place, we regressed each neuron’s firing rate against elapsed time (10 discrete, 3s bins), place (12 regions; Figures 2.S1 and 2.S2), navigation-event (Search or Dig), and their first-order interactions. We then identified neurons for which removing the main effect of time or the interaction between time and another variable caused a significant decline in model performance, relative to a null distribution of circularly-shifted firing rates (see Methods). Additionally, to ensure that time and place were sufficiently behaviorally decorrelated, we allowed subjects to exit the base through only one of three doors on a given trial (left, right, or center; counterbalanced across trials), requiring them to vary their routes through the mine. This manipulation severed all but weaker correlations ($r < 0.2$) between temporal and spatial bins, with the exception that subjects always began navigation at the mine base (Figure 2.S3). Models with additional covariates for head direction, movement, visible objects and landmarks, and dig times yielded qualitatively similar results (Figure 2.S4).

Holding place constant, we observed many neurons that fired in a time-dependent manner during navigation (Figure 2.3A). Most of these time-coding neurons were context-specific, with a significant number of neurons ($n = 64$, 14%) representing interactions between time and navigation-event, while the number of neurons with a significant main effect of time ($n = 23$, 5%) was at chance level (Figure 2.3C). In this respect, time cells during navigation differed markedly from delay time cells that fired analogously between Delay₁ and Delay₂. In addition, classifiers trained on neural firing during delays failed to predict time above chance during navigation (Figure 2.S5), and population neural activity was negatively correlated between delay and navigation events, such that neurons that were more active during delays

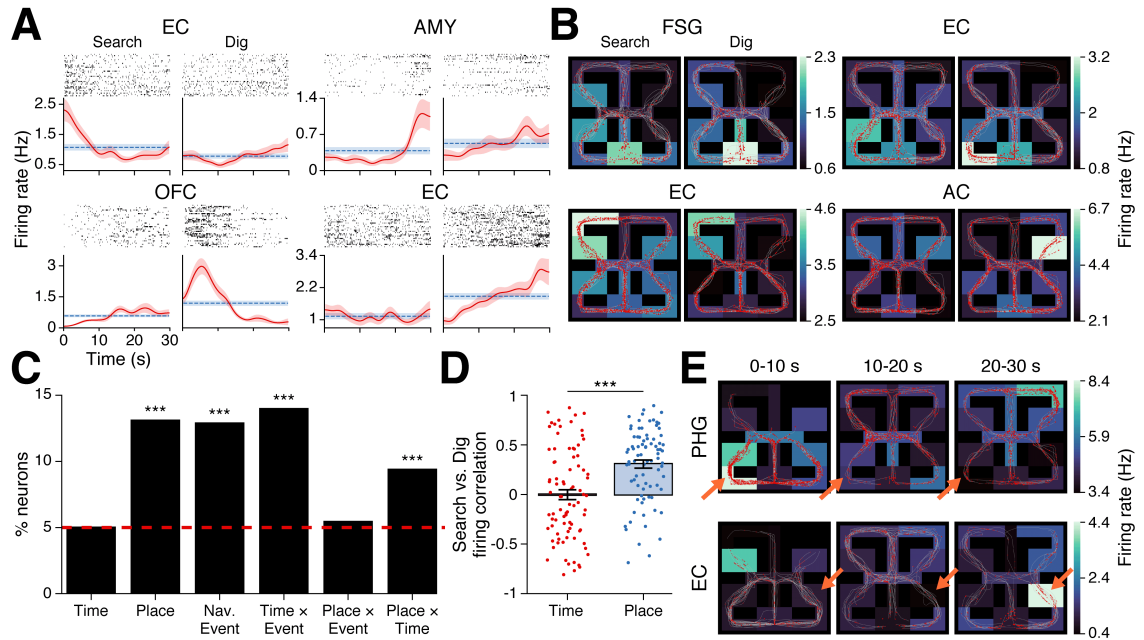


Figure 2.3: Time and place cells during navigation. (A) Four time \times navigation-event-specific neurons in the entorhinal cortex (top-left, bottom-right), amygdala (top-right), and orbitofrontal cortex. (B) Four place cells in the fusiform gyrus (top-left), entorhinal cortex (top-right, bottom-left), and anterior cingulate. Paths traveled (white lines) and spikes (red circles) are overlaid on firing rate heatmaps (colorbar) in each mine region. The left subpanel for each neuron in (A) and (B) shows activity during Search events, and the right subpanel shows activity during Dig events. (C) Percent of neurons that responded significantly to each main effect and interaction (red line: Type 1 error rate). *** $p < 0.0001$, binomial test with Bonferroni-Holm correction. (D) Correlated firing rates between Search and Dig events, computed: (Left bar) across time bins, for neurons with a main effect of time or a time \times navigation-event interaction (each point = one neuron); (Right bar) across mine regions, for neurons with a main effect of place or a place \times navigation-event interaction. *** $p < 0.0001$, Welch's t -test. (E) Firing rates in each mine region for two place \times time interaction cells in the parahippocampal gyrus (top) and entorhinal cortex, averaged across all Search and Dig events during the first, middle, and last 10s of each event (left to right subpanels).

were usually less active during navigation, and vice versa (Figure 2.S6). Insofar as neurons encoded time during navigation, they therefore did not adhere to the delay time code.

Most time \times navigation-event neurons fired in a time-modulated manner during one navigation event but had a flat or unrelated firing rate during the other, similar to the place cell phenomenon of ‘global remapping’ [27]. For example, the entorhinal cortex neuron shown in the bottom-right Figure 2.3A subpanel fired at a uniform rate throughout Search events but increased its firing rate more than threefold from the beginning to end of Dig events. As during delays, firing rate peaks for time \times navigation-event cells spanned entire event durations and were overrepresented near navigation onset (Figure 2.S7). Time \times navigation-event cell proportions did not differ significantly between regions, nor did we find regional differences between other behavioral variables during navigation (Table 2.S2).

Classifiers trained on population neural activity during navigation echoed the single-neuron results, decoding time within 3.8 ± 0.2 s on held-out test trials (chance: 10.1 ± 0.2 s), with increasing error at later times from event onset (Figure 2.S8, A and C). However, contrasting the delay results, time cell cross-classifiers that were trained and tested on different navigation events failed to generalize, performing no better than chance ($p > 0.05$, paired t -test; Figure 2.S8, B and D). Thus, while the two delays were represented by an overlapping time cell code, Search and Dig events used orthogonal codes.

As in untimed navigation studies [42, 92, 93, 104, 127], a significant number of neurons ($n = 60$, 13%) encoded place as a main effect during timed navigation, and these ‘place cells’ exhibited a wide range of receptive fields in different regions of the mine (Figure 2.3, B and C). In contrast, the number of neurons with a significant place \times navigation-event interaction ($n = 25$, 6%) did not exceed chance. This result revealed a dissociation between time cell and place cell responses to changes in task context, with place cells remaining stable between Search and Dig events while time cells remapped. We confirmed this conclusion by comparing correlations between Search and Dig firing rates: (1) across time bins, for each of the 85 neurons with a main effect of time or a time \times navigation-event interaction

($r = 0.0 \pm 0.05$ SEM across neurons); and (2) across spatial regions, for each of the 82 neurons with a main effect of place or a place \times navigation-event interaction ($r = 0.31 \pm 0.04$; Figure 2.3D). Despite this remapping dissociation, time cells and place cells did not differ significantly in number or in time and place coding strength, respectively ($p > 0.05$, Welch's t -test comparing likelihood ratio z -scores versus null distributions; see Methods).

Prior animal and human studies have found that place cells are often influenced by additional variables including head direction, goal location, and visual cues [42, 92, 116, 209]. We asked if time similarly modulates place representations by identifying neurons whose activity reflected interactions between place and time, controlling for their main effects. We identified 43 such place \times time cells (9%) whose firing rates at a given location depended on the time it was visited relative to navigation onset (Figure 2.3E). These neurons were significantly more prevalent than chance, including in models that further controlled for head direction and visual landmarks (Figure 2.S4). Thus, while time and place were generally represented by different neuronal populations, a small number of neurons conveyed information about joint spatiotemporal context, reflecting a higher level of feature abstraction.

Finally, we identified a significant number of neurons ($n = 59$, 13%) that encoded navigation-event independent of time and place, half of which fired preferentially during Search events and half during Dig events. These navigation-event-specific cells overlapped minimally with delay-event-specific cells described previously (Figure 2.2B), and consequently all four trial events were represented by distinct groups of neurons.

2.3.3. Representing time over long durations

During both delay and navigation events, the neural time code gradually erodes (Figure 2.2, E and G and Figure 2.S8, A and C), as reported previously in animals [15, 119, 189]. Given this loss of temporal information, how do we retain a sense of time over long durations? Behavioral studies of temporal memory suggest that some events might act as ‘landmarks’ in time by realigning the internal clock with the external passage of time [55]. Landmarks play a paraallel role in spatial navigation, where they can correct cumulative path integration

error and offer an alternative to direction-based navigation [122, 147].

The *Goldmine* task contained two levels of temporal structure: time within each delay and navigation event, and time across the four events in a trial (Figure 2.1A). If neurons used the boundaries between these events as temporal landmarks, we reasoned that: (1) it should be possible to decode time across the whole trial at once, and (2) decoding accuracy should decrease steadily within each trial event but increase following the transition from one event to the next.

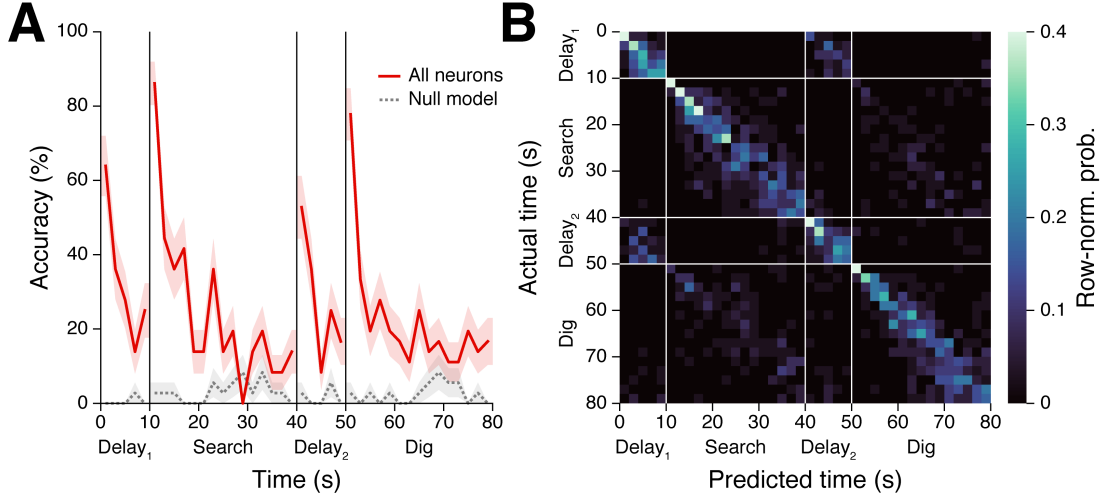


Figure 2.4: Decoding time across the trial. (A) Prediction accuracy by time for classifiers trained to decode 2s time bins from all neuron firing rates, using actual (solid, red line) or circularly-shifted (gray, dotted line) time bins. (B) Confusion matrix for classifiers trained on actual (non-shifted) time bins. Matrix rows sum to 1, with each value indicating the mean probability across held-out test trials.

To evaluate these hypotheses, we trained classifiers to decode time (40, 2s bins) from all neuron firing rates across the 80s trial, then tested them on held-out trials (Figure 2.4). As classifiers merely selected the most probable time bin without knowing anything about the trial event structure, above-chance performance can only be explained by the distinctiveness of neural patterns in each time bin, relative to others. Consistent with our first hypothesis, classifier accuracy on held-out trials was well above chance (observed: $25 \pm 3\%$ SEM across trials; chance: 2.5%), and classifier-predicted times were closely aligned with actual

times throughout the trial duration (Figure 2.4B). Consistent with the second hypothesis, classifier accuracy increased sharply at the beginning of each delay and navigation event then decreased at a predictable rate over time (Figure 2.4A). Population neural activity was therefore sufficient to decode time across multiple events in the trial.

2.4. Discussion

Our study reveals neurons in the MTL and mPFC that encode time and space during exploration in a virtual environment for fixed durations. Time cells activated at rest in the absence of movement or other external contextual change, while distinct time cells and place cells emerged during navigation and exhibited divergent responses to changing tasks. These results demonstrate a neuron-level code for spatiotemporal context in the human brain, in which time and space are simultaneously represented but not wholly conjoined.

Fixing the duration of navigation events allowed us to investigate concomitant temporal and spatial codes, and we find the brain maintains largely independent time and place representations within a given context. Our data moreover reveal a novel dissociation between place cell and time cell responses, with place cells firing similarly between gold searching and digging tasks while time cells completely remapped. This result could reflect differences in how subjects perceived time and place in *Goldmine*, akin to differences in how people judge the time and place of events in daily life. That is, place cells were stable because subjects needed to return to the same locations during gold searching and digging, while time cells remapped to track the temporal progression of these events (first search, then dig) within each trial. This interpretation implies that different experimental conditions could elicit a reversed remapping effect in which place cell activity varies across contexts for which time cells are stable, with implications for how events within these contexts are later organized in memory [32].

Two recent studies in humans described neurons with temporally correlated activity during verbal list learning [199] and image sequence learning [161] tasks. These studies provided initial evidence for neuronal time coding under conditions in which subjects had to attend to

sequential information. Here we extend these findings to show that time codes are present even in the absence of task engagement, serial item presentation, or changing external stimuli. This finding suggests that neurons map time by default, providing a stable scaffold onto which events are bound to their times of occurrence across diverse contexts. Our task additionally enabled direct comparison between human and animal neuronal responses to time, revealing broadly conserved qualities across species. Specifically, we find that human time cells: (1) span entire event durations [62, 112, 144]; (2) accumulate error in the absence of external cues [15, 119, 189]; (3) remap between events for which context discrimination (here gold searching versus digging) is behaviorally adaptive [62, 112, 144, 189]; (4) are encoded independently of place [103, 113, 163, 166]; and (5) reside in the MTL [15, 72, 137, 144, 167, 169, 194] and mPFC [28, 190].

It is worth noting that we designed our paradigm to bear strong resemblance to the tasks in which time cells were originally discovered and subsequently investigated in rodents [40, 112, 144]. We found that time and place were both robustly encoded after accounting for potentially confounding variables including task, visual cues, and head direction. However, we acknowledge that in addition to quantifiable variables, latent factors (e.g. attention, planning, or anticipation) could additionally influence neuronal responses and are difficult to fully dismiss. While this concern is valid for both human and animal time cell studies, we see two paths forward: (1) employing alternative task designs across which the similarities and differences in time cell activity can be judged; and (2) using causal manipulations, such as direct stimulation, to determine how perturbing neuronal activity in specific regions affects the ability to make temporal judgments.

While we observed significant numbers of time cells and place cells in multiple regions within the MTL and mPFC, understanding regional differences in time and place coding properties is critical for interpreting these neurons' function. However, such analyses are currently infeasible due to limited sample size and high inter-subject variability in electrode recording location and quality. Further caution in interpreting our findings is warranted as subjects

are patients with neurological conditions, although consistency with animal studies lends considerable support to these data.

Episodic memory is distinguished from other forms of memory by the recall of events together with the unique, spatiotemporal contexts in which they occurred – the ‘what,’ ‘when,’ and ‘where’ of experience [196, 197]. Neural representations of these features are thought to converge in the MTL, where neurons fire selectively to image categories and multimodal percepts (‘what’) [61, 154, 156], and to specific locations and orientations in an environment (‘where’) [42, 92, 93, 104, 127]. Here we confirm a single-neuron basis for encoding ‘when’ an event occurs, separably from encoding ‘where.’ We further show that ensembles of time cells and event-specific cells support a neural code for time across multiple temporal scales. Each element of episodic memory – time, place, and event-related content – is therefore linked to its own neural code, the convergence of which provides a biological foundation for Tulving’s defining view of memory, 50 years ago [196].

2.5. Methods

2.5.1. Subjects

We analyzed behavioral and single-unit data from 10 neurosurgical patients with drug-resistant epilepsy who completed a total of 12 testing sessions. Clinical teams determined the location and number of implanted electrodes, based on clinical criteria. All testing was performed under informed consent after the nature and possible consequences of the experiment were explained, and experiments were approved by institutional review boards at the University of California, Los Angeles and the University of Pennsylvania.

2.5.2. Electrophysiological recording

Patients were stereotactically implanted with 7-12 Behnke-Fried electrodes with $40\mu\text{m}$ diameter microwire extensions (eight high-impedance recording wires and one low-impedance reference wire per depth electrode) that capture local field potentials (LFPs) and extracellular spike waveforms [54]. Microwire electrophysiology data were amplified and recorded at 30kHz on a Blackrock Microsystems (Salt Lake City, UT) recording system or at 32kHz on a Neuralynx (Tucson, AZ) recording system.

2.5.3. Spike sorting

Automated spike detection and sorting were performed using the WaveClus3 software package in Matlab [155]. We then manually reviewed each unit for inclusion by evaluating waveform shape, amplitude, and consistency, along with spike time auto-correlation, inter-spike intervals, and firing consistency across the session, and we rejected units that were likely contaminated by artifacts, in keeping with field-standard spike evaluation criteria [66, 74]. For electrodes with multiple units that passed this inclusion check, we merged units whose waveform features could not be well-separated in principle components space, retaining for analysis a combination of single- and multi-units. Spike sorting was performed by D.R.S., blinded to electrode recording region, and independently reviewed by I.F.

2.5.4. Task description

Subjects played a first-person, virtual navigation game called *Goldmine*, in which they explored an underground mine while alternating between searching for visible gold and then digging for this gold, now hidden from view, at remembered gold locations. Testing sessions lasted for approximately one hour, and they consisted of a short tutorial sequence followed by 36 experimental trials. Every trial consisted of four timed and two untimed events in the following sequence:

1. Delay₁ (10s): Subject waits in the mine base. Game controls are turned off, and the subject sees a static image of the center base door. This image is identical across delays, and the subject is in exactly the same location, facing the same direction, on every delay.
2. Gold Search (30s): A 1s beep denotes the start of the Gold Search event, during which the subject may freely search the mine for one or more golds that appear on the ground in randomized locations on every trial. Concurrent with the beep that signals the start of Gold Search, a 1s instruction message, centered onscreen, tells the subject how many golds there are to find. Game controls are also reactivated, and one of three doors (to the left, right, or center) opens to allow the subject to exit the base. If the left or right door opens, an arrow appears onscreen for 1s (overlapping with the instruction message) to indicate which way the subject should turn.
3. Return-to-base₁ (variable time): All gold vanishes, and a message onscreen instructs the subject to navigate back to the mine base. As soon as the subject re-enters the base, or if they were already in the base at the end of Gold Search, the screen goes black for 2s except for a message that instructs the subject to envision the route they will take during the upcoming Gold Dig event. Across all trials, the median duration for this event was 2s (the minimum duration), and the 75th percentile was 8.9s.
4. Delay₂ (10s): Subject waits in the mine base. As during Delay₁, game controls are

deactivated, and the subject sees a static image of the center base door. Delay₁ and Delay₂ are overtly identical events, differing only by their order within the trial sequence.

5. Gold Dig (30s): A 1s beep denotes the start of the Gold Dig event, during which the subject attempts to return to gold locations from the preceding Gold Search event and dig for gold, now hidden from view. Concurrent with the beep that signals the start of Gold Dig, a 1s instruction message, centered onscreen, tells the subject how many golds there are to dig (equal to the number of golds to find during Gold Search). Game controls are reactivated, and the same door that opened during Gold Search is reopened, allowing the subject to exit the base.
6. Return-to-base₂ (variable time): Digging is disabled, and a message onscreen instructs the subject to navigate back to the mine base. As soon as the subject reenters the base, or if they were already in the base at the end of Gold Dig, the screen goes black for 2s except for a message that instructs the subject to prepare for the upcoming Gold Search event. Across all trials, the median duration for this event was 2s (the minimum duration), and the 75th percentile was 7.4s.

After 36 trials, a “game over” screen appeared and showed subjects their final score, the number of golds successfully dug, and their digging accuracy. Subjects were aware of the 30s time limits during Gold Search and Gold Dig and of a “short waiting time” between each navigation event, but they were never explicitly instructed to attend to time during the experiment. Instead, they were told that their goal was to maximize their score by digging up as many golds as possible, as accurately as possible. They were also asked to remain focused, still, and silent throughout testing – including during delays – unless they needed to ask the experimenter a clarifying question. Voluntary breaks were programmed after 12 and 24 completed trials. Subjects were also taught to press a ‘manual pause’ button if they needed to pause the game for any reason during testing. We did not analyze trials with manual pauses (1.9% of all trials; min = 0, max = 3 per session).

The game was played from a first-person perspective, with the (invisible) avatar being $2m$ tall and moving forward at a constant $4m/s$. Subjects rotated their view by moving the mouse, moved forward by clicking and holding the left mouse button, and dug (during Gold Dig only) by pressing the spacebar. Releasing the left mouse button caused movement to immediately stop, although head rotation was still possible.

Subjects could retrieve one gold on each of the first two trials. Thereafter, the number of golds, n_{gold} , varied such that if a subject had successfully retrieved all golds on both of the last two trials, the next trial would have $n_{gold} + 1$ golds. However, if the subject failed to retrieve all golds on both of the last two trials, respectively, the next trial would have $\max(n_{gold} - 1, 1)$ golds. Otherwise, the number of golds stayed the same. Subjects received 10 points for each gold retrieved, with a correct dig occurring anywhere within $4m$ of the nearest gold. A crosshairs on the ground in front of the subject indicated where their digging was targeted. Each gold could be retrieved only once, and only golds from the most recent Gold Search event could be retrieved. Subjects were not required to move, or dig, if they did not elect to do so. There was no limit on how many digs could be attempted, but every incorrect dig subtracted 2 points from the overall score. The current score was always visible in the top-right corner of the screen, and current task instructions (how many golds to find or dig) were always visible in the top-left corner of the screen.

Before beginning the main experiment, subjects completed a 10min tutorial with 3 practice trials that taught them the game rules and controls and allowed them to practice moving through the virtual space. The tutorial occurred in a different environment than the one used during the main experiment, although trial events used the same timing (10s delay and 30s navigation events).

The virtual environment was designed to be moderately challenging for patients to learn, capable of being fully explored within 30s, and visually sparse so as to minimize behavioral confounds with time and place. The environment was $27m$ long \times $27m$ wide and featured $531m^2$ of traversable space, including $477m^2$ in the mine and $54m^2$ in the base. The envi-

ronment was vertically, horizontally, and diagonally symmetrical except for the base, which served as the sole orienting landmark. Tall rock walls surrounded the mine on all four sides, and inner rock walls were of uniform height ($4m$) and appearance. The floor of the mine was flat and evenly patterned. Each gold occupied $1m^2$ of space, and all golds were visually identical. Gold locations were selected by the computer at random at the start of every trial, with the only condition being that gold could not overlap with the base, any walls, or any already created golds.

Goldmine was programmed in Unity, with scripts written in C#. The paradigm ran on a Macbook Pro at 60 frames-per-second. A cord connected the laptop to a digital-analogue converter that sent patterned pulses to the recording system, for the purpose of later synchronizing electrophysiological and behavioral data.

2.5.5. Single-neuron responses to task variables

Delay events. For each neuron, we used ordinary least squares regression to fit the number spikes (unsmoothed) in 1s increments across the 36 Delay₁ and 36 Delay₂ events, as a function of time (10 discrete bins, each 1s in duration), delay-event (Delay₁ or Delay₂), and their interaction. We then calculated the likelihood ratio, LR , between this model and 3 reduced models that dropped the parameters for each main effect and interaction, respectively. For example, in the case of time, we compared the original model to a reduced model in which all time-bin parameters were removed while delay-event and time-bin \times delay-event parameters were retained. LR is calculated as:

$$LR = -2 \ln \frac{L(m_1)}{L(m_2)} \quad (2.1)$$

Where $L(m_1)$ is the likelihood of the reduced model, given the data, and $L(m_2)$ is the likelihood of the original model, given the data. A higher LR indicates that the reduced model fit the data increasingly worse than the fit obtained from the original model, and LR can therefore be interpreted as a measure of the extent to which a set of parameters (e.g.

time bins) improves dependent variable prediction (firing rate) over and above the variance explained by the remaining parameters (delay-event and time-bin \times delay-event).

Next, we generated a null distribution for each neuron by shuffling event labels (i.e. permuting Delay₁ and Delay₂ labels, without replacement) and circularly-shifting spike counts by a uniform, random integer between 0 and 9, independently across delays. This manipulation served to decouple cross-trial associations between the behavioral parameters and a neuron’s firing rate while preserving both the number of spikes in each time bin and the autocorrelation in firing rates over time. We repeated this process 1,000 times per neuron, recalculating *LRs* between full model and reduced model fits with each iteration. We then compared these null distribution *LRs* to those obtained from the real data, calculating an empirical *p*-value as $p = \frac{r+1}{n+1}$, where *r* is the number of null replicates with an *LR* greater than or equal to the real *LR*, and *n* is the total number of replicates [138]. We considered a neuron significant for a given main effect or interaction if $p < 0.05$. Finally, we used binomial tests to determine if the number of significant neurons exceeded the 5% Type 1 error rate, Bonferroni-Holm corrected for multiple comparisons across the 2 main effects and 1 interaction term of interest. The results from these models are described in the text and shown in Figure 2.2 and Table 2.S2.

Navigation events. The same procedure was used to analyze firing rate correlations with behavior during navigation as during delays, but with a different combination independent variables. Specifically, ordinary least squares regression was used to model the number of spikes (unsmoothed) in 500ms increments across the 36 Gold Search and 36 Gold Dig events, as a function of time (10 discrete bins, each 3s in duration), place (i.e. subjects’ current location within the 12 mine regions in Figure 2.S1), navigation-event (Gold Search or Gold Dig), and their first-order interactions (time \times delay-event, place \times delay-event, and time \times place). For each neuron, we calculated *LRs* between this model and 6 reduced models that dropped the parameters for each main effect and interaction term, in turn. Empirical *p*-values were obtained relative to null distributions that shuffled navigation event labels and

circularly-shifted spike count vectors at random within each navigation event, and neurons were considered significant for a given main effect or interaction if $p < 0.05$. Finally, we used binomial tests to determine if the number of significant neurons exceeded the 5% Type 1 error rate, Bonferroni-Holm corrected for multiple comparisons across the 3 main effects and 3 interaction terms of interest. The results from these models are described in the text and shown in Figure 2.3, Table 2.S2, and Figures 2.S7 and 2.S8.

We also tested models with additional covariates for virtual head direction (8 angles corresponding to North [the starting direction], Northeast, East, Southeast, South, Southwest, West, and Northwest), player movement (whether the in-game avatar was moving or rotating), base visibility (whether the base was currently visible from the player’s vantage), gold visibility (whether gold was currently visible from the player’s vantage; applied to Gold Search only), gold digging (whether the player had just performed a dig action; applied to Gold Dig only), head-direction \times navigation-event, player-movement \times navigation-event, and base-visibility \times navigation-event. Figure 2.S3 shows the mean correlations, across subjects, between all pairs of behavioral parameters.

2.5.6. Neural response differences by brain region

As electrode coverage and the number of recorded neurons per region varied between subjects, we used a permutation-based method that accounted for between-subject differences to analyze regional differences in the proportion of significantly-responding neurons to each behavioral variable of interest (see Table 2.S2). For each behavioral variable, we first performed a χ^2 independence test on the contingency table that listed the number of significantly-responding neurons by region, across all subjects. We then shuffled the neuron-to-region assignment at random within each subject and recalculated the χ^2 statistic 1,000 times to obtain a null distribution. Lastly, an empirical p -value was obtained that described the extent to which the proportion of significantly-responding neurons by region differed to a greater extent than was observed in the shuffled data [138]. As no p -value passed the significance threshold after adjusting for multiple comparisons, no post-hoc tests were performed.

We performed this analysis using 3 regions-of-interest: the hippocampus, surrounding medial temporal lobe (combining amygdala, entorhinal cortex, and parahippocampal gyrus/medial bank of the fusiform gyrus), and medial prefrontal cortex (combining orbitofrontal cortex, anterior cingulate, and supplementary motor area). We excluded from these analyses 46 neurons that were located in more sparsely-sampled neocortical regions due to insufficient sample size.

2.5.7. Classifying time from population neural activity

We used the scikit-learn library [146] to train multi-class, nonlinear (radial basis function) support vector machines to identify discrete, 2s time bins based on population neuron firing rates. We trained separate classifiers on Delay₁, Delay₂, Gold Search, and Gold Dig events, respectively (Figure 2.2, E to H, and Figure 2.S8), as well as training classifiers across all four of these events combined (Figure 2.4).

For each of these conditions, we used the following procedure: First, missing firing rates from the 1.9% of discarded trials (see Task description) were replaced using median imputation. Next, we z -scored firing rates across all time bins and trials in a given analysis, separately for each neuron. Lastly, we trained support vector machines using a nested cross-validation (CV) procedure that split data into train/test/validate folds at the trial level (5 inner folds, 36 outer folds). The inner CV served to identify optimal values for two hyperparameters of the radial basis function kernel: C , which determines the strength of parameter regularization; and γ , which determines the radius of influence for each support vector. For each inner fold, we tested 100 pairs of hyperparameter values, each chosen at random from a continuous, log-uniform distribution between $1e^{-9}$ and $1e^9$. The best-performing hyperparameter values were then used to retrain a classifier across the 35 train/validate trials and generate predictions on the held-out test trial. This procedure was repeated over each fold of the outer CV, yielding predictions for each time bin, for all 36 trials.

To evaluate classifier performance, we trained null classifiers that replicated the above procedure, but with time bins being circularly-shifted by a uniform, random integer between

0 and 1 minus the number of time bins, independently on every trial. Paired *t*-tests were used to compare mean prediction errors (absolute value of the difference between actual and classifier-predicted times) across trials for classifiers trained on actual versus circularly-shifted time bins.

Cross-event decoders used the same decoders that were trained separately on each trial event, as described above, but then predicted times from neural firing rates during a different event than the one that was used for training. The following cross-decoders were evaluated (train → test):

1. Delay: Delay₁ → Delay₂, Delay₂ → Delay₁
2. Navigation: Gold Search → Gold Dig, Gold Dig → Gold Search
3. Delay to navigation: Delay₁ → Gold Search, Delay₁ → Gold Dig, Delay₂ → Gold Search, Delay₂ → Gold Dig. As the event durations differed, we tested three mappings for each of these combinations: First 10s of navigation, last 10s of navigation, and relative time as a percentage of event duration.

2.5.8. Code dependencies

Neural firing and behavioral data were analyzed using Python version 3.9.7 and JupyterLab version 3.1.745 [101], along with the following, open source Python packages: Matplotlib (version 3.0.3) [85], NumPy (version 1.19.1) [65], pandas (version 1.1.5) [121], SciPy (1.5.2) [201], seaborn (version 0.11.1) [202], Scikit-learn (version 0.23.2) [146], and Statsmodels (version 0.12.1) [173].

2.5.9. Data availability

All subject de-identified data are freely available for use upon request to the corresponding authors. Python code and JupyterLab notebooks used for all data preprocessing and analyses can be downloaded at https://github.com/dschonhaut/time_cells.

2.6. Supplementary Material

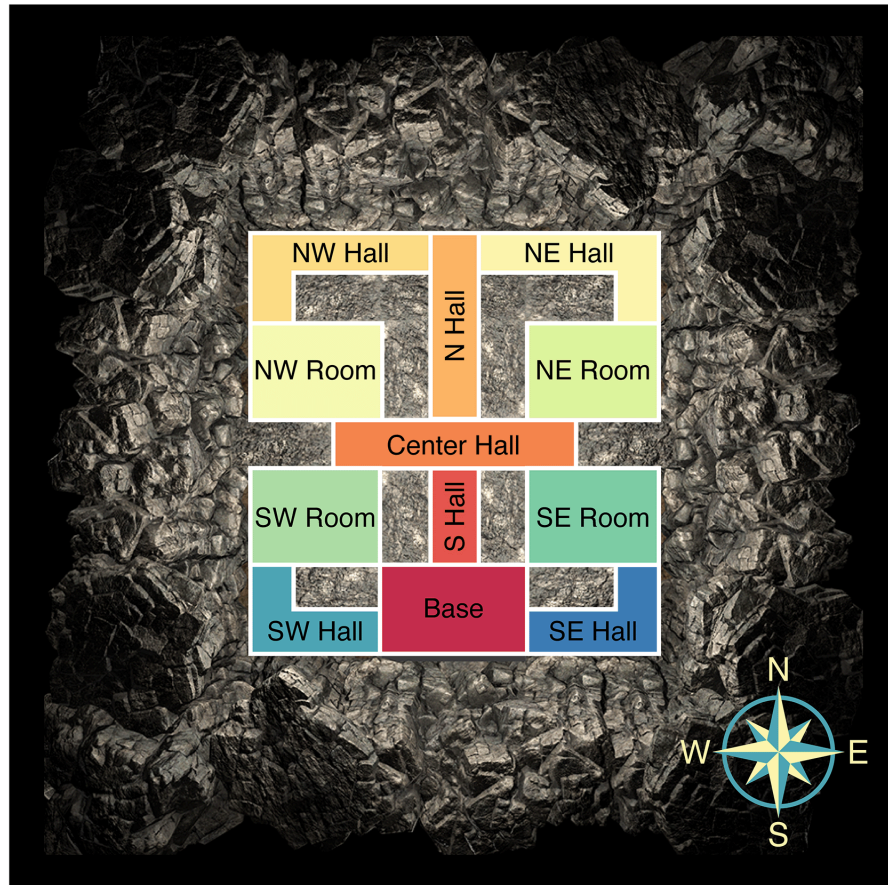


Figure 2.S1: Mine regions. Overhead map of the 12 mine regions that were used in regression models fit to each neuron's firing rate during Gold Search and Gold Dig events.

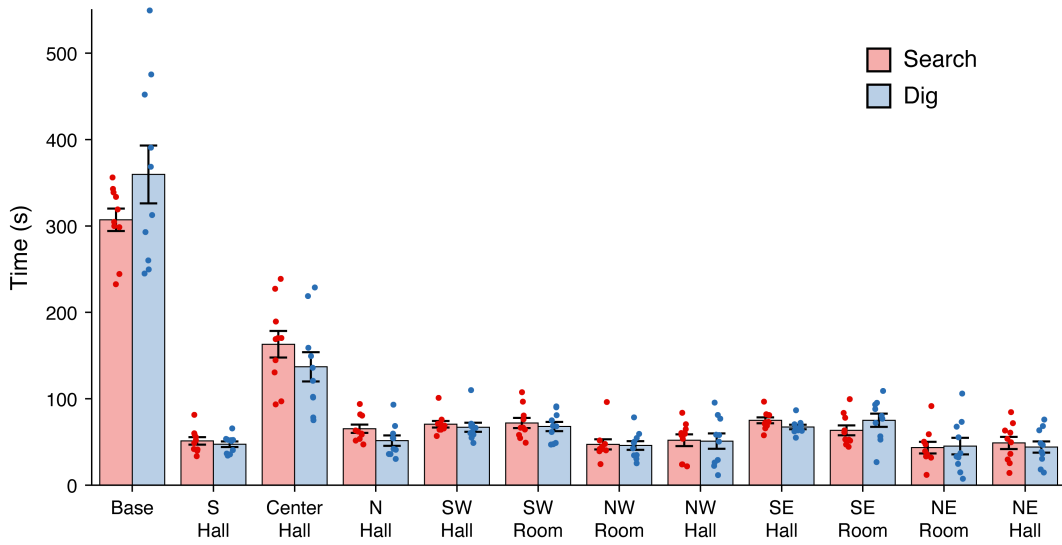


Figure 2.S2: Time spent in each mine region. Bar graph shows how much time subjects spent in each mine region during Gold Search (red, left bars) and Gold Dig (blue, right bars). Bars and error bars show the mean and standard error across subjects, respectively, and overlaid points correspond to individual subjects.

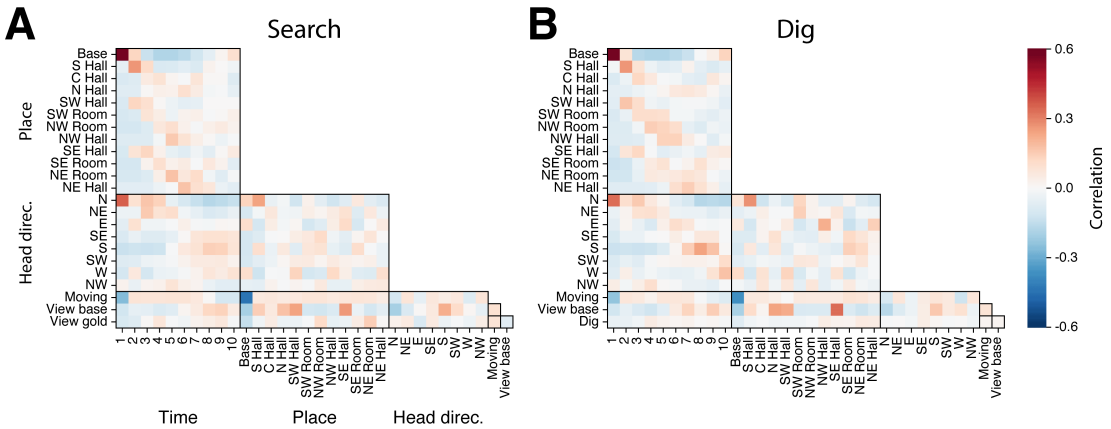


Figure 2.S3: Behavioral parameter correlations. Colormap values show the mean Pearson correlations, across subjects, between each pair of behavioral parameters during Gold Search (**A**) and Gold Dig (**B**). Each time bin corresponds to a 3s duration.

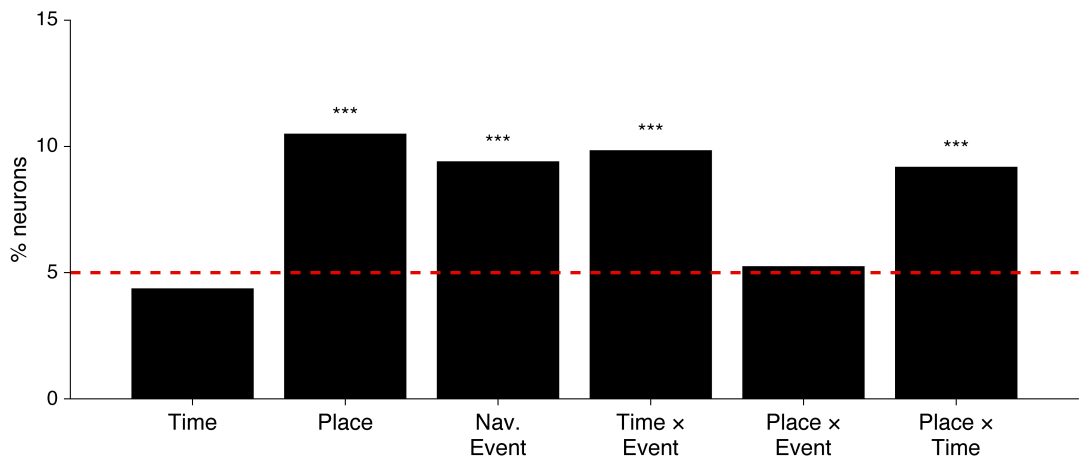


Figure 2.S4: Single-neuron response rates under alternative model specification. Percent of neurons that responded significantly to each main effect and interaction (red line: Type 1 error rate) when adding covariates for head direction, movement, visible objects and landmarks, and dig times. *** $p < 0.0001$, binomial test with Bonferroni-Holm correction. Compare to Figure 2.3C.

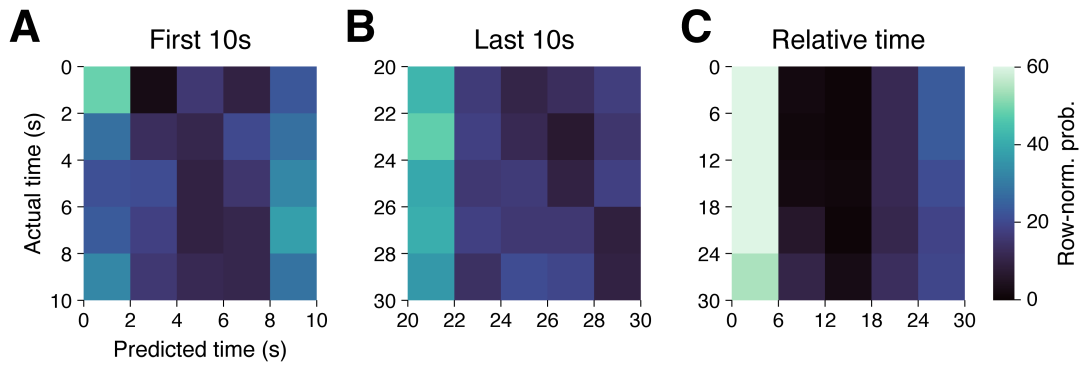


Figure 2.S5: Delay-to-navigation time decoding. Figure panels show confusion matrices for classifiers that were trained to decode time from all neuron firing rates during delay events, then used to predict time during the first 10s (**A**), last 10s (**B**), and time relative to event duration (**C**) during navigation. Matrix rows sum to 1, with each value indicating the mean probability across held-out test trials.

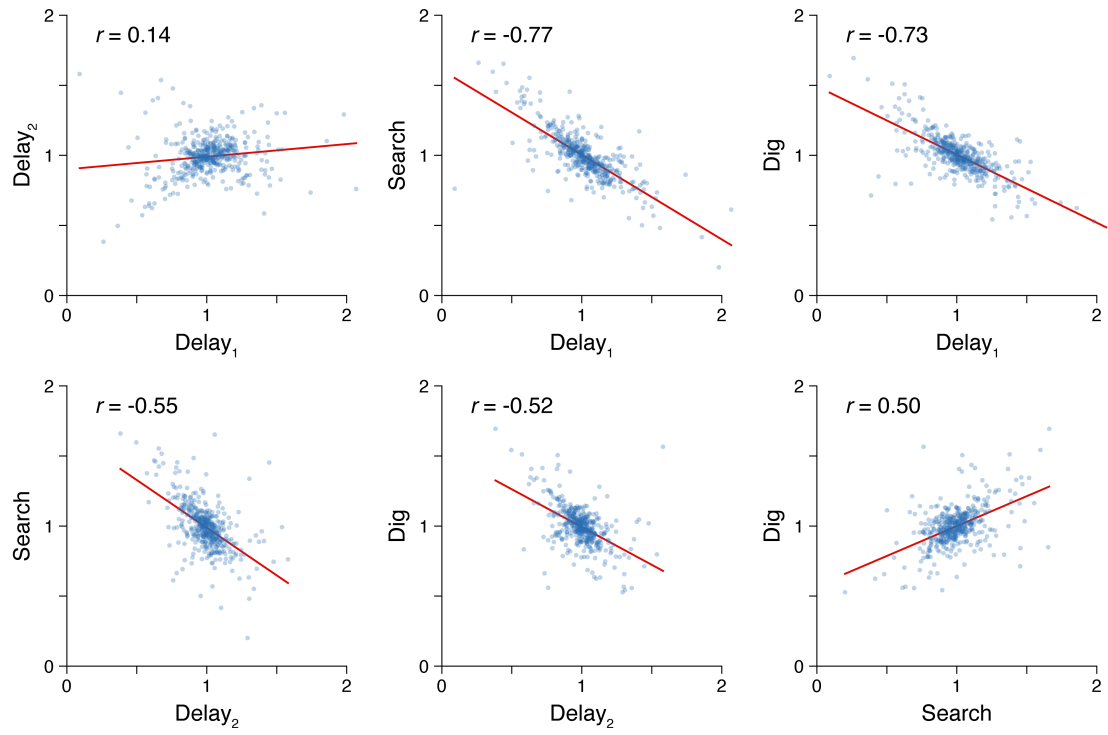


Figure 2.S6: Firing rate correlations between trial event pairs. Figure panels show Pearson correlations between normalized firing rates in each pair of trial events, across all neurons in the study (each dot = one neuron). Each neuron's firing rate was calculated across time bins and trials within each delay and navigation event, respectively, then normalized by dividing each event's mean firing rate by the grand average firing rate across the four events.

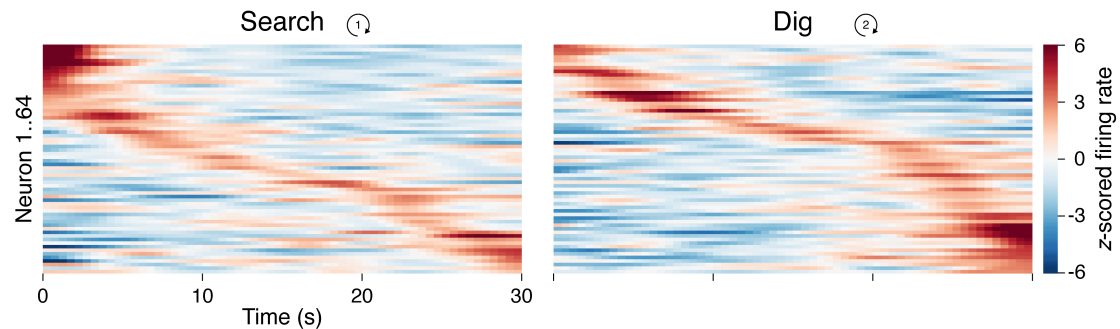


Figure 2.S7: Firing rates over time for all time \times navigation-event cells.
 Heatmaps depict z -scored firing rates across the 30s navigation events, averaged across trials, for all time \times navigation-event-specific neurons (each row = one neuron), sorted separately by the time of maximum z -scored firing during Gold Search (left) and Gold Dig (right).

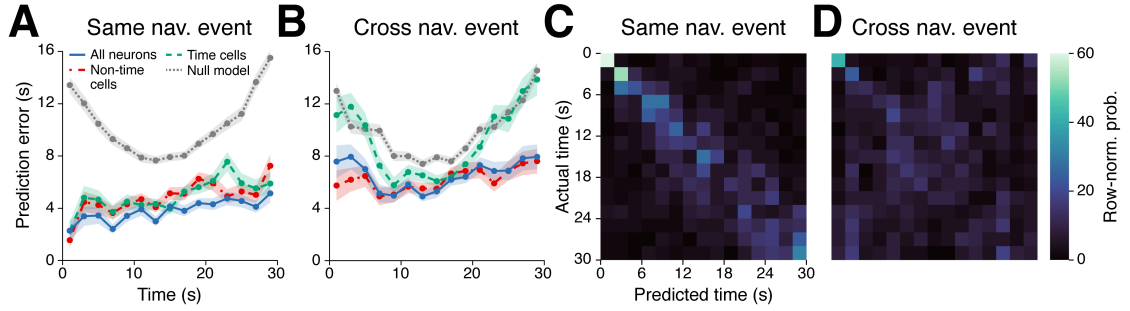


Figure 2.S8: Classifying time during navigation from population neural firing.

(A) Mean \pm SEM prediction errors, across trials, for classifiers that were trained and tested on the same navigation event (e.g. both Gold Search) to decode time from firing rates of all neurons (solid, blue line), the 119 neurons that responded to time as a main effect or interaction with other variables (dashed, green line), 338 neurons that did not respond significantly to time (dash-dot, red line), and chance-level results from null model classifiers (dotted, gray line). (B) Same as in (A), but for classifiers that were trained and tested on different navigation events (e.g. Gold Search \rightarrow Gold Dig). (C and D) Confusion matrices for same navigation event (C) and cross-event (D) time cell classifiers.

Subject	HPC	AMY	EC	PHG/FSG	HSG	mOCC	mPFC	Other	Sum
1**	19	6	5	23	0	13	0	0	66
2	5	0	0	19	0	0	0	0	24
3	11	5	1	0	0	0	1	7	25
4	9	6	10	0	0	0	8	0	33
5**	11	19	42	0	21	0	7	2	102
6	0	25	24	15	0	0	1	0	65
7	9	13	15	9	0	0	27	0	73
8	3	9	0	0	0	0	1	0	13
9	4	6	3	0	0	0	0	0	13
10	14	3	0	8	0	0	15	3	43
Sum	85	92	100	74	21	13	60	12	457

Table 2.S1: Neurons by subject and region. Number of neurons (single- and multi-units) recorded from each subject, in each region. HPC = hippocampus; AMY = amygdala; EC = entorhinal cortex; PHG/FSG = parahippocampal gyrus/medial bank of the fusiform gyrus; HSG = Heschl's gyrus; mOCC = medial occipital cortex; mPFC = medial prefrontal cortex (including medial orbitofrontal, anterior cingulate, and pre-supplementary motor area). Subjects are listed in the order tested. * Sample from one patient. ** Subjects with two sessions of data.

Trial events	Behav. variable	HPC	AMY	EC	PHG/FSG	HSG*	mOCC*	mPFC	Other
Delay ₁ , Delay ₂	Time	10 (12%)	22 (24%)	21 (21%)	22 (30%)	4 (19%)	5 (38%)	13 (22%)	2 (17%)
Delay ₁ , Delay ₂	Delay-event	11 (13%)	15 (16%)	25 (25%)	9 (12%)	0 (0%)	2 (15%)	6 (10%)	2 (17%)
Delay ₁ , Delay ₂	Time × Delay-event	4 (5%)	7 (8%)	4 (4%)	1 (1%)	3 (14%)	2 (15%)	5 (8%)	0 (0%)
Search, Dig	Time	2 (2%)	4 (4%)	4 (4%)	8 (11%)	0 (0%)	2 (15%)	2 (3%)	1 (8%)
Search, Dig	Place	7 (8%)	6 (7%)	15 (15%)	16 (22%)	1 (5%)	3 (23%)	11 (18%)	1 (8%)
Search, Dig	Navigation-event	8 (9%)	13 (14%)	12 (12%)	12 (16%)	1 (5%)	2 (15%)	10 (17%)	1 (8%)
Search, Dig	Time × Nav.-event	9 (11%)	10 (11%)	22 (22%)	8 (11%)	0 (0%)	2 (15%)	12 (20%)	1 (8%)
Search, Dig	Place × Nav.-event	4 (5%)	3 (3%)	6 (6%)	4 (5%)	1 (5%)	0 (0%)	6 (10%)	1 (8%)
Search, Dig	Place × Time	5 (6%)	8 (9%)	8 (8%)	8 (11%)	6 (29%)	4 (31%)	4 (7%)	0 (0%)

Table 2.S2: Neuron responses by region. Number and percentage of neurons in each region, across subjects, with significant responses to each behavioral variable. * Sample from one patient.

CHAPTER 3

MTL NEURONS PHASE-LOCK TO HUMAN HIPPOCAMPAL THETA

This chapter has been adapted from Schonhaut DR, Ramayya AG, Solomon EA, Herweg NA, Fried I, Kahana MJ (2022) MTL neurons phase-lock to human hippocampal theta. *bioRxiv*, 2022. doi: <https://doi.org/10.1101/2022.12.19.521101>

3.1. Abstract

Memory formation depends on neural activity across a network of regions, including the hippocampus and broader medial temporal lobe (MTL). Interactions between these regions have been studied indirectly using functional MRI, but the bases for inter-regional communication at a cellular level remain poorly understood. Here we evaluate the hypothesis that oscillatory currents in the hippocampus synchronize the firing of neurons both within and outside the hippocampus. We recorded extracellular spikes from 1,854 single- and multi-units simultaneously with hippocampal local field potentials (LFPs) in 28 neurosurgical patients who completed virtual navigation experiments. A majority of hippocampal neurons phase-locked to oscillations in the slow (2-4Hz) or fast (6-10Hz) theta bands, with a significant subset exhibiting nested slow theta \times beta frequency (13-20Hz) phase-locking. Outside of the hippocampus, phase-locking to hippocampal oscillations occurred only at theta frequencies and primarily among neurons in the entorhinal cortex and amygdala. Extrahippocampal neurons phase-locked to hippocampal theta even when theta did not appear locally. These results indicate that spike-time synchronization with hippocampal theta is a defining feature of neuronal activity in the hippocampus and structurally-connected MTL regions. Theta phase-locking could mediate flexible communication with the hippocampus to influence the content and quality of memories.

3.2. Introduction

The hippocampus is the operational hub of a spatially distributed episodic memory system that enables us to remember past experiences in rich detail, together with the space and time that they occurred [39, 131]. To serve in this capacity, the hippocampus must maintain precise but flexible connections with the rest of the memory system. Understanding the mechanisms that govern inter-regional connections among regions supporting episodic memory is a major concern of systems neuroscience, and progress in this area could accelerate efforts to develop treatments for memory disorders and age-related memory decline.

A leading hypothesis is that theta (2-10Hz) oscillations within the hippocampus facilitate interactions between the hippocampus and other brain regions [22, 49, 131]. Hippocampal neurons are more receptive to synaptic excitation at specific theta phases [99], so well-timed inputs can more effectively drive activity than inputs at random phases [58]. Long-term potentiation and long-term depression in the rodent hippocampus are also theta phase-dependent [83, 86, 145], providing a putative link between the phase at which inputs arrive and how strongly they are encoded. Experimental evidence for this hypothesis comes largely from studies in the rat medial prefrontal cortex (mPFC), a downstream target of hippocampal area CA1. mPFC neurons phase-lock to hippocampal theta during short-term memory tasks [87, 175, 178], and stronger phase-locking predicts better performance [9, 60, 88, 96] and greater information transfer between mPFC and hippocampal neurons [90, 141]. Phase-locking to hippocampal theta is also prevalent among cells in many other regions, including the entorhinal cortex (EC), amygdala, parietal cortex, thalamic nucleus reuniens, and some subcortical and brainstem nuclei [11, 52, 60, 90, 102, 178]. Theta phase-synchronization could thus be a general mechanism for relaying information between the hippocampus and a broad network of memory-related regions.

In humans, macroelectrode local field potential (LFP) recordings in epilepsy patients have revealed sporadically-occurring theta oscillations in the hippocampus and cortex during spatial navigation and episodic memory engagement [1, 43, 107, 183, 200, 203, 204, 213]. Studies

relating theta power to memory have produced equivocal results [71], but macroscale theta phase-synchronization within the medial temporal lobe (MTL) and PFC has consistently correlated with better memory performance [6, 105, 180, 206, 214]. Considerably less is known about how oscillations relate to neuronal firing in humans than in rodents. An early study in epilepsy patients found that a large percentage of MTL and neocortical neurons phase-locked to theta (among other frequency) oscillations in their local vicinity as subjects navigated through a virtual environment [91], and another study discovered MTL neurons phase-locked more strongly to locally-recorded theta oscillations while subjects viewed images that they later recognized than those that they forgot [165]. These findings indicate that neural activity within the human episodic memory system is organized in part by a theta phase code. However, oscillatory phase coding of neuronal responses outside the hippocampus have not been well studied in humans, and the hypothesis that hippocampal theta facilitates inter-regional communication lacks empirical validation. To address this question, we leveraged the rare opportunity to record single- and multi-neuron activity simultaneously with LFP oscillations in multiple brain regions, including the hippocampus, in 28 neurosurgical patients implanted with intracranial electrodes.

3.3. Results

Subjects were implanted with depth electrodes in the hippocampus, EC, amygdala, parahippocampal gyrus (PHG), superior temporal gyrus (STG), orbitofrontal cortex (OFC), and anterior cingulate cortex (ACC). Using microwires that extended from the tips of these depth probes, we recorded extracellular spikes from 1,854 single- and multi-units (hereafter called ‘neurons’; Table 3.1) as subjects navigated through a virtual environment while completing one of several spatial memory tasks whose data we pooled for this analysis (see Methods). In total, we identified 10-71 (median=30.0) neurons per session across 55 recording sessions, and the firing rates of these neurons were log-normally distributed (median=2.0Hz). In addition, every subject had at least one microwire bundle implanted in the hippocampus, permitting neuronal firing to be analyzed simultaneously with oscillatory activity in the hippocampal LFP.

Region	Subjects	Neurons	Firing rate (Hz)
Hippocampus	27	391	1.6 (0.6, 4.7)
Entorhinal cortex	19	341	2.3 (1.0, 5.5)
Amygdala	23	439	1.5 (0.6, 3.7)
Parahippocampal gyrus	15	217	2.2 (0.8, 4.5)
Superior temporal gyrus	5	139	3.4 (1.4, 8.6)
Orbitofrontal cortex	15	193	2.0 (0.9, 4.9)
Anterior cingulate cortex	8	134	3.1 (1.4, 6.8)
Total	28	1,854	2.0 (0.8, 5.0)

Table 3.1: Neurons by region. Table shows how many subjects had 1+ neurons in each brain region, how many neurons were recorded in each region, and the median, lower, and upper quartile firing rates for these neurons.

3.3.1. Identifying oscillations in hippocampal microwire LFPs

Existing studies that reported oscillatory properties of the human hippocampus during navigation have primarily utilized implanted macroelectrodes that integrate activity over hundreds of thousands of neurons [1, 43, 200, 203, 204]. As microwires used in the present study record at far smaller spatial scales, we first considered whether comparable oscillatory properties are observed in microwires as in macroelectrode LFPs. We focused on 1-30Hz signals for this analysis, avoiding higher frequencies at which spike-related artifacts can complicate LFP interpretation [23, 115, 160]. Many individual electrodes showed peaks in spectral power that rose above the background 1/f line in session-averaged LFP spectrograms (Figure 3.1A), indicating the potential presence of oscillatory activity [34]. The frequency and magnitude of these spectral peaks varied considerably across subjects (compare Figure 3.1A subpanels) yet were nearly exclusively observed between 2-20Hz.

To determine if spectral peaks were associated with sustained oscillations versus asynchronous, high-amplitude events, we used the BOSC (Better OSCillation) detection method to identify time-resolved oscillatory ‘bouts’ in each hippocampal microwire recording [207]. Briefly, BOSC (alternatively called ‘P-episode’) defines an oscillatory bout according to two threshold criteria, such that spectral power at a given frequency must exceed: (1) a statistically-defined amplitude above the 1/f spectrum, for (2) a minimum defined duration

(we used 3 cycles; see Methods for more details). Figure 3.1B shows an example hippocampal LFP in which an initially aperiodic, ‘1/f-like’ signal transitioned into a strong, 6Hz oscillation that persisted for 6 cycles, with the BOSC-defined oscillatory bout highlighted in pink.

Across subjects, hippocampal oscillatory bouts were present between ~1-6% of the time at the examined frequencies (Figure 3.1C; Figure 3.S1 shows oscillatory prevalence in other regions for comparison). The prevalence of these oscillations was not uniform across frequencies, but instead clustered around three, well-separated bands with peaks at 3Hz, 7Hz, and 15Hz, respectively. These frequencies are consistent with the hippocampal slow theta (alternatively ‘delta’; 2-4Hz), fast theta (6-10Hz), and beta band rhythms (13-20Hz) previously described in macroelectrode recordings, and the prevalence of oscillatory bouts in our data was comparable to these earlier studies [43, 63, 107, 204]. Oscillatory prevalence varied between these frequency bands ($\chi^2(2) = 13.9$, $p < 0.0001$, likelihood ratio test between linear mixed-effects models testing frequency band as a fixed effect and holding subject as a random effect), such that slow theta appeared more prevalent than fast theta ($z = 2.4$, $p = 0.0336$, post-hoc pairwise z -tests, Bonferroni-Holm corrected for multiple comparisons) or beta ($z = 3.9$, $p = 0.0002$). Fast theta and beta oscillations occurred at similar rates ($z = 1.5$, $p = 0.1218$). These findings indicate that the human hippocampus exhibits several distinct, low frequency oscillations that are conserved across spatial scales spanning several orders of magnitude, from microwire to macroelectrode fields. Moreover, theta oscillations are the predominant oscillatory component of the hippocampal LFP during virtual navigation.

3.3.2. Individual neuron phase-locking to hippocampal oscillations

Having confirmed the presence of hippocampal theta and beta oscillations, we next asked how these oscillations interacted with the timing of neuronal firing throughout recorded regions (Table 3.1). We quantified the phase-locking strength of individual neurons to ipsilateral hippocampal oscillations at a range of frequencies from 1-30Hz. A neuron’s phase-locking

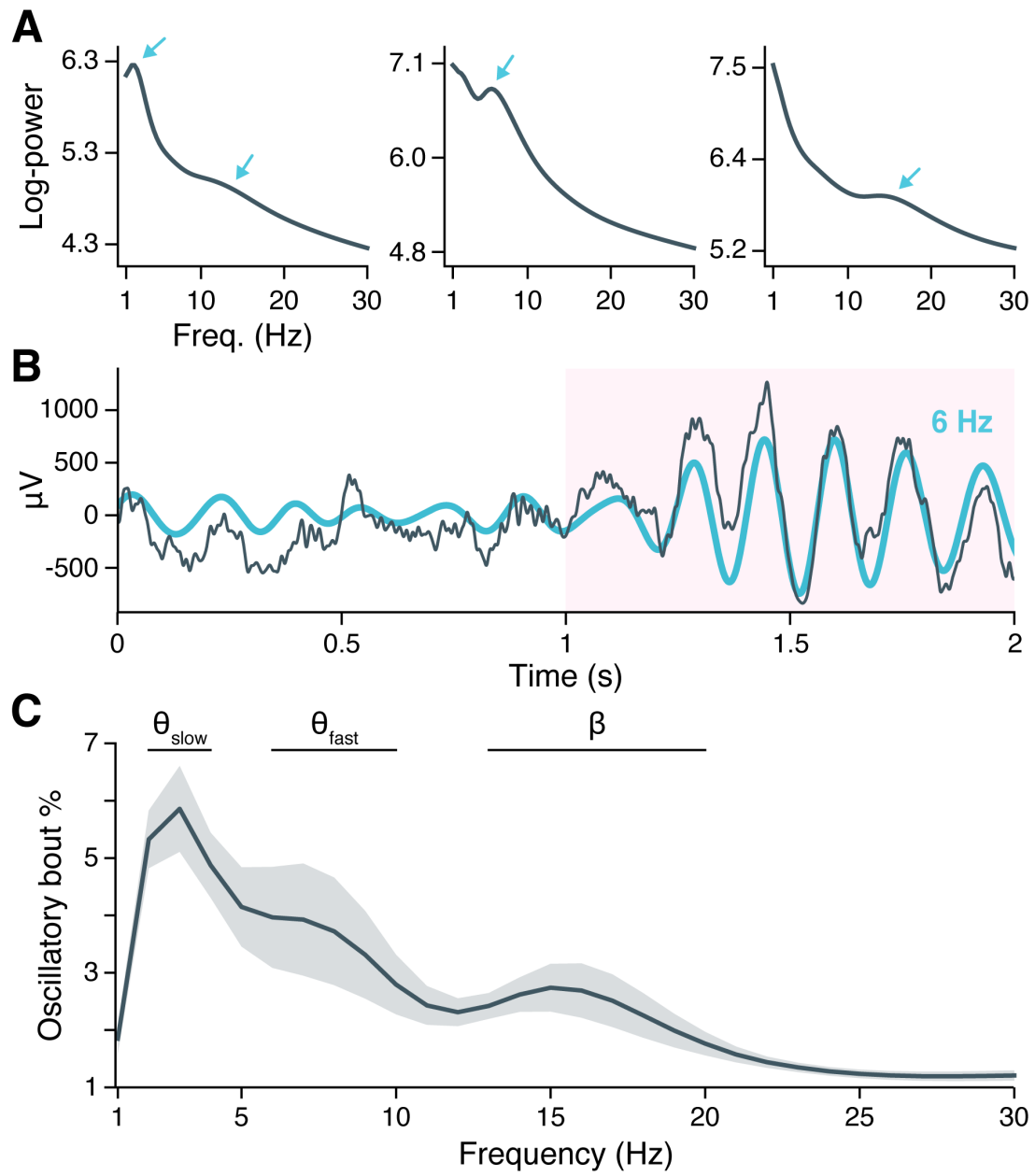


Figure 3.1: Neural oscillations in the hippocampus. (A) Spectral power across the recording session is shown for hippocampal LFPs from three example subjects. Arrows indicate spectral peaks above the background $1/f$ spectrum. (B) A hippocampal LFP trace (gray line = raw LFP, cyan line = 6Hz filtered LFP) is shown immediately before and during a BOSC-detected theta oscillation, highlighted in pink. (C) Mean \pm SEM percent time, across subjects, that BOSC-detected oscillations were present in hippocampal LFPs at each frequency from 1-30Hz.

strength was defined as the mean resultant length (MRL) of hippocampal LFP phases across spike times at a given frequency, z -scored against a null distribution of MRLs obtained by circularly-shifting the neuron's spike train 10,000 times at random (see Methods). To control for the possibility that some neurons might phase-lock to asynchronous events in the hippocampal LFP, such as sharp waves or interictal discharges [162, 179], we restricted our analysis to spikes that coincided with BOSC-detected oscillatory bouts at each frequency, excluding 11% of neurons for which the number of included spikes was insufficient to accurately gauge phase-locking (see Methods).

Figure 3.2A illustrates the phase-locking of an EC neuron whose spikes appear in raster format above a simultaneously-recorded, 3s hippocampal LFP trace exhibiting slow theta rhythmicity. The neuron fired in bursts of 2-8 spikes on a majority of theta cycles, with each burst generally aligned with the theta cycle peak, while nearly no spikes occurred near the theta trough. Next, we examined the population phase-locking statistics for this neuron across the recording session (Figure 3.2C). Computing the mean hippocampal LFP trace surrounding each spike (the 'spike-triggered average LFP'), we confirmed that the neuron preferentially fired just after the theta peak, with synchronous theta oscillations extending more than a full cycle before and after spike onset (Figure 3.2C, left subpanel, blue line). As a control, we also examined a spike-triggered average LFP drawn at random from the null distribution, which showed a nearly flat line consistent with absent phase-locking (Figure 3.2C, left subpanel, gray line). Graphing this neuron's phase-locking strength at frequencies from 1-30Hz revealed that phase-locking to hippocampal oscillations occurred only in the slow theta band, peaking at 3Hz (Figure 3.2C, middle subpanel). Finally, the circular histogram of spike-coincident, 3Hz hippocampal LFP phases showed that most spikes occurred within a quarter-cycle after the theta peak (Figure 3.2C, right subpanel). Figure 3.2B and D-J applies this analysis to representative neurons in the hippocampus, EC, amygdala, and OFC that phase-locked to LFP oscillations in the hippocampus. Most neurons exhibited unimodal peaks in phase-locking strength, most commonly in the theta range.

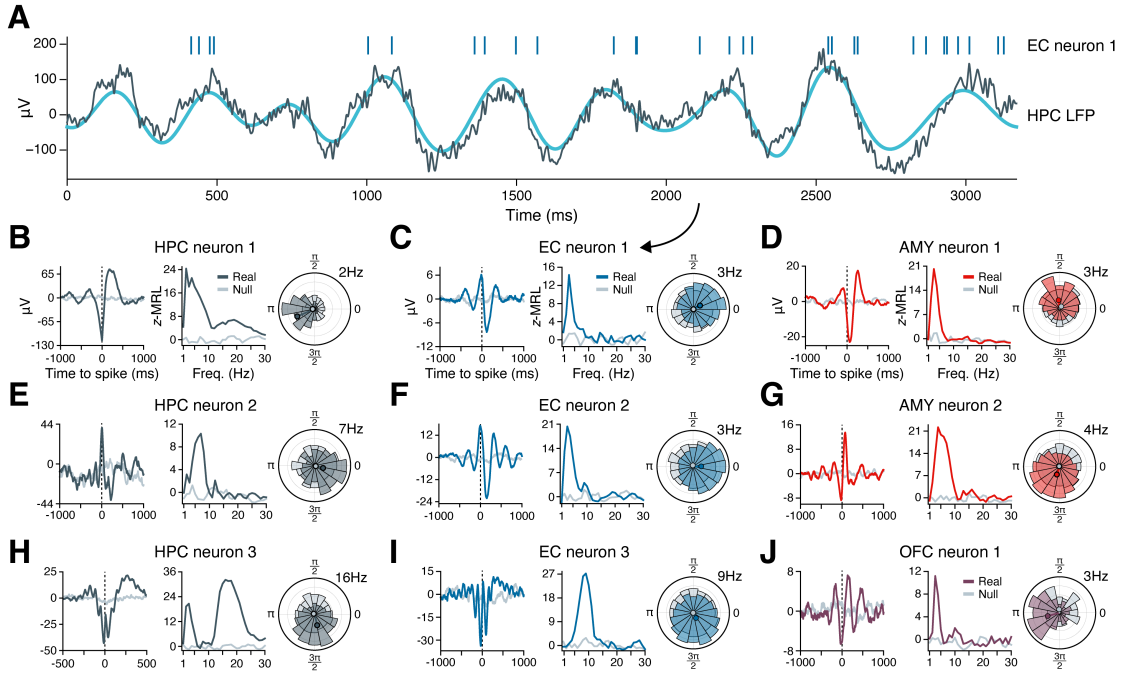


Figure 3.2: Example phase-locking to hippocampal oscillations. (A) Spikes from an EC neuron (top, vertical lines) are shown alongside LFP activity in the hippocampus during a slow theta oscillation (gray line = raw LFP, cyan line = 3Hz filtered LFP). Panel (C) shows phase-locking statistics for this neuron across the recording session. (B-J) Shown are nine neurons in the HPC (left column), EC (middle column), AMY (right column, top two rows), and OFC (right column, bottom row) that phase-locked to oscillatory signals in the hippocampus while subjects navigated through a virtual environment. The left subpanel for each neuron shows the mean hippocampal LFP centered on the time of each spike. The middle subpanel shows the phase-locking strength at each frequency relative to a null distribution of circularly-shifted spikes. The right subpanel shows the spike-phase distribution at the maximum phase-locking frequency. Dark gray (HPC), blue (EC), red (AMY) and purple (OFC) lines correspond to true spike times, while light gray lines correspond to circularly-shifted spike times from a single draw from the null distribution. HPC = hippocampus; EC = entorhinal cortex; AMY = amygdala; OFC = orbitofrontal cortex.

3.3.3. Regional differences in hippocampal phase-locking

We next examined phase-locking at the population level, first considering the percentage of neurons in each region that significantly phase-locked to ipsilateral hippocampal LFP oscillations, irrespective of frequency. For each neuron, we derived an empirical phase-locking *p*-value by comparing the neuron's maximum phase-locking strength, across frequencies, to its null distribution of maximum phase-locking strengths (see Methods). We then applied false discovery rate (FDR) correction at $\alpha = 0.05$ to the distribution of *p*-values within each region. Finally, for each region outside the hippocampus, we performed the same analyses and statistical corrections with respect to LFP oscillations in each neuron's local region (proximal to the electrode where a neuron was recorded). This last step allowed us to directly compare phase-locking rates to local versus remote hippocampal influences.

Figure 3.3A illustrates these analyses. As expected, neurons within the hippocampus phase-locked to hippocampal oscillations at the highest rate among recorded regions, with 59% of hippocampal neurons being significantly phase-locked after FDR-correction. High phase-locking rates to the hippocampus were also found for neurons in the EC (41%) and amygdala (29%), with phase-locking rates in the EC being significantly higher than those in the amygdala ($z = 3.6$, $p = 0.0004$, post-hoc pairwise *z*-test from a logistic mixed-effects model testing neuron region as a fixed effect and holding subject as a random effect). Whereas amygdala neurons phase-locked to local oscillations at significantly higher rates (46%) than to oscillations in the hippocampus ($\chi^2(1) = 32.6$, $p < 0.0001$), neurons in the EC phase-locked to local (40%) and hippocampal oscillations at indistinguishable rates ($\chi^2(1) = 0.2$, $p = 0.6672$) (likelihood ratio tests between logistic mixed-effects models testing oscillation region as a fixed effect and holding subject as a random effect).

These results stood in stark contrast to all remaining regions, where phase-locking to the hippocampus occurred at rates below 5%. Phase-locking to local oscillations was nonetheless prevalent in the PHG (24%) and STG (49%), indicating that many of these neurons were rhythmically entrained, just not by oscillations in the hippocampus. In two regions of the

prefrontal cortex, local phase-locking rates were relatively low (16% of OFC neurons and 6% of ACC neurons) although still significantly higher than phase-locking rates to the hippocampus (OFC: $\chi^2(1) = 20.9$, $p < 0.0001$; ACC: $\chi^2(1) = 5.6$, $p = 0.0178$; likelihood ratio tests between logistic mixed-effects models, as above). Altogether, these results highlight a triad of regions in the hippocampus, EC, and amygdala with strong spike-time synchronization to hippocampal oscillations, while neurons in more remote, cortical regions known to interact with hippocampal-dependent processes [39, 159, 182] were minimally entrained by hippocampal rhythms.

3.3.4. Frequencies of hippocampal phase-locking

Individual neuron examples suggested that phase-locking to the hippocampus occurred most commonly at theta frequencies (Figure 3.2), although our analysis of hippocampal LFPs revealed oscillations extending up to ~ 20 Hz (Figure 3.1). Does this observation of preferential theta phase-locking hold at the population level, and does the frequency of hippocampal phase-locking vary by a neuron's region-of-origin? To answer these questions, we generated heatmaps of phase-locking strength by frequency for all neurons that phase-locked significantly to hippocampal oscillations at *any* frequency, as defined in the previous section (Figure 3.3B; these neurons correspond to the dark gray bars in Figure 3.3A). We made separate heatmaps for neurons in the hippocampus, EC, amygdala, and remaining regions, respectively, sorting the neurons in each region by frequency of maximum phase-locking strength. Figure 3.S2 shows analogous heatmaps for neurons in each region with respect to local, rather than hippocampal, oscillations (matching the light gray bars in Figure 3.3A).

In the hippocampus, neurons phase-locked to local oscillations predominately between 2-20Hz. Only a few neurons phase-locked weakly at higher frequencies, which may be largely attributable to false discoveries (Figure 3.3B, far-left subpanel). Within the 2-20Hz range, phase-locking was not unimodal, but instead clustered around three distinct peaks in the slow theta, fast theta, and beta bands. Most hippocampal neurons phase-locked to only a single band, with the exception of neurons that phase-locked maximally to beta oscillations, which

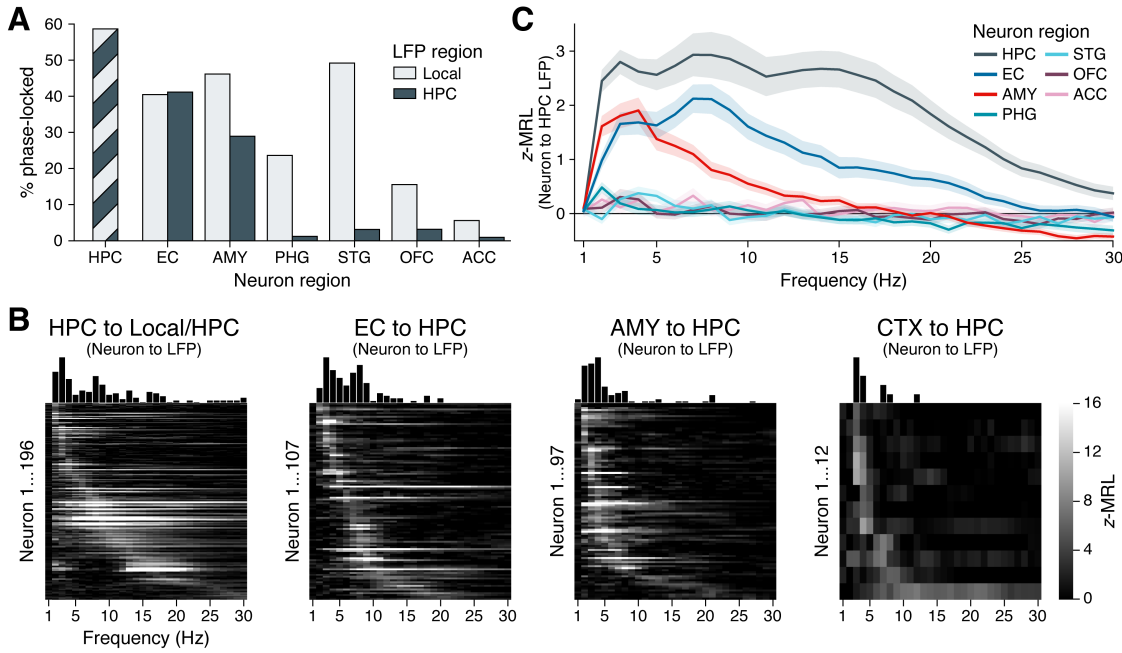


Figure 3.3: Phase-locking to hippocampal oscillations by region and frequency.

(A) Bars show the percentage of neurons in each region that phase-locked to locally-recorded LFP oscillations (light gray) and hippocampal LFP oscillations (dark gray). (Note that local and hippocampal LFP is identical for hippocampal neurons.) Phase-locking significance was set at FDR-corrected $p < 0.05$ within each bar group. (B) Heatmaps show the phase-locking strength (z -MRL; color scale intensity) by hippocampal LFP oscillation frequency (x-axis) for all significantly phase-locked neurons (y-axis; each row = one neuron) in the HPC, EC, AMY, and remaining regions (CTX), respectively. Neurons in each region are sorted from top to bottom by frequency of maximum phase-locking strength. Neurons depicted match the dark gray bars in (A). (C) Mean \pm SEM phase-locking strength by hippocampal oscillation frequency is shown for all neurons in each region, regardless of their individual phase-locking significance as depicted in (A) and (B). HPC = hippocampus; EC = entorhinal cortex; AMY = amygdala; PHG = parahippocampal gyrus; STG = superior temporal gyrus; OFC = orbitofrontal cortex; ACC = anterior cingulate cortex.

also showed a near-universal tendency to phase-lock strongly to slow theta (see for example Figure 3.2H). These neurons may best be classified as nested slow theta \times beta phase-locking neurons, which to our knowledge have not previously been reported. In contrast, we did not observe nested phase-locking between fast theta and beta oscillations or between any other pair of frequency bands.

Among neurons outside the hippocampus, phase-locking to hippocampal oscillations occurred within a more constrained frequency range, between 2-10Hz (Figure 3.3B, left three subpanels). In the EC, similar numbers of neurons showed preferential phase-locking to slow and fast hippocampal theta, respectively. In the amygdala and remaining cortical regions, this balance shifted: only a few neurons phase-locked to fast hippocampal theta, while most neurons were entrained exclusively by slow theta. Thus, while hippocampal neurons phase-locked to both theta and beta bands, for neurons outside the hippocampus, spike-time synchronization with hippocampal oscillations was restricted to theta frequencies.

We confirmed these conclusions in a secondary analysis that examined the mean phase-locking strength at each frequency across all neurons in each region, regardless of individual phase-locking significance (Figure 3.3C). This approach benefited from not requiring an explicit significance threshold to be defined. Instead, we assumed that if the neurons in a given region *did not* phase-lock measurably to the hippocampus, then the mean phase-locking strength across these neurons would approach zero (no difference versus the null distribution) at increasing sample size. Indeed, population phase-locking strengths were close to zero across frequencies for neurons in the PHG, STG, OFC, and ACC, consistent with the relative absence of individually phase-locked neurons in these regions. In contrast, neurons in the EC and amygdala both showed strong phase-locking to slow hippocampal theta frequencies, while EC but not amygdala neurons exhibited a secondary rise in phase-locking strength to fast hippocampal theta. Finally, neurons in the hippocampus showed stronger phase-locking to hippocampal oscillations at all frequencies than neurons in any other region, with peaks in phase-locking strength at all three (slow theta, fast theta, and

beta) oscillatory bands.

3.3.5. Local oscillation effects on remote hippocampal phase-locking

Our data reveal that neurons not only within the hippocampus, but in remote regions – particularly the entorhinal cortex and amygdala – are entrained by hippocampal theta phase. How do these remote spike-phase associations occur? One possibility, given the strength of phase-locking to local oscillations (Figure 3.S2), is that phase-locking to the hippocampus is an indirect phenomenon, facilitated by transient phase coupling between oscillations in different regions (Figure 3.S3, blue arrows). In rodents, however, neurons in some regions phase-lock to hippocampal theta even in the absence of a local theta rhythm [175], suggesting that inter-regional oscillatory coupling is not a strict requirement for remote spike-phase associations to occur (Figure 3.S3, red arrow).

To examine how inter-regional oscillatory coupling contributed to remote spike-phase associations, we first considered the co-occurrence of oscillatory bouts in the hippocampus and in each extrahippocampal region. We reasoned that if remote spike-phase associations were mediated by oscillatory coupling, then regions where neurons phase-locked to the hippocampus at higher rates should also show higher levels of oscillatory co-occurrence. Consistent with this hypothesis, hippocampal oscillations overlapped more with oscillations in the EC and amygdala than with oscillations in the STG, OFC, and ACC at most frequencies (Figure 3.4A; overlap calculated using the Dice similarity coefficient). However, hippocampal and PHG oscillations also overlapped strongly despite the relative absence of PHG neuron phase-locking to the hippocampus (Figure 3.3A) and abundant PHG neuron phase-locking to local theta (Figure 3.3 3.S2). Moreover, the overlap between local and hippocampal oscillations never exceeded 20% in any region at any frequency, indicating that neurons could, in principle, phase-lock to hippocampal oscillations independent of local oscillations, and vice versa. Altogether these results provide a mixed view for the hypothesis that inter-regional oscillatory coupling and remote spike-phase associations are interchangeable.

Next, we directly compared how remote phase-locking to the hippocampus varied as a func-

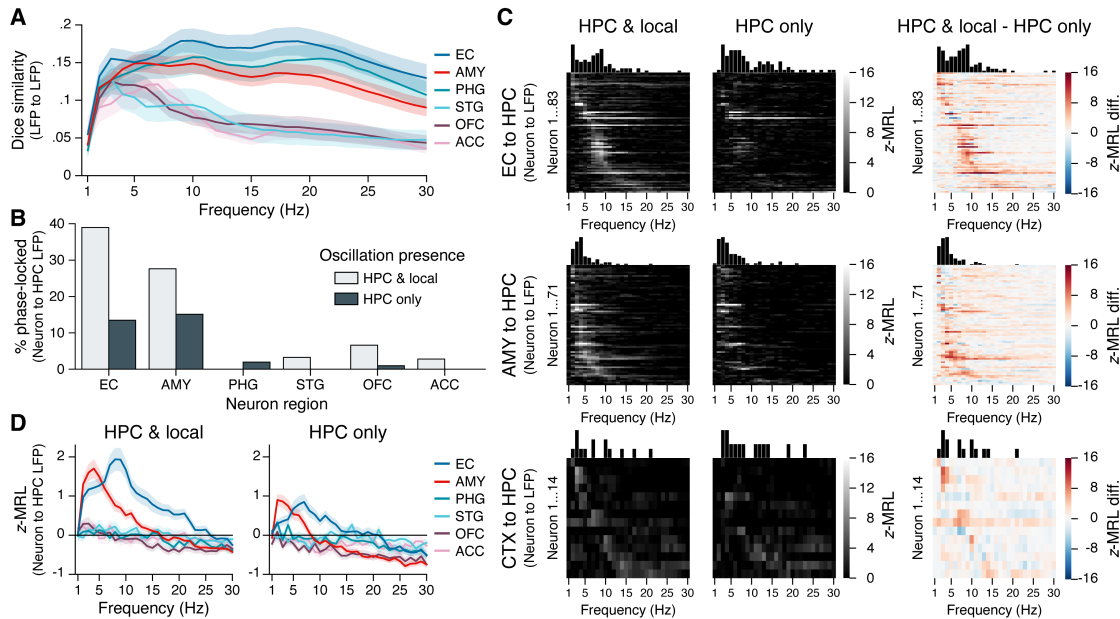


Figure 3.4: Phase-locking to hippocampal oscillations with and without co-occurring local oscillations. (A) Mean \pm SEM Dice coefficient across subjects shows the percent overlap between oscillatory bouts in the hippocampus and in each extrahippocampal region. (B) Bars show the percentage of neurons in each region that phase-locked to hippocampal oscillations when local oscillations were present (light gray) or absent (dark gray). Phase-locking significance was set at FDR-corrected $p < 0.05$ within each bar group. (C) Heatmaps show the phase-locking strength by hippocampal LFP oscillation frequency for all significantly phase-locked neurons in the EC (top row), AMY (middle row), and remaining regions (CTX; bottom row), when hippocampal and local oscillations co-occurred (left column) versus when only hippocampal oscillations occurred (middle column). The right column shows the left column minus middle column values. Neurons in each region are sorted from top to bottom by frequency with the maximum phase-locking strength, and the sorting order is constant across columns within each row. Neurons depicted match the union of light gray and dark gray bars in (B). (D) Phase-locking to the hippocampus is shown during co-occurring local and hippocampal oscillations (left) or only hippocampal oscillations (right). Each subpanel shows the mean \pm SEM phase-locking strength by hippocampal oscillation frequency for all neurons in each region, regardless of their individual phase-locking significance as depicted in (B) and (C). HPC = hippocampus; EC = entorhinal cortex; AMY = amygdala; PHG = parahippocampal gyrus; STG = superior temporal gyrus; OFC = orbitofrontal cortex; ACC = anterior cingulate cortex.

tion of local phase-locking effects. For each extrahippocampal neuron, we subdivided spikes into two categories: (1) spikes that occurred when an oscillation was present in *both* the hippocampus and a neuron's local region, and (2) spikes that occurred when an oscillation was present in the hippocampus but *not* the neuron's local region. As chance-level phase-locking values are sample size dependent, for each neuron we matched the number of spikes in each group, at each frequency, excluding neurons with insufficient sample size (<50 spikes at any frequency; see Methods). We then applied the same methods for determining phase-locking strength and significance as described in the previous section.

Figure 3.4B shows the results from these analyses. FDR-corrected phase-locking rates during co-occurring local and hippocampal oscillations were comparable to phase-locking rates when all spikes were included (see Figure 3.3A), with high phase-locking to hippocampal oscillations occurring among neurons in the EC and amygdala and minimal phase-locking among neurons in other regions. In contrast, when hippocampal oscillations occurred without co-occurring local oscillations, phase-locking rates to the hippocampus declined by nearly two-thirds in the EC (from 39% of neurons to 14%) and by half in the amygdala (from 28% to 15%), while phase-locking to the hippocampus in other regions mostly vanished. Phase-locking strength to the hippocampus decreased specifically at theta frequencies, and even neurons that remained significantly phase-locked in the absence of local oscillations showed reduced phase-locking strength (Figure 3.4C). We also considered the reverse analysis, asking whether phase-locking to local oscillations depended on the presence of co-occurring oscillations in the hippocampus. While local phase-locking rates in the amygdala and neocortex were unaffected by hippocampal oscillation presence, in the EC the percentage of locally phase-locked neurons was reduced by more than half when hippocampal oscillations were absent (Figure 3.S4).

Finally, we confirmed these findings at the population level by computing the mean phase-locking strength across all neurons in each region, without regard to phase-locking significance, while still matching the number of spikes at each frequency between conditions in

which local and hippocampal oscillations co-occurred versus only hippocampal oscillations occurred. As in Figure 3.3C, when local and hippocampal oscillations co-occurred, EC and amygdala neurons both phase-locked strongly to slow hippocampal theta, phase-locking to fast hippocampal theta was restricted to EC neurons, and other regions showed negligible phase-locking to hippocampal oscillations at any frequency (Figure 3.4D, left subpanel). When local theta was absent, the strength of EC and amygdala neuron phase-locking to hippocampal theta was reduced by half, while still remaining well above chance (Figure 3.4D, right subpanel). Collectively, these results provide direct evidence that inter-regional LFP-LFP theta coupling augments but is not strictly required for extrahippocampal neuron phase-locking to hippocampal theta.

3.4. Discussion

By combining datasets of single- and multi-neuron recordings in human subjects, we provide an empirical test of the hypothesis that LFP oscillations in the hippocampus synchronize the timing of neuronal firing both within the hippocampus and in functionally associated regions. Consistent with prior studies, we identify sporadic, oscillatory bouts in hippocampal LFPs within slow theta (2-4Hz), fast theta (6-10Hz), and beta (13-20Hz) bands while subjects engaged in virtual navigation. Individual hippocampal neurons phase-lock to oscillations in each of these bands, including a previously undiscovered group of neurons that phase-lock to nested slow theta and beta rhythms. Outside the hippocampus, phase-locking to hippocampal oscillations occurs in both a regionally-specific (primarily EC and amygdala neurons) and frequency-specific (theta frequency preferring) manner. We further show a dissociation between region and frequency in the selective phase-locking of EC neurons to fast hippocampal theta, whereas neurons in all regions outside the hippocampus show some level of phase-locking to slow hippocampal theta. Finally, we provide the first direct evidence in humans that LFP-LFP coupling enhances spike-time synchronization between regions, as extrahippocampal neurons phase-lock approximately twice as strongly to hippocampal theta during co-occurring local theta oscillations versus when local theta is absent. Taken together, these findings reveal a fundamental relationship between MTL neuron firing and

hippocampal theta phase that underscores a hypothesized role for theta oscillations in routing the information contents of memory.

We note a particularly striking difference between phase-locking rates to hippocampal theta in the EC and amygdala (\sim 30-40% of neurons) relative to all other recorded regions, which phase-lock minimally (<5%) despite their associations with hippocampal-dependent processes [39, 159, 182]. This result is consistent with structural anatomy, as the hippocampus maintains strong, reciprocal connections with the EC and amygdala while connections to neocortex are sparser [2]. Still, given evidence in rodents that some mPFC neurons project directly to the hippocampus [157], phase-lock to hippocampal theta [87, 90, 141, 175, 178], and are critical for memory retrieval [157, 210], we expected that ACC and OFC neurons would show stronger associations with hippocampal theta than we observed. One possibility is that strong phase-locking to hippocampal theta occurs in the EC and amygdala by default, whereas phase-locking among neurons in the mPFC and other cortical areas is task-dependent. Consistently, a recent study in humans found that ACC and pre-supplementary motor area neurons phase-locked to hippocampal theta during a task-switching experiment in which subjects alternated between making recognition memory-based or categorization-based decisions [129]. To the best of our knowledge, this is the only other study that has reported extrahippocampal phase-locking to hippocampal theta in humans, although it will be interesting for future work to consider how phase-locking rates vary by region under different task and stimulus conditions.

We find two differences in hippocampal phase-locking properties between the EC and amygdala. First, as in neocortical regions, amygdala neurons phase-lock at higher rates to local than hippocampal oscillations, and local and hippocampal phase-locking occur at least somewhat independently. By contrast, EC neurons phase-lock to local and hippocampal theta oscillations at indistinguishable rates, and phase-locking is greatly disrupted when EC and hippocampal theta bouts are out of sync. It is worth noting that in rodents, EC and hippocampal theta are phase-shifted but otherwise largely interchangeable, with EC inputs

playing a major role in hippocampal theta generation [20]. Theta phase synchronization between these regions is critical to explain many circuit-level phenomena in rodents, including grid cell and place cell interactions, phase precession, and encoding/retrieval phase separation [13, 16, 52, 67, 140]. Theta occurs more sporadically in humans and other primates than in rodents, and may differ between mammals in other ways not yet well understood [19, 45, 193]. Still, our results indicate that as in rodents, EC and hippocampal neurons in humans retain a uniquely high degree of spike-time synchronization with an overlapping theta rhythm.

The second difference between EC and amygdala neurons concerns the frequency of hippocampal phase-locking, with neurons in both regions phase-locking to slow hippocampal theta but only EC neurons phase-locking measurably to fast theta. This result may be placed in context with recent observations that hippocampal theta frequency varies along the longitudinal axis of the hippocampus, with faster theta occurring more posteriorly [63, 148], where the density of EC relative to amygdalar afferents is greater [185]. While most of our hippocampal electrodes were located anteriorly and precluded a direct analysis of EC and amygdala phase-locking by hippocampal electrode position, this hypothesis may be worth examining in a different dataset.

We note an important difference in our methodological approach compared to prior studies that examined spike-LFP phase relations in humans [91, 98, 128, 153, 165, 205]. These studies typically analyzed either all spikes or a large majority of spikes during time windows of interest, sometimes excluding spikes when spectral power fell below a predefined threshold, e.g. the bottom 25th percentile. Here we wished to strictly test the hypothesis that neurons phase-lock to neural *oscillations* in the hippocampus, as defined by intervals when spectral power exceeds the $1/f$ spectrum by a significant amount for a sustained duration [35, 207]. We considered this approach especially important given the sporadic nature of oscillatory bouts in human LFP recordings and the prevalence of asynchronous, high power artifacts—interictal discharges [162], sharp-wave ripples [179], duplicate spikes across channels [29],

and movement or other non-neural artifacts that escape algorithmic detection. In our experience, phase-locking analyses that did not restrict spikes to verified oscillations produced qualitatively similar group-level results as we report here, but included many individual cases of likely spurious phase-locking to non-oscillatory signals. This methodological difference might explain discrepancies between our results and earlier findings that hippocampal neurons phase-lock to local oscillations at a wider range of frequencies, e.g. 20-30Hz, that we did not observe [91].

This study has several important limitations. First, all subjects had pharmacoresistant epilepsy, and we cannot rule out that some results might stem from pathological activity. However, we sought to reduce this potential by analyzing spikes only during oscillatory bouts, and we are encouraged by the general agreement between our results and those in rodents. A second limitation concerns the quality of unit isolation, as we recorded spikes from single microwires with limited ability to resolve spiking contributions from different neurons. Although some studies in humans have attempted to distinguish between single-units and multi-units and between excitatory and inhibitory neurons, unit quality metrics from microwires do not leave us with high confidence in the accuracy with which these distinctions can be made, while the potential for better quality unit recordings using tetrodes or Neuropixels may soon provide clarity with respect to cell-type-specific differences [25, 31]. In the meantime, we believe it is unlikely that this limitation would change any of our main conclusions, which do not depend on knowing if a unit is truly “single” versus a combination of several neighboring cells.

Still little is known about the relations between theta phase-locking and human cognition. Prior studies have focused on the behavioral correlates of phase-locking to local theta rhythms within the MTL; for example, successful image encoding was found to depend on theta phase-locking strength among hippocampal and amygdala neurons [165], while another study found that MTL neurons can represent contextual information in their theta firing phase [205]. Here we show that hippocampal theta oscillations also inform the timing

of neuronal firing in regions beyond the hippocampus, positioning theta oscillations at the interplay between local circuit computations and inter-regional communication. It remains unknown if behavioral or brain-state dissociations can be found between local and inter-regional phase-locking, or between spike-LFP and LFP-LFP phase synchronization. Such analyses could be well positioned to unite findings from animal and human studies and advance a more mechanistic account of hippocampal-dependent processes across multiple levels of scale, from single neurons to macroscopic fields.

3.5. Methods

3.5.1. Participants

Subjects were 28 patients with pharmacoresistant epilepsy who were implanted with depth electrodes to monitor seizure activity. Clinical teams determined the location and number of implanted electrodes in each patient. We performed bedside cognitive testing on a laptop computer. All testing was completed under informed consent. Experiments were approved by institutional review boards at the University of California, Los Angeles and the University of Pennsylvania.

3.5.2. Spatial navigation tasks

We analyzed data from 55 recording sessions (1-4 sessions per subject, mean duration = 33.6min). During each session, subjects played one of several first-person navigation games in which they freely explored a virtual environment and retrieved objects or navigated to specific locations. The details of these experiments have been previously described [42, 92, 172]; for the purposes of the present study, we pooled data across these studies to generate a large sample for conducting electrophysiological analyses. We analyzed intervals in which subjects could freely navigate through the virtual environment.

3.5.3. Recording equipment

Each subject was implanted with six to 12 Behnke-Fried depth electrodes that feature macro-electrode contacts for clinical monitoring and 40 μ m diameter, platinum-iridium microwires for measuring microscale local field potentials (LFPs) and extracellular action potentials [54].

Electrode localizations were confirmed by the clinical team using post-operative structural MRIs or post-operative CT scans co-registered to pre-operative structural MRIs. Microwires were packaged in bundles of eight high-impedance recording wires and one low-impedance wire that served as the recording reference. Each microwire bundle was threaded through the center of a depth probe and extended 5mm from the implanted end. As microwires splay out during implantation and cannot reliably be visualized on post-operative scans, electrode localizations are regarded with a ~5mm radius of uncertainty that preclude analyses at the level of regional substructures or hippocampal layers or subfields. Microwire LFPs were amplified and sampled at 28-32kHz on a Neuralynx Cheetah (Neuralynx, Tucson, AZ) or Blackrock NeuroPort (Blackrock Microsystems, Salt Lake City, UT) recording system.

3.5.4. Spike-sorting

We performed semi-automatic spike sorting and quality inspection on each microwire channel using the WaveClus software package in Matlab [155], as previously described [42, 172]. We isolated 0-8 units on each microwire channel, retaining both single-units and multi-units for subsequent analysis while removing units with low amplitude waveforms relative to the noise floor, non-neuronal shapes, inconsistent firing across the recording session, or other data quality issues. Spikes that clustered into separate clouds in reduced dimensional space were retained as separate units, while spikes that clustered into single clouds were merged. Repeated testing sessions occurred on different days, and we spike-sorted and analyzed these data separately.

3.5.5. LFP preprocessing and spectral feature extraction

Microwire LFPs were downsampled to 1000Hz, bandpass filtered between 0.1-80Hz using a zero-phase Hann window, and notch-filtered at 60Hz to remove electrical line noise. Bandpass frequencies were selected to reduce signal drift at the low end and spike waveform artifacts (or other high-amplitude noise) at the high end, while maintaining sufficient distance from frequencies of interest for analysis. Lastly, we identified and removed a small number of dead or overly noisy channels, identified as those for which the mean, cross-frequency spec-

tral power differed by >2 standard deviations from the mean spectral power across channels in each microwire bundle. The remaining LFP channels were manually inspected prior to further analysis as a secondary quality inspection step. Lastly, we extracted instantaneous spectral power and phase estimates for each preprocessed LFP channel by convolving the time domain signal with 5-cycle complex wavelets at 30 frequencies, linearly-spaced from 1-30Hz.

3.5.6. Oscillatory bout identification

For each LFP channel, we identified time-resolved oscillatory bouts at the 30 frequencies defined in the previous section using the BOSC (Better OSCillation) detection method, as described previously [207]. BOSC defines an oscillatory bout according to two threshold criteria: a power threshold, P_T , and a duration threshold, D_T . P_T is set to the 95th percentile of the theoretical χ^2 probability distribution of power values at each frequency, under the null hypothesis that powers can be modeled as a straight power law decaying function (the ‘1/f’ spectrum). Defining P_T for each frequency of interest requires first finding a best fit for 1/f. We obtained this fit by implementing the recently-developed FOOOF (Fitting Oscillations & One-Over F) algorithm, which uses an iterative fitting procedure to decompose the power spectrogram into oscillatory components and a 1/f background fit [34]. To avoid assuming that the 1/f spectrum was stationary across the recording session, we divided the LFP into 30s epochs and re-fit 1/f (and P_T , by extension) in each epoch. Finally, we set $D_T = 3/f$, consistent with the convention used in previous studies [1, 43, 203], such that power at a given frequency f must exceed P_T for a minimum of 3 cycles for an oscillatory bout to be detected.

Oscillatory prevalence was calculated within three frequency bands of interest, defined as slow theta (2-4Hz), fast theta (6-10Hz), and beta (13-20Hz). For each subject, we calculated the average oscillatory bout percentage across recording sessions, hippocampal microwire channels, and frequencies within each band. The resulting matrix provided a single measure of hippocampal LFP oscillation prevalence within each band, from each subject. Differences

between bands were assessed using a linear mixed-effects model to account for repeated samples within-subject.

3.5.7. Phase-locking strength and significance

We computed phase-locking strengths at 30 frequencies (1-30Hz with 1Hz spacing) between each neuron's spike times and oscillations in the hippocampus, as well as between each neuron's spike times and oscillations in the neuron's local region (other microwires in the same bundle, excluding the neuron's own recording wire due to spike contamination of the LFP). For both of these comparisons, we retained only spikes that coincided with BOSC-detected oscillatory bouts to avoid reporting spike-phase associations with non-oscillatory LFP phenomena. Phase-locking strength was then calculated as follows: First, we calculated the mean resultant length (MRL) of hippocampal LFP phases across spike times at each frequency, respectively. The MRL is equal to the sum of phase angle unit vectors divided by the total number of samples, yielding a measure from 0 to 1 that indicates the extent to which the phase distribution is unimodal. This metric is sample size dependent, with low n yielding artificially high MRLs due to chance clustering of phases. For this reason, we excluded neurons with <50 spikes at all frequencies of interest. Several other factors can artificially inflate the MRL, including nonuniform phase distributions in an underlying LFP signal, or autocorrelated spike times [175]. To control for these potential confounds, we used a permutation-based procedure in which we circularly-shifted each neuron's spike train at random and then recalculated MRLs at each frequency, repeating this process 10,000 times per neuron to generate a null distribution. We then calculated phase-locking strength as the true MRL at each frequency z -scored against null distribution MRLs at the corresponding frequencies.

To determine which neurons phase-locked significantly to local and hippocampal oscillations, respectively, we calculated an empirical p -value for each neuron by comparing its maximum phase-locking strength across frequencies to its null distribution of maximum phase-locking strengths, using the formula $p = \frac{r+1}{n+1}$, where r is the number of permuted values \geq the true

value for a given test statistic, and n is the total number of permutations [138]. Finally, we false discovery rate (FDR)-corrected p -values using the adaptive linear step-up procedure, which controls the expected proportion of true null hypotheses among rejected nulls for both independent and positively-dependent test statistics, and has greater statistical power than the commonly used Benjamini-Hochberg procedure [10]. FDR correction was applied separately to p -values from each neuron region \times LFP region (local or hippocampal) pair to control the expected proportion of false positives within each of these groups. Neurons with FDR-corrected $p < 0.05$ were deemed significantly phase-locked.

3.5.8. Inter-regional oscillatory co-occurrence

Co-occurrence rates were determined between hippocampal and extrahippocampal oscillatory bouts by quantifying the Dice coefficient between each hippocampal electrode and each ipsilateral, extrahippocampal electrode. The Dice coefficient measures the similarity from 0 to 1 between two sets A and B , with 0 indicating that the sets do not overlap and 1 indicating that A and B are equal: $Dice = \frac{2|A \cap B|}{|A|+|B|}$, where $|A|$ and $|B|$ correspond to the number of elements in each set and $|A \cap B|$ is the number of elements common to both sets. We calculated these values using binarized oscillation detection vectors (oscillation present or absent) as defined in “Oscillatory bout identification,” separately at each 1-30Hz frequency.

3.5.9. Phase-locking to hippocampal oscillations during co-occurring or absent local oscillations

We divided spikes from each extrahippocampal neuron into two groups according to the following criteria: (1) BOSC-detected oscillations were present in both the hippocampus and a neuron’s local region, or (2) BOSC-detected oscillations were present in the hippocampus but not the neuron’s local region (Figure 3.4). These spike subsets were determined separately for each 1-30Hz frequency. Phase-locking strengths were then calculated separately within each spike group, at each frequency, and significance determined relative to null distributions as described in “Phase-locking strength and significance.” As chance-level phase-locking values are sample size dependent, for each neuron we matched the number of

spikes in each group, at each frequency, excluding neurons with insufficient sample size (<50 spikes at any frequency). For example, for neuron i at frequency j , if 200 spikes occurred when local and hippocampal oscillations were both present and 150 spikes occurred when only hippocampal oscillations were present, we selected 150 spikes from the first group at random and proceeded to calculate phase-locking strength in each group. The same analytical approach was applied to a supplemental analysis (Figure 3.S4 in which extrahippocampal spikes were subdivided as: (1) local and hippocampal oscillations were both present, or (2) local oscillations were present but hippocampal oscillations were absent.

3.5.10. Statistics

Linear and logistic mixed-effects models with fixed slopes and random intercepts were performed using the lme4 package in R [5]. All models included a single random effect of subject and a single fixed effect of interest, as stated in each result. p -values were obtained from likelihood ratio tests between nested models (with versus without including the fixed effect). We adopted this approach to control for inter-subject differences in our data that would be overlooked when using conventional methods, like linear regression, that assume independence between neurons. This approach was particularly important for comparing effects between regions, as each subject had electrodes placed in only a subset of the regions that we analyzed. For models in which the independent variable was a categorical measure with three or more levels, if the likelihood ratio test revealed a significant effect ($p < 0.05$), we performed post-hoc, pairwise z -tests on the fitted model terms with Bonferroni-Holm correction for multiple comparisons where noted in the Results.

3.5.11. Software

Mixed-effects models were fit using the lme4 package in R [5]. Spike-sorting was performed using the WaveClus software package in Matlab [155]. All additional analyses were performed, and plots generated, using code that was developed in-house in Python 3, utilizing standard libraries and the following, publicly-available packages: astropy, fooof, matplotlib, mne, numpy, pandas, seaborn, scipy, statsmodels, and xarray.

3.5.12. Data availability

The data used in this study is publicly available for download from the Cognitive Electrophysiology Data Portal (http://memory.psych.upenn.edu/Electrophysiological_Data). This dataset includes de-identified, raw EEG data; spike-sorted unit data; and pre-processed phase-locking data. All data analysis code and JupyterLab notebooks can be freely downloaded at the public GitHub repository: https://github.com/dschonhaut/phase_locking.

3.6. Acknowledgments

We are grateful to the patients for their participation and thank hospital staff and researchers who were involved in data acquisition. This work was supported by the National Science Foundation GRFP grant (D.R.S.), NIH U01 (NS113198 to M.J.K.) and NINDS (NS033221 and NS084017 to I.F.), and Deutsche Forschungsgemeinschaft (DFG) Grant HE 8302/1-1 (N.A.H.).

3.7. Author Contributions

D.R.S. and M.J.K. designed the experiments. IF performed surgical procedures and supervised recordings and data collection. D.R.S. analyzed the data. D.R.S. wrote the manuscript with feedback from all authors.

3.8. Competing Interests

The authors declare no competing interests.

3.9. Supplementary Material

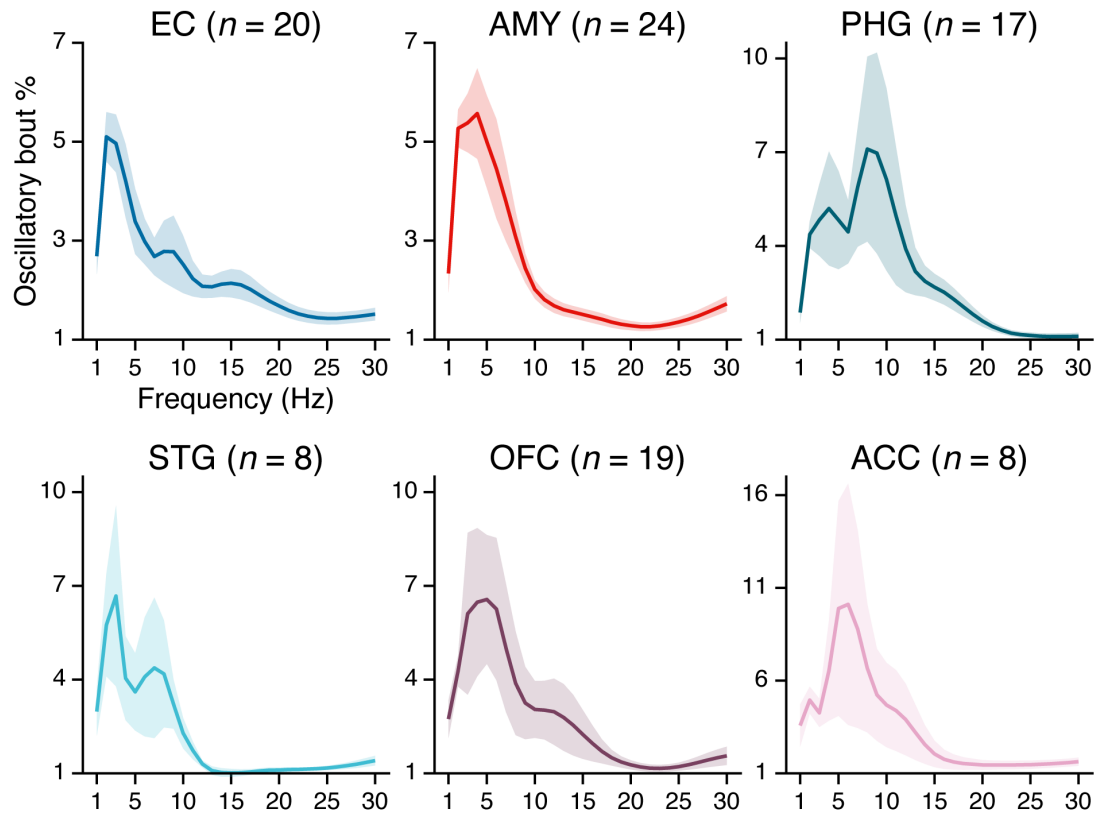


Figure 3.S1: Neural oscillations outside the hippocampus. Subpanels show the mean \pm SEM percent time, across n subjects, that BOSC-detected oscillations were present in each region at 1-30Hz frequencies. (Note the differences in y-axis scaling due to higher variance at lower sample sizes.)

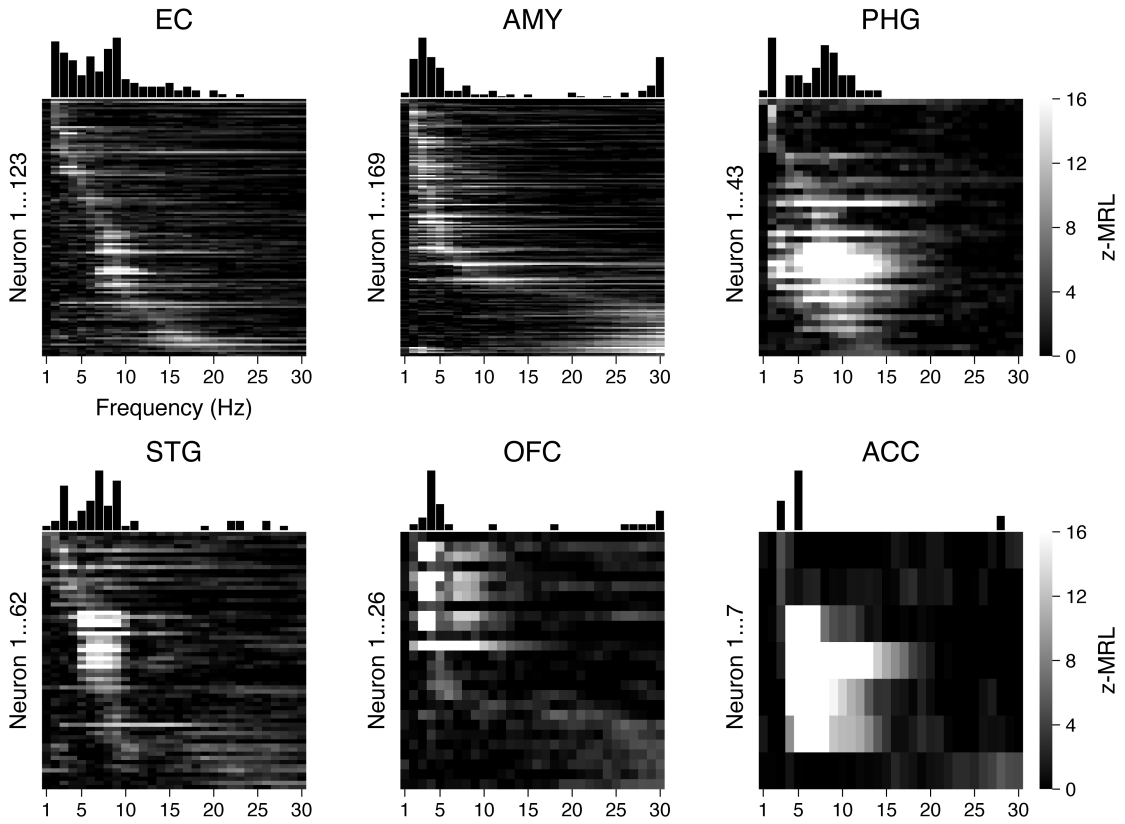


Figure 3.S2: Phase-locking to local oscillations. Heatmaps show the phase-locking strength (z -MRL; color scale intensity) by local oscillation frequency (x-axis) for all significantly phase-locked neurons (y-axis; each row = one neuron) in each region, respectively. Neurons in each region are sorted from top to bottom by frequency of maximum phase-locking strength. Neurons depicted match the light gray bars in Figure 3.3A.

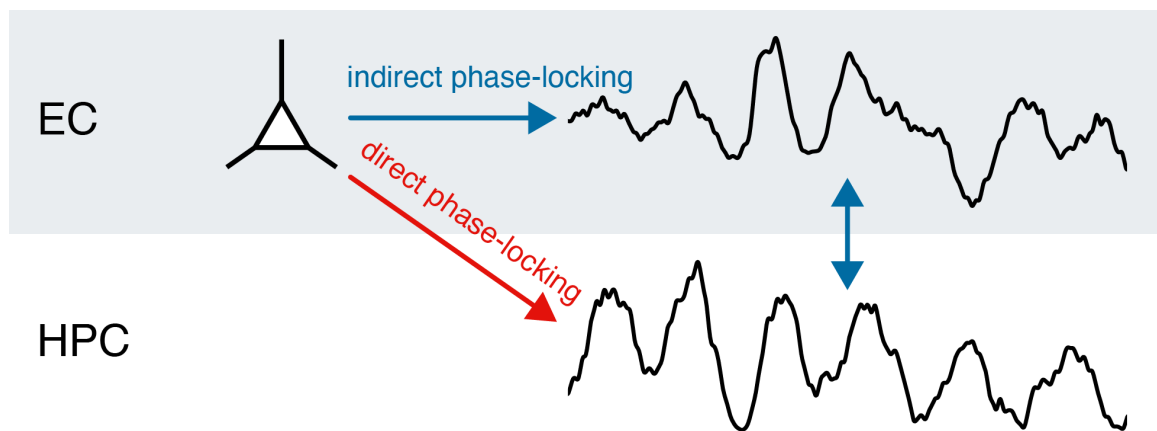


Figure 3.S3: Two explanations for remote phase-locking to hippocampal theta.
 Figure illustration shows two ways in which phase-locking of extrahippocampal neurons to hippocampal theta could occur. In the first scenario, an EC neuron phase-locks to the local theta rhythm, which in turn exhibits phase-synchrony with hippocampal theta (“indirect phase-locking,” blue arrow). In the second scenario, the EC neuron is directly entrained to hippocampal theta, such that phase-locking can occur even absent a local theta rhythm (“direct phase-locking,” red arrow).

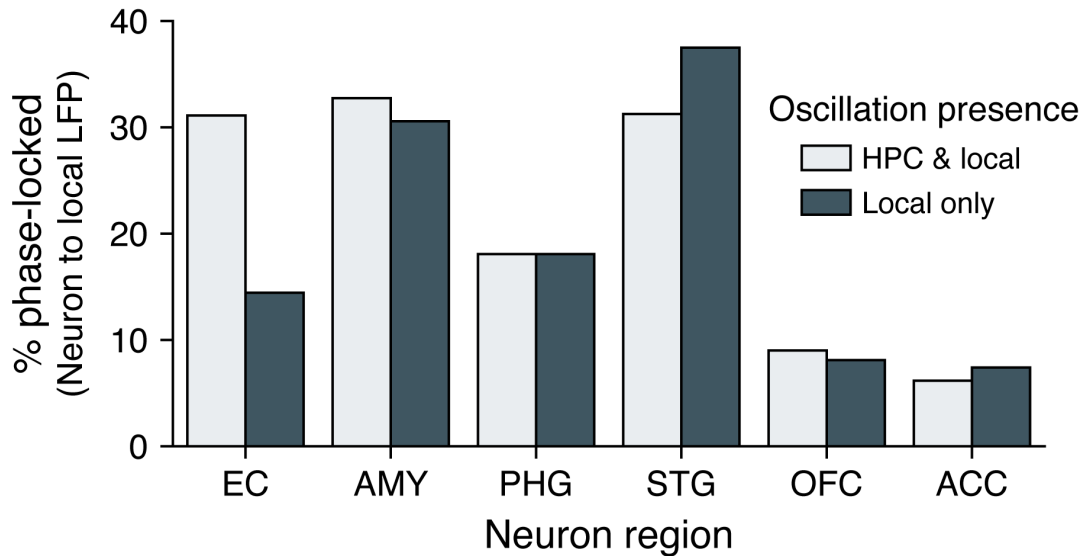


Figure 3.S4: Phase-locking to local oscillations with and without co-occurring hippocampal oscillations. Bars show the percentage of neurons in each region that phase-locked to local oscillations when hippocampal oscillations were present (light gray) or absent (dark gray). Phase-locking significance was set at FDR-corrected $p < 0.05$ within each bar group.

CHAPTER 4

GENERAL DISCUSSION

In the preceding chapters, I set out to advance two areas of study in the domain of human neuron recordings. First, I asked how neurons construct a code for time during everyday-like events, and how this temporal code converges with neural representations of space. Second, I considered how neurons in different regions of the memory system communicate with each other during the kinds of complex, virtual navigation settings that were explored in the time cell experiment. In particular, I sought to test the hypothesis that hippocampal theta oscillations help to coordinate the timing of neuronal firing in different regions. I conclude with a few thoughts outlining particularly promising future directions for these research topics, and where the common ground between them lies. I also touch on possible roadblocks to implementing successful follow-up experiments given limitations of the available data, offering alternative approaches that could be considered.

4.1. Time cells

In Chapter 2, I showed that time-coding neurons appear widely throughout the MTL and mPFC during delay and navigation intervals, such that time and task interval could be simultaneously decoded from population firing patterns with reasonable accuracy. Yet the conclusions we can draw at present are limited by the number and quality of neurons recorded per subject and the number of included subjects. With the task staying mostly as-is, simply collecting more data should bring clearer answers on two of the most important, unresolved questions that extend from our study: First, can we separate time-coding neurons into multiple classes according to the functions they use to compute time? For example, although we interpreted our findings mainly in the context of time cells with Gaussian fields akin to those described in the rodent hippocampus [144], we acknowledge that other forms of time coding (including, but not limited to, exponential ramping [15, 194]) are both possible and might interact with Gaussian time cells. Second, how does the distribution of these time cell classes vary by brain region? A straight read of the literature in animals suggests

that Gaussian time cells are concentrated in the hippocampus and mPFC while exponential ramping neurons are enriched in the lateral EC. However, studies in animals typically record from only one or two regions at a time, displaying strong selection bias and often an absence of control regions, which leaves them vulnerable to over-interpreting the regional specificity of neuronal responses. For this reason, I believe it is an open but important question to resolve regional differences in the strength and properties of time (and place) coding.

When we set out in search of human time cells, one early decision that we made was to mimic the style of classic time cell experiments in rodents, enabling direct comparisons between human and rodent neuron responses. This decision meant that we would not instruct or explicitly incentivize subjects to attend to time during delay intervals, which carried a calculated risk of finding no timing effects. Now that we know that time cells *do* materialize during task-free delays, there is a series of experiments that have been completed in rodents and would be worth pursuing in humans for the sake of cross-species comparison. These follow-up experiments might also prove useful for delineating between classes of time coding neurons, as described above.

1. What happens when a learned delay duration is unexpectedly changed, e.g. from 10s to 15s? In rodents, this manipulation has a tendency to cause time cell remapping [112, 189]. However, we already saw that in humans, most delay time cells did not remap between first and second trial delays, whereas rodent time cells do remap under analogous conditions. A simple variation of the current, 36-trial experiment would set the delays at 10s over the first 12 trials, 15s over the second 12, and then revert to 10s during the final 12 trials. I predict that time cells will remap when the delay is set to 15s but recover their original fields over the final 12 trials.
2. What effect does changing a contextual feature other than duration have on time cell stability? We had predicted, incorrectly, that differences in the surrounding contexts of the two trial delays (one before gold search, one before gold dig) would be sufficient to induce time cell remapping. However, it remains possible that changing context

during the delays would still have this effect. For example, the first and last 12 trials might occur in the mine base as it is currently designed, then switch to a visually redesigned but otherwise identical mine base from trials 13-24, reverting back to the original base over the last 12 trials.

3. What happens when delays are not inserted between encoding and retrieving periods, but instead occur between tasks that lack a memory component? One early explanation for time cells proposed that they bridge otherwise empty intervals between connected events. For example, a rodent might need to hold a specific odor in mind for a fixed amount of time before having to make a decision based on that odor's identity [40]. Initial evidence in rodents suggested that delay time coding was lost in the absence of memory-dependent tasks [144], although later findings contradicted this conclusion [169]. This question could be tested in *Goldmine* by alternating between two unrelated task intervals. For example, after Delay₁ subjects could spend 30s navigating to a series of locations in a virtual environment, and after Delay₂ they could spend 30s dodging creatures that appear in the environment and chase them (akin to Pac-Man). A second approach outside the virtual navigation context would be to show subjects a sequence of images for exactly 5s each, or for 3-7s drawn randomly from a uniform distribution (this could be done in alternating blocks). If time cells require only a stable temporal interval but do not need to bridge connected events, they should be reliably found in the 5s stimulus blocks but not in the variable time blocks. This design has the advantage of including a strong control against purely stimulus-driven responses and works within the context of other experiments of likely research interest (e.g. finding cells with stimulus-selective responses, or in the guise of a recognition memory task).

With regard to time and space coding during navigation, I showed that neuron-level codes for time and space emerged in parallel while subjects navigated a virtual environment. Moreover, although significant numbers of neurons represented time *or* place, respectively, a

subset of neurons encoded conjunctive time \times place interactions. This analysis was possible to conduct because of a trick we employed in the maze design that required subjects to alter their routes at the beginning of each navigation interval, going left, right, or straight depending on which door to the mine opened. This had the effect of sufficiently decorrelating time, place, and head direction parameters that they could be separated in a multiple regression model. However, as shown in Figure 2.S3, many weak correlations remained in the behavioral data despite this manipulation, and the fact that subjects always had to begin and end each navigation interval in the same location meant that the degree of correlation between time and place varied over time. To gain a clearer perspective on how time, place, and time \times place cells collectively represent a spatiotemporal environment, change with experience, and vary between brain regions, it will be necessary to more fully decorrelate time, place, and head direction. A decent way to accomplish this may be to separate the delay location from the navigation environment, for example by teleporting subjects from the mine to an offsite base at the end of each navigation interval, then teleporting them to a random location and orientation in the mine at the start of the next trial. Some trial-and-error testing may be needed to design an environment that: (1) achieves nearly full decorrelation of time, place, and head direction; (2) subjects can learn to navigate effectively over the course of the testing session; and (3) subjects traverse each part of the environment in roughly equal proportions. Something like a circular track cut through by two, perpendicular lines (a plus-symbol inside of a donut) with strategically-placed landmarks would meet these criteria, but alternative designs should be considered and a pragmatic choice selected.

Possibly the most important question pertaining to time cells and place cells concerns their importance, if any, to episodic memory. Contextual reinstatement models of memory predict that having a stable neural code for spatiotemporal context should facilitate associative connections between events in memory [79, 152]. For example, if events i and j both occur at location (x, y) and time z on trials t and $t + 1$, respectively, then all else being equal, reinstating the memory associated with j will more likely retrieve the memory associated with i than if j had occurred at location $(x - 3, y + 7)$ or at time $z + 10$, or *especially*

if both (x, y) and z were shifted in this manner. Versions of this phenomenon have been found in verbal memory studies describing associative intrusion errors [97], joint temporal-semantic clustering in categorized free recall [151], and transitive associations in paired associates learning with double-function pairs [78]. Yet to my knowledge cross-trial time and place associations have not been convincingly examined. If time cells and place cells act as neural mediators for inter-item associations across similar spatiotemporal contexts, then the trialwise accuracy of neural decoders for time and place might be shown to correlate with the strength of inter-item associations. Along with these implicit associations, we can make a related hypothesis that time cells contribute to explicit temporal memory (and similarly, place cells to spatial memory). This might be tested by having subjects locate and retrieve unique objects within a virtual environment (as in Deuker et al. [32]) rather than learning the locations of identical objects, as in the current *Goldmine* experiment. After each encoding interval, subjects could then complete a temporal memory test in which they place each object on a timeline that reflects when they encountered it, and a spatial memory test in which they place each object on a top-down map of the virtual environment that reflects where they found it (counterbalancing the testing order across trials). This paradigm would provide single-subject measures of temporal and spatial memory and would allow correlating trial-wise accuracy of neural time and place decoders with temporal and spatial memory performance.

From a feasibility standpoint, in preliminary work I found that time and space decoding from population firing patterns exceeds chance in a majority of subjects who completed the existing *Goldmine* paradigm. However, these single-subject decoders were prone to blind spots (times or locations that could not be predicted because no recorded neuron had an overlapping receptive field). It is possible that successfully implementing the proposed experiment will require being able to record more and higher quality neurons per subject, or training decoders on a combination of neural firing data and LFP spectral features. To the first possibility, pilot experiments using tetrodes and Neuropixels have recently been conducted in humans and offer the potential to collect orders of magnitude more unit firing

data per subject [25, 31]. However, these technologies are not yet widely available for human subjects research, and many neurosurgeons may be hesitant to implant new devices without there being a clear, clinical benefit for patients. In the meantime, Herweg et al. [70] recently demonstrated the feasibility of performing subject-level spatial decoding from LFP features in a different virtual navigation paradigm tested in humans. Combining neural firing and LFP data may therefore prove fruitful for investigating the neural associates of temporal and spatial memory.

4.2. Theta phase-locking

In Chapter 3, I showed that high percentages of neurons in the hippocampus, EC, and amygdala phase-lock to hippocampal theta oscillations while subjects navigate through virtual space. Phase-locking to hippocampal theta was also evident among some neurons in regions less connected to the hippocampus, including parahippocampal gyrus and orbitofrontal cortex, although this effect washed out at the group level due to absent cortico-hippocampal interactions in a majority of neurons from these regions. As in previous studies that recorded from the human hippocampus using macroelectrodes [43, 63, 107, 204], I found that hippocampal theta occurred in two, separated bands: a slow theta (2-4Hz) oscillation that some neurons in all regions phase-locked to, and a fast theta (6-10Hz) oscillation that only hippocampal and EC neurons phase-locked to. Lastly, I demonstrated that hippocampal theta phase-locking is enhanced by but does not depend on theta synchronization between regions, as significant numbers of EC and amygdala neurons phase-locked to hippocampal theta even in the absence of a local theta rhythm. Together, these findings support a role for hippocampal theta in synchronizing neural activity both within the hippocampus and in other regions of the episodic memory network.

My work sets up but does not address the behavioral question; namely, what is the point of theta phase-locking in relation to hippocampal function and episodic memory? Oscillatory coupling has typically been interpreted as facilitating communication between regions by modulating the gain of activity from one region on another [22, 49, 58, 131]. This is because,

in rodents at least, hippocampal interneurons fire at preferential theta phases, creating windows of heightened inhibition when the same excitatory input is less likely to discharge a hippocampal pyramidal cell than when inhibitory tone is reduced [99]. A related hypothesis contends that the hippocampal theta rhythm is separated into two functional windows: an ‘encoding’ phase when hippocampal neurons are more receptive to external excitatory drive, and a ‘retrieval’ phase when activity is driven more by connections within the hippocampus (notably CA3 inputs to CA1) [52, 68, 176]. This does not imply that the hippocampus enters into an encoding phase all at once; rather, hippocampal theta acts as a traveling wave along the longitudinal axis with a phase gradient imposed at any given moment [110, 213], so hippocampal neurons enter into receptive theta phases in a staggered manner. Combining these hypotheses, I propose that one function of hippocampal theta phase-locking is to facilitate information transfer from remote brain regions to the hippocampus, in the process transforming neural representations of current environmental stimuli into long-term memory traces. My findings indicate that most of this information transfer is routed through the EC and amygdala, given their uniquely high rates of phase-locking to hippocampal theta. These regions may therefore serve as gatekeepers separating information that is perceived in the moment from content that is later retrievable.

The ‘information transfer’ hypothesis of hippocampal theta phase-locking can be tested in several ways. First, experimental manipulations at the time of encoding that increase or decrease memory performance should have corresponding effects on phase-locking strength to hippocampal theta. We might also expect these effects to be regionally-specific; for example, instructing subjects to attend to the locations and background details of a set of images versus their emotional attributes could have opposite effects on EC versus amygdala neuron phase-locking to hippocampal theta, respectively. Following work described in Chapter 2 and future analyses outlined in the preceding section, we can also examine whether instructing subjects to attend to the time or place that they encounter objects in a virtual environment modulates the extent of hippocampal theta phase-locking by exponential ramping neurons in the lateral EC versus grid cells in the medial EC. Finally, if phase-locking supports

information transfer to the hippocampus, as hypothesized, theta phase-locking effects might in turn correlate with the prevalence of hippocampal time cells and place cells under each experimental condition.

Although the described analyses cannot be pursued in the current *Goldmine* paradigm, I conducted preliminary analyses that showed that EC and amygdala neurons phase-locked to hippocampal theta at significantly higher rates, and with greater phase-locking strengths, during navigation intervals when subjects actively explored a virtual environment than during delays when external stimuli were held constant. This effect was stronger when comparing neural firing to hippocampal theta than to local theta phase, and no differences in firing rate were found at the population level between navigation and delay intervals. These preliminary results are consistent with the hypothesis that hippocampal theta phase-locking is behavior-dependent and selectively increased during active encoding and exploration intervals over periods of quiet restfulness. The data further suggest that the timing and rate of neuronal firing provide complementary keys for parsing neural circuit computations, despite the large majority of human neuron studies having focused on rate-based codes [53, 164].

4.3. Looking ahead

In summary, here I describe novel work on the means through which neurons in the hippocampus and other memory-related regions represent time and space in the human brain, and how the timing of neuronal firing in this memory network is clocked against an internal hippocampal theta rhythm. The intersection between these fields will provide a more integrated view of neural coding that reconciles roles for firing rate-based representations and oscillatory phase coding, as well as distinguishing between local and distal spike-field interactions. Although much of this ground remains still to be covered, I propose several modified experiments that build on our initial time cell paradigm and will facilitate analyses into the functions of time cells, place cells, and theta phase-locking in parallel. I end this dissertation with several things learned and many more questions opened than answered. Continued work along these directions offers great promise for providing new and foundational insights

into the neurobiological mechanisms of time, space, and memory.

BIBLIOGRAPHY

- [1] Aghajan ZM, Schuette P, Fields TA, Tran ME, Siddiqui SM, Hasulak NR, Tcheng TK, Eliashiv D, Mankin EA, Stern J, Fried I, Suthana N (2017) Theta oscillations in the human medial temporal lobe during real-world ambulatory movement. *Curr. Biol.* 27:3743–3751.e3.
- [2] Amaral DG (2011) Memory: Anatomical organization of candidate brain regions In *Comprehensive Physiology*, pp. 211–294. John Wiley and Sons, Ltd.
- [3] Astur RS, Taylor LB, Mamelak AN, Philpott L, Sutherland RJ (2002) Humans with hippocampus damage display severe spatial memory impairments in a virtual Morris water task. *Behav. Brain Res.* 132:77–84.
- [4] Azari NP, Auday BC, Cross HA (1989) Effect of instructions on memory for temporal order. *Bull. Psychon. Soc.* 27:203–205.
- [5] Baayen RH, Davidson DJ, Bates DM (2008) Mixed-effects modeling with crossed random effects for subjects and items. *Journal of Memory and Language* 59:390–412.
- [6] Babiloni C, Vecchio F, Mirabella G, Buttiglione M, Sebastiano F, Picardi A, Di Gennaro G, Quarato PP, Grammaldo LG, Buffo P, Esposito V, Manfredi M, Cantore G, Eusebi F (2009) Hippocampal, amygdala, and neocortical synchronization of theta rhythms is related to an immediate recall during Rey auditory verbal learning test. *Hum. Brain Mapp.* 30:2077–2089.
- [7] Barker GR, Bird F, Alexander V, Warburton EC (2007) Recognition memory for objects, place, and temporal order: A disconnection analysis of the role of the medial prefrontal cortex and perirhinal cortex. *J. Neurosci.* 27:2948–2957.
- [8] Bellmund JLS, Deuker L, Doeller CF (2019) Mapping sequence structure in the human lateral entorhinal cortex. *eLife* p. e45333.
- [9] Benchenane K, Peyrache A, Khamassi M, Tierney PL, Gioanni Y, Battaglia FP, Wiener SI (2010) Coherent theta oscillations and reorganization of spike timing in the hippocampal-prefrontal network upon learning. *Neuron* 66:921–936.
- [10] Benjamini Y, Krieger AM, Yekutieli D (2006) Adaptive linear step-up procedures that control the false discovery rate. *Biometrika* 93:491–507.
- [11] Bienvenu TC, Busti D, Magill PJ, Ferraguti F, Capogna M (2012) Cell-type-specific recruitment of amygdala interneurons to hippocampal theta rhythm and noxious stimuli in vivo. *Neuron* 74:1059–1074.

- [12] Bohbot VD, Kalina M, Stepankova K, Spackova N, Petrides M, Nadel L (1998) Spatial memory deficits in patients with lesions to the right hippocampus and to the right parahippocampal cortex. *Neuropsychologia* 36:1217–1238.
- [13] Bonnevie T, Dunn B, Fyhn M, Hafting T, Derdikman D, Kubie JL, Roudi Y, Moser EI, Moser MB (2013) Grid cells require excitatory drive from the hippocampus. *Nat. Neurosci.* 16:309–317.
- [14] Bostock E, Muller RU, Kubie JL (1991) Experience-dependent modifications of hippocampal place cell firing. *Hippocampus* 1:193–205.
- [15] Bright IM, Meister ML, Cruzado NA, Tiganj Z, Buffalo EA, Howard MW (2020) A temporal record of the past with a spectrum of time constants in the monkey entorhinal cortex. *Proc. Natl. Acad. Sci. U. S. A.* 117:20274–20283.
- [16] Burgess N, Barry C, O’Keefe J (2007) An oscillatory interference model of grid cell firing. *Hippocampus* 17:801–812.
- [17] Burt CD (1992a) Reconstruction of the duration of autobiographical events. *Mem. Cognit.* 20:124–132.
- [18] Burt CD (1992b) Retrieval characteristics of autobiographical memories: Event and date information. *Appl. Cogn. Psychol.* 6:389–404.
- [19] Bush D, Burgess N (2019) Neural oscillations: Phase coding in the absence of rhythmicity. *Curr. Biol.* 29:R55–R57.
- [20] Buzsáki G (2002) Theta oscillations in the hippocampus. *Neuron* 33:325–340.
- [21] Buzsáki G (2006) *Rhythms of the brain* Oxford University Press, New York, NY.
- [22] Buzsáki G (2010) Neural syntax: Cell assemblies, synapsembles, and readers. *Neuron* 68:362–385.
- [23] Buzsáki G, Anastassiou CA, Koch C (2012) The origin of extracellular fields and currents—EEG, ECoG, LFP and spikes. *Nat. Rev. Neurosci.* 13:407–20.
- [24] Chen AC, Etkin A (2013) Hippocampal network connectivity and activation differentiates post-traumatic stress disorder from generalized anxiety disorder. *Neuropsychopharmacology* 38:1889–1898.
- [25] Chung JE, Sellers KK, Leonard MK, Gwilliams L, Xu D, Dougherty ME, Kharazia V, Metzger SL, Welkenhuysen M, Dutta B, Chang EF (2022) High-density single-unit human cortical recordings using the Neuropixels probe. *Neuron* 110:2409–2421.e3.

- [26] Colgin LL (2020) Five decades of hippocampal place cells and EEG rhythms in behaving rats. *J. Neurosci.* 40:54–60.
- [27] Colgin LL, Moser EI, Moser MB (2008) Understanding memory through hippocampal remapping. *Trends Neurosci.* 31:469–477.
- [28] Cruzado NA, Tiganj Z, Brincat SL, Miller EK, Howard MW (2020) Conjunctive representation of what and when in monkey hippocampus and lateral prefrontal cortex during an associative memory task. *Hippocampus* 30:1332–1346.
- [29] Dehnen G, Kehl MS, Darcher A, Müller TT, Macke JH, Borger V, Surges R, Mormann F (2021) Duplicate detection of spike events: A relevant problem in human single-unit recordings. *Brain Sci.* 11:761.
- [30] Dennis EL, Thompson PM (2014) Functional brain connectivity using fMRI in aging and Alzheimer’s disease. *Neuropsychol. Rev.* 24:49–62.
- [31] Despouy E, Curot J, Reddy L, Nowak LG, Deudon M, Sol JC, Lotterie JA, Denuelle M, Maziz A, Bergaud C, Thorpe SJ, Valton L, Barbeau EJ (2020) Recording local field potential and neuronal activity with tetrodes in epileptic patients. *J. Neurosci. Methods* 341:108759.
- [32] Deuker L, Bellmund JL, Schröder TN, Doeller CF (2016) An event map of memory space in the hippocampus. *eLife* 5:e16534.
- [33] DeVito LM, Eichenbaum H (2011) Memory for the order of events in specific sequences: Contributions of the hippocampus and medial prefrontal cortex. *J. Neurosci.* 31:3169–3175.
- [34] Donoghue T, Haller M, Peterson EJ, Varma P, Sebastian P, Gao R, Noto T, Lara AH, Wallis JD, Knight RT, Shestyuk A, Voytek B (2020) Parameterizing neural power spectra into periodic and aperiodic components. *Nat. Neurosci.* 23:1655–1665.
- [35] Donoghue T, Schawronkow N, Voytek B (2022) Methodological considerations for studying neural oscillations. *Eur. J. Neurosci.* 55:3502–3527.
- [36] Downes JJ, Mayes AR, MacDonald C, Hunkin NM (2002) Temporal order memory in patients with Korsakoff’s syndrome and medial temporal amnesia. *Neuropsychologia* 40:853–861.
- [37] DuBrow S, Davachi L (2014) Temporal memory is shaped by encoding stability and intervening item reactivation. *J. Neurosci.* 34:13998–14005.
- [38] DuBrow S, Davachi L (2016) Temporal binding within and across events. *Neurobiol. Learn. Mem.* 134:107–114.

- [39] Eichenbaum H (2000) A cortical–hippocampal system for declarative memory. *Nat. Rev. Neurosci.* 1:41–50.
- [40] Eichenbaum H (2014) Time cells in the hippocampus: A new dimension for mapping memories. *Nat. Rev. Neurosci.* 15:732–744.
- [41] Eichenbaum H, Dudchenko P, Wood E, Shapiro M, Tanila H (1999) The hippocampus, memory, and place cells: Is it spatial memory or a memory space? *Neuron* 23:209–226.
- [42] Ekstrom AD, Kahana MJ, Caplan JB, Fields TA, Isham EA, Newman EL, Fried I (2003) Cellular networks underlying human spatial navigation. *Nature* 425:184–188.
- [43] Ekstrom AD, Caplan JB, Ho E, Shattuck K, Fried I, Kahana MJ (2005) Human hippocampal theta activity during virtual navigation. *Hippocampus* 15:881–889.
- [44] Ekstrom AD, Copara MS, Isham EA, chun Wang W, Yonelinas AP (2011) Dissociable networks involved in spatial and temporal order source retrieval. *Neuroimage* 56:1803–1813.
- [45] Eliav T, Geva-Sagiv M, Yartsev MM, Finkelstein A, Rubin A, Las L, Ulanovsky N (2018) Nonoscillatory phase coding and synchronization in the bat hippocampal formation. *Cell* 175:1119–1130.e15.
- [46] Ezzyat Y, Davachi L (2014) Similarity breeds proximity: Pattern similarity within and across contexts is related to later mnemonic judgments of temporal proximity. *Neuron* 81:1179–1189.
- [47] Farovik A, Dupont LM, Eichenbaum H (2010) Distinct roles for dorsal CA3 and CA1 in memory for sequential nonspatial events. *Learn. Mem.* 17:801–806.
- [48] Feldman DE (2012) The spike-timing dependence of plasticity. *Neuron* 75:556–571.
- [49] Fell J, Axmacher N (2011) The role of phase synchronization in memory processes. *Nat. Rev. Neurosci.* 12:105–118.
- [50] Fell J, Ludowig E, Rosburg T, Axmacher N, Elger CE (2008) Phase-locking within human mediotemporal lobe predicts memory formation. *Neuroimage* 43:410–419.
- [51] Fell J, Klaver P, Lehnertz K, Grunwald T, Schaller C, Elger CE, Fernández G (2001) Human memory formation is accompanied by rhinal-hippocampal coupling and decoupling. *Nat. Neurosci.* 4:1259–1264.
- [52] Fernández-Ruiz A, Oliva A, Nagy GA, Maurer AP, Berényi A, Buzsáki G (2017) Entorhinal-CA3 dual-input control of spike timing in the hippocampus by theta-gamma coupling. *Neuron* 93:1213–1226.e5.

- [53] Fried I, Rutishauser U, Cerf M, Kreiman G (2014) *Single neuron studies of the human brain: Probing cognition* MIT Press, Cambridge, MA.
- [54] Fried I, Wilson CL, Maidment NT, Engel Jr. J, Behnke E, Fields TA, Macdonald KA, Morrow JW, Ackerson L (1999) Cerebral microdialysis combined with single-neuron and electroencephalographic recording in neurosurgical patients. *J. Neurosurg.* 91:697–705.
- [55] Friedman WJ (1993) Memory for the time of past events. *Psychol. Bull.* 113:44–66.
- [56] Friedman WJ (2004) Time in autobiographical memory. *Soc. Cogn.* 22:591–605.
- [57] Friedman WJ, Wilkins AJ (1985) Scale effects in memory for the time of events. *Mem. Cognit.* 13:168–175.
- [58] Fries P (2005) A mechanism for cognitive dynamics: Neuronal communication through neuronal coherence. *Trends Cogn. Sci.* 9:474–480.
- [59] Fries P (2015) Rhythms for cognition: Communication through coherence. *Neuron* 88:220–235.
- [60] Fujisawa S, Buzsáki G (2011) A 4 Hz oscillation adaptively synchronizes prefrontal, VTA, and hippocampal activities. *Neuron* 72:153–165.
- [61] Gelbard-Sagiv H, Mukamel R, Harel M, Malach R, Fried I (2008) Internally generated reactivation of single neurons in human hippocampus during free recall. *Science* 322:96–101.
- [62] Gill PR, Mizumori SJ, Smith DM (2011) Hippocampal episode fields develop with learning. *Hippocampus* 21:1240–1249.
- [63] Goyal A, Miller J, Qasim SE, Watrous AJ, Zhang H, Stein JM, Inman CS, Gross RE, Willie JT, Lega B, Lin JJ, Sharan A, Wu C, Sperling MR, Sheth SA, McKhann GM, Smith EH, Schevon C, Jacobs J (2020) Functionally distinct high and low theta oscillations in the human hippocampus. *Nat. Commun.* 11:2469.
- [64] Grady CL, McIntosh AR, Craik FI (2003) Age-related differences in the functional connectivity of the hippocampus during memory encoding. *Hippocampus* 13:572–586.
- [65] Harris CR, Millman KJ, van der Walt SJ, Gommers R, Virtanen P, Cournapeau D, Wieser E, Taylor J, Berg S, Smith NJ, Kern R, Picus M, Hoyer S, van Kerkwijk MH, Brett M, Haldane A, del Río JF, Wiebe M, Peterson P, Gérard-Marchant P, Sheppard K, Reddy T, Weckesser W, Abbasi H, Gohlke C, Oliphant TE (2020) Array programming with NumPy. *Nature* 585:357–362.
- [66] Harris KD, Quiroga RQ, Freeman J, Smith SL (2016) Improving data quality in neu-

- ronal population recordings. *Nat. Neurosci.* 19:1165–1174.
- [67] Hasselmo ME (2005) What is the function of hippocampal theta rhythm? - Linking behavioral data to phasic properties of field potential and unit recording data. *Hippocampus* 15:936–949.
- [68] Hasselmo ME, Bodelón C, Wyble BP (2002) A proposed function for hippocampal theta rhythm: Separate phases of encoding and retrieval enhance reversal of prior learning. *Neural Comput.* 14:793–817.
- [69] Healey MK, Long NM, Kahana MJ (2019) Contiguity in episodic memory. *Psychon. Bull. Rev.* 26:699–720.
- [70] Herweg NA, Kunz L, Schonhaut DR, Brandt A, Wanda PA, Sharan AD, Sperling MR, Schulze-Bonhage A, Kahana MJ (2020) A learned map for places and concepts in the human MTL.
- [71] Herweg NA, Solomon EA, Kahana MJ (2020) Theta oscillations in human memory. *Trends Cogn. Sci.* 24:208–227.
- [72] Heys JG, Dombeck DA (2018) Evidence for a subcircuit in medial entorhinal cortex representing elapsed time during immobility. *Nat. Neurosci.* 21:1574–1582.
- [73] Heys JG, Wu Z, Allegra Mascaro AL, Dombeck DA (2020) Inactivation of the medial entorhinal cortex selectively disrupts learning of interval timing. *Cell Rep.* 32:108163.
- [74] Hill DN, Mehta SB, Kleinfeld D (2011) Quality metrics to accompany spike sorting of extracellular signals. *J. Neurosci.* 31:8699–8705.
- [75] Hintzman DL (2004) Time versus items in judgment of recency. *Mem. Cogn.* 32:1298–1304.
- [76] Hintzman DL, Block RA, Summers JJ (1973) Contextual associations and memory for serial position. *J. Exp. Psychol.* 97:220–229.
- [77] Howard MW, MacDonald CJ, Tiganj Z, Shankar KH, Du Q, Hasselmo ME, Eichenbaum H (2014) A unified mathematical framework for coding time, space, and sequences in the hippocampal region. *J. Neurosci.* 34:4692–4707.
- [78] Howard MW, Jing B, Rao VA, Provyn JP, Datey AV (2009) Bridging the gap: Transitive associations between items presented in similar temporal contexts. *J. Exp. Psychol. Learn. Mem. Cogn.* 35:391–407.
- [79] Howard MW, Kahana MJ (2002) A distributed representation of temporal context. *J. Math. Psychol.* 46:269–299.

- [80] Howard MW, Shankar KH, Aue WR, Criss AH (2015) A distributed representation of internal time. *Psychol. Rev.* 122:24–53.
- [81] Howard MMW, Eichenbaum H (2015) Time and space in the hippocampus. *Brain Res.* 1621:345–54.
- [82] Hsieh LT, Gruber MJ, Jenkins LJ, Ranganath C (2014) Hippocampal activity patterns carry information about objects in temporal context. *Neuron* 81:1165–1178.
- [83] Huerta PT, Lisman JE (1995) Bidirectional synaptic plasticity induced by a single burst during cholinergic theta oscillation in CA1 in vitro. *Neuron* 15:1053–1063.
- [84] Huerta PT, Sun LD, Wilson MA, Tonegawa S (2000) Formation of temporal memory requires NMDA receptors within CA1 pyramidal neurons. *Neuron* 25:473–480.
- [85] Hunter JD (2007) Matplotlib: A 2D graphics environment. *Comput. Sci. Eng.* 9:90–95.
- [86] Hyman JM, Wyble BP, Goyal V, Rossi CA, Hasselmo ME (2003) Stimulation in hippocampal region CA1 in behaving rats yields long-term potentiation when delivered to the peak of theta and long-term depression when delivered to the trough. *J. Neurosci.* 23:11725–31.
- [87] Hyman JM, Zilli EA, Paley AM, Hasselmo ME (2005) Medial prefrontal cortex cells show dynamic modulation with the hippocampal theta rhythm dependent on behavior. *Hippocampus* 15:739–749.
- [88] Hyman JM, Zilli EA, Paley AM, Hasselmo ME (2010) Working memory performance correlates with prefrontal-hippocampal theta interactions but not with prefrontal neuron firing rates. *Front. Integr. Neurosci.* 4:2.
- [89] Iglói K, Doeller CF, Berthoz A, Rondi-Reig L, Burgess N (2010) Lateralized human hippocampal activity predicts navigation based on sequence or place memory. *Proc. Natl. Acad. Sci. U. S. A.* 107:14466–14471.
- [90] Ito HT, Moser EI, Moser MB (2018) Supramammillary nucleus modulates spike-time coordination in the prefrontal-thalamo-hippocampal circuit during navigation. *Neuron* 99:576–587.e5.
- [91] Jacobs J, Kahana MJ, Ekstrom AD, Fried I (2007) Brain oscillations control timing of single-neuron activity in humans. *J. Neurosci.* 27:3839–3844.
- [92] Jacobs J, Kahana MJ, Ekstrom AD, Mollison MV, Fried I (2010) A sense of direction in human entorhinal cortex. *Proc. Natl. Acad. Sci. U. S. A.* 107:6487–6492.
- [93] Jacobs J, Weidemann CT, Miller JF, Solway A, Burke JF, Wei XX, Suthana N, Sperling

- MR, Sharan AD, Fried I, Kahana MJ (2013) Direct recordings of grid-like neuronal activity in human spatial navigation. *Nat. Neurosci.* 16:1188–1190.
- [94] Janssen SM, Chessa AG, Murre JM (2006) Memory for time: How people date events. *Mem. Cogn.* 34:138–147.
- [95] Jenkins LJ, Ranganath C (2010) Prefrontal and medial temporal lobe activity at encoding predicts temporal context memory. *J. Neurosci.* 30:15558–15565.
- [96] Jones MW, Wilson MA (2005) Theta rhythms coordinate hippocampal-prefrontal interactions in a spatial memory task. *PLoS Biol.* 3:e402.
- [97] Kahana MJ, Howard MW, Polyn SM (2008) Associative retrieval processes in episodic memory. *Learn. Mem. A Compr. Ref.* pp. 1–24.
- [98] Kamiński J, Brzezicka A, Mamelak AN, Rutishauser U (2020) Combined phase-rate coding by persistently active neurons as a mechanism for maintaining multiple items in working memory in humans. *Neuron* 106:256–264.e3.
- [99] Kamondi A, Acsády L, Wang XJ, Buzsáki G (1998) Theta oscillations in somata and dendrites of hippocampal pyramidal cells in vivo: Activity-dependent phase-precession of action potentials. *Hippocampus* 8:244–261.
- [100] Kesner RP, Hopkins RO, Fineman B (1994) Item and order dissociation in humans with prefrontal cortex damage. *Neuropsychologia* 32:881–891.
- [101] Kluyver T, Ragan-Kelley B, Pérez F, Granger B, Bussonnier M, Frederic J, Kelley K, Hamrick J, Grout J, Corlay S, Ivanov P, Avila D, Abdalla S, Willing C (2016) Jupyter Notebooks—A publishing format for reproducible computational workflows. *Position. Power Acad. Publ. Play. Agents Agendas* pp. 87–90.
- [102] Kocsis B, Vertes RP (1992) Dorsal raphe neurons: Synchronous discharge with the theta rhythm of the hippocampus in the freely behaving rat. *J. Neurophysiol.* 68:1463–1467.
- [103] Kraus BJ, Robinson RJ, White JA, Eichenbaum H, Hasselmo ME (2013) Hippocampal "time cells": Time versus path integration. *Neuron* 78:1090–1101.
- [104] Kunz L, Brandt A, Reinacher P, Staresina B, Reifenstein E, Weidemann C, Herweg N, Tsitsiklis M, Kempter R, Kahana M, Schulze-Bonhage A, Jacobs J (2020) A neural code for egocentric spatial maps in the human medial temporal lobe. *Neuron* pp. 1–16.
- [105] Kunz L, Wang L, Lachner-Piza D, Zhang H, Brandt A, Dümpelmann M, Reinacher PC, Coenen VA, Chen D, Wang WX, Zhou W, Liang S, Grewe P, Bien CG, Bierbrauer A, Schröder TN, Schulze-Bonhage A, Axmacher N (2019) Hippocampal theta phases

organize the reactivation of large-scale electrophysiological representations during goal-directed navigation. *Sci. Adv.* 5:eaav8192.

- [106] Kurosaki Y, Terasawa Y, Ibata Y, Hashimoto R, Umeda S (2020) Retrospective time estimation following damage to the prefrontal cortex. *J. Neuropsychol.* 14:135–153.
- [107] Lega BC, Jacobs J, Kahana M (2012) Human hippocampal theta oscillations and the formation of episodic memories. *Hippocampus* 22:748–761.
- [108] Lehn H, Steffenach HA, Van Strien NM, Veltman DJ, Witter MP, Håberg AK (2009) A specific role of the human hippocampus in recall of temporal sequences. *J. Neurosci.* 29:3475–3484.
- [109] Leutgeb S, Leutgeb JK, Barnes CA, Moser EI, McNaughton BL, Moser MB (2005) Independent codes for spatial and episodic memory in hippocampal neuronal ensembles. *Science* 309:619–623.
- [110] Lubenov EV, Siapas AG (2009) Hippocampal theta oscillations are travelling waves. *Nature* 459:534–539.
- [111] MacDonald CJ, Carrow S, Place R, Eichenbaum H (2013) Distinct hippocampal time cell sequences represent odor memories in immobilized rats. *J. Neurosci.* 33:14607–14616.
- [112] MacDonald CJ, Lepage KQ, Eden UT, Eichenbaum H (2011) Hippocampal "time cells" bridge the gap in memory for discontiguous events. *Neuron* 71:737–749.
- [113] MacDonald CJ, Tonegawa S (2021) Crucial role for CA2 inputs in the sequential organization of CA1 time cells supporting memory. *Proc. Natl. Acad. Sci. U. S. A.* 118.
- [114] Mankin EA, Sparks FT, Slayyeh B, Sutherland RJ, Leutgeb S, Leutgeb JK (2012) Neuronal code for extended time in the hippocampus. *Proc. Natl. Acad. Sci. U. S. A.* 109:19462–19467.
- [115] Manning JR, Jacobs J, Fried I, Kahana MJ (2009) Broadband shifts in local field potential power spectra are correlated with single-neuron spiking in humans. *J. Neurosci.* 29:13613–13620.
- [116] Manns JR, Eichenbaum H (2009) A cognitive map for object memory in the hippocampus. *Learn. Mem.* 16:616–624.
- [117] Manns JR, Howard MW, Eichenbaum H (2007) Gradual changes in hippocampal activity support remembering the order of events. *Neuron* 56:530–540.
- [118] Matell MS, Meck WH (2004) Cortico-striatal circuits and interval timing: Coincidence detection of oscillatory processes. *Cogn. Brain Res.* 21:139–170.

- [119] Mau W, Sullivan DW, Kinsky NR, Hasselmo ME, Howard MW, Eichenbaum H (2018) The same hippocampal CA1 population simultaneously codes temporal information over multiple timescales. *Curr. Biol.* 28:1499–1508.e4.
- [120] Mayes AR, Isaac CL, Holdstock JS, Hunkin NM, Montaldi D, Downes JJ, MacDonald C, Cezayirli E, Roberts JN (2001) Memory for single items, word pairs, and temporal order of different kinds in a patient with selective hippocampal lesions. *Cogn. Neuropsychol.* 18:97–123.
- [121] McKinney W (2011) pandas: A foundational python library for data analysis and statistics.
- [122] McNaughton BL, Barnes CA, Gerrard JL, Gothard K, Jung MW, Knierim JJ, Kudrimoti H, Qin Y, Skaggs WE, Suster M, Weaver KL (1996) Deciphering the hippocampal polyglot: The hippocampus as a path integration system. *J. Exp. Biol.* 199:173–185.
- [123] Meck WH, Church RM, Olton DS (1984) Hippocampus, time, and memory. *Behav. Neurosci.* 98:3–22.
- [124] Meyer-Lindenberg AS, Olsen RK, Kohn PD, Brown T, Egan MF, Weinberger DR, Berman KF (2005) Regionally specific disturbance of dorsolateral prefrontal-hippocampal functional connectivity in schizophrenia. *Arch. Gen. Psychiatry* 62:379–386.
- [125] Miall C (1989) The storage of time intervals using oscillating neurons. *Neural Comput.* 1:359–371.
- [126] Michon JA, Jackson JL (1984) Attentional effort and cognitive strategies in the processing of temporal information. *Ann. N. Y. Acad. Sci.* 423:298–321.
- [127] Miller JF, Neufang M, Solway A, Brandt A, Trippel M, Mader I, Hefft S, Merkow M, Polyn SM, Jacobs J, Kahana MJ, Schulze-Bonhage A (2013) Neural activity in human hippocampal formation reveals the spatial context of retrieved memories. *Science* 342:1111–1114.
- [128] Minxha J, Adolphs R, Fusi S, Mamelak AN, Rutishauser U (2020) Flexible recruitment of memory-based choice representations by the human medial frontal cortex. *Science* 368:eaba3313.
- [129] Minxha J, Mosher C, Morrow JK, Mamelak AN, Adolphs R, Gothard KM, Rutishauser U (2017) Fixations gate species-specific responses to free viewing of faces in the human and macaque amygdala. *Cell Rep.* 18:878–891.
- [130] Montchal ME, Reagh ZM, Yassa MA (2019) Precise temporal memories are supported by the lateral entorhinal cortex in humans. *Nat. Neurosci.* 22:284–288.

- [131] Moscovitch M, Cabeza R, Winocur G, Nadel L (2016) Episodic memory and beyond: The hippocampus and neocortex in transformation. *Annu. Rev. Psychol.* 67:105–134.
- [132] Moser EI, Moser MB, McNaughton BL (2017) Spatial representation in the hippocampal formation: A history. *Nat. Neurosci.* 20:1448–1464.
- [133] Moser MB, Rowland DC, Moser EI (2015) Place cells, grid cells, and memory. *Cold Spring Harb. Perspect. Biol.* 7:a021808–a021808.
- [134] Mulders PC, van Eijndhoven PF, Schene AH, Beckmann CF, Tendolkar I (2015) Resting-state functional connectivity in major depressive disorder: A review. *Neurosci. Biobehav. Rev.* 56:330–344.
- [135] Murdock BB (1976) Item and order information in short-term serial memory. *J. Exp. Psychol. Gen.* 105:191–216.
- [136] Naya Y, Chen H, Yang C, Suzuki WA, Squire LR (2017) Contributions of primate prefrontal cortex and medial temporal lobe to temporal-order memory. *Proc. Natl. Acad. Sci. U. S. A.* 114:13555–13560.
- [137] Naya Y, Suzuki WA (2011) Integrating what and when across the primate medial temporal lobe. *Science* 333:773–776.
- [138] North BV, Curtis D, Sham PC (2002) A note on the calculation of empirical P values from Monte Carlo procedures. *Am. J. Hum. Genet.* 71:439–441.
- [139] Noulhiane M, Pouthas V, Hasboun D, Baulac M, Samson S (2007) Role of the medial temporal lobe in time estimation in the range of minutes. *Neuroreport* 18:1035–1038.
- [140] O’Keefe J, Burgess N (2005) Dual phase and rate coding in hippocampal place cells: Theoretical significance and relationship to entorhinal grid cells. *Hippocampus* 15:853–866.
- [141] Padilla-Coreano N, Canetta S, Mikofsky RM, Alway E, Pasco J, Myroshnychenko MV, Garcia-Garcia AL, Warren R, Teboul E, Blackman DR, Morton MP, Hupalo S, Tye KM, Kellendonk C, Kupferschmidt DA, Gordon JA (2019) Hippocampal-prefrontal theta transmission regulates avoidance behavior. *Neuron* 104:601–610.e4.
- [142] Palombo DJ, Di Lascio JM, Howard MW, Verfaellie M (2019) Medial temporal lobe amnesia is associated with a deficit in recovering temporal context. *J. Cogn. Neurosci.* 31:236–248.
- [143] Palombo DJ, Reid AG, Thavabalasingam S, Hunsberger R, Lee AC, Verfaellie M (2020) The human medial temporal lobe is necessary for remembering durations within a sequence of events but not durations of individual events. *J. Cogn. Neurosci.* 32:497–507.

- [144] Pastalkova E, Itskov V, Amarasingham A, Buzsáki G (2008) Internally generated cell assembly sequences in the rat hippocampus. *Science* 321:1322–1327.
- [145] Pavlides C, Greenstein YJ, Grudman M, Winson J (1988) Long-term potentiation in the dentate gyrus is induced preferentially on the positive phase of theta-rhythm. *Brain Research* 439:383–387.
- [146] Pedregosa F, Varoquaux G, Gramfort A, Michel V, Thirion B, Grisel O, Blondel M, Prettenhofer P, Weiss R, Dubourg V, Vanderplas J, Passos A, Cournapeau D, Brucher M, Perrot M, Duchesnay É (2011) Scikit-learn: Machine learning in python. *J. Mach. Learn. Res.* 12:2825–2830.
- [147] Peer M, Brunec IK, Newcombe NS, Epstein RA (2020) Structuring knowledge with cognitive maps and cognitive graphs. *Trends Cogn. Sci.* 25:37–54.
- [148] Penner C, Minxha J, Chandravadia N, Mamelak AN, Rutishauser U (2022) Properties and hemispheric differences of theta oscillations in the human hippocampus. *Hippocampus* 32:335–341.
- [149] Petrides M (1985) Deficits on conditional associative-learning tasks after frontal- and temporal-lobe lesions in man. *Neuropsychologia* 23:601–614.
- [150] Polyn SM, Kragel J, McCluey JD, Burke JF (2019) Altering the flow of mental time: A test of retrieved-context theory.
- [151] Polyn SM, Erlikhman G, Kahana MJ (2011) Semantic cuing and the scale insensitivity of recency and contiguity. *J. Exp. Psychol. Learn. Mem. Cogn.* 37:766–775.
- [152] Polyn SM, Norman KA, Kahana MJ (2009) A context maintenance and retrieval model of organizational processes in free recall. *Psychol. Rev.* 116:129–156.
- [153] Qasim SE, Fried I, Jacobs J (2021) Phase precession in the human hippocampus and entorhinal cortex. *Cell* 184:3242–3255.e10.
- [154] Quiroga RQ, Mukamel R, Isham EA, Malach R, Fried I (2008) Human single-neuron responses at the threshold of conscious recognition. *Proc. Natl. Acad. Sci. U. S. A.* 105:3599–3604.
- [155] Quiroga RQ, Nadasdy Z, Ben-Shaul Y (2004) Unsupervised spike detection and sorting with wavelets and superparamagnetic clustering. *Neural Comput.* 16:1661–1687.
- [156] Quiroga RQ, Kraskov A, Koch C, Fried I (2009) Explicit encoding of multimodal percepts by single neurons in the human brain. *Curr. Biol.* 19:1308–1313.
- [157] Rajasethupathy P, Sankaran S, Marshel JH, Kim CK, Ferenczi E, Lee SY, Berndt

- A, Ramakrishnan C, Jaffe A, Lo M, Liston C, Deisseroth K (2015) Projections from neocortex mediate top-down control of memory retrieval. *Nature* 526:653–659.
- [158] Ranganath C, Heller A, Cohen MX, Brozinsky CJ, Rissman J (2005) Functional connectivity with the hippocampus during successful memory formation. *Hippocampus* 15:997–1005.
- [159] Ranganath C, Ritchey M (2012) Two cortical systems for memory-guided behaviour. *Nat. Rev. Neurosci.* 13:713–26.
- [160] Ray S (2015) Challenges in the quantification and interpretation of spike-LFP relationships. *Curr. Opin. Neurobiol.* 31:111–118.
- [161] Reddy L, Zoefel B, Possel JK, Peters JC, Dijksterhuis D, Poncet M, van Straaten EC, Baayen JC, Idema S, Self MW (2021) Human hippocampal neurons track moments in a sequence of events. *J. Neurosci.* 41:6714–25.
- [162] Reed CM, Mosher CP, Chandravadia N, Chung JM, Mamelak AN, Rutishauser U (2020) Extent of single-neuron activity modulation by hippocampal interictal discharges predicts declarative memory disruption in humans. *J. Neurosci.* 40:682–693.
- [163] Robinson NT, Priestley JB, Rueckemann JW, Garcia AD, Smeglin VA, Marino FA, Eichenbaum H (2017) Medial entorhinal cortex selectively supports temporal coding by hippocampal neurons. *Neuron* 94:677–688.e6.
- [164] Rutishauser U, Reddy L, Mormann F, Sarnthein J (2020) The architecture of human memory: Insights from human single-neuron recordings. *J. Neurosci.* 00:JN–SY–1648–20.
- [165] Rutishauser U, Ross IB, Mamelak AN, Schuman EM (2010) Human memory strength is predicted by theta-frequency phase-locking of single neurons. *Nature* 464:903–907.
- [166] Sabariego M, Schönwald A, Boublil BL, Zimmerman DT, Ahmadi S, Gonzalez N, Leibold C, Clark RE, Leutgeb JK, Leutgeb S (2019) Time cells in the hippocampus are neither dependent on medial entorhinal cortex inputs nor necessary for spatial working memory. *Neuron* 102:1235–1248.e5.
- [167] Sakon JJ, Naya Y, Wirth S, Suzuki WA (2014) Context-dependent incremental timing cells in the primate hippocampus. *Proc. Natl. Acad. Sci. U. S. A.* 111:18351–18356.
- [168] Sala-Llonch R, Bartrés-Faz D, Junqué C (2015) Reorganization of brain networks in aging: A review of functional connectivity studies. *Front. Psychol.* 6:663.
- [169] Salz DM, Tiganj Z, Khasnabish S, Kohley A, Sheehan D, Howard MW, Eichenbaum H (2016) Time cells in hippocampal area CA3. *J. Neurosci.* 36:7476–7484.

- [170] Schapiro AC, Gregory E, Landau B, McCloskey M, Turk-Browne NB (2014) The necessity of the medial temporal lobe for statistical learning. *J. Cogn. Neurosci.* 26:1736–1747.
- [171] Schapiro AC, Kustner LV, Turk-Browne NB (2012) Shaping of object representations in the human medial temporal lobe based on temporal regularities. *Curr. Biol.* 22:1622–1627.
- [172] Schonhaut DR, Aghajan ZM, Kahana MJ, Fried I (2022) A neural code for spatiotemporal context.
- [173] Seabold S, Perktold J (2010) Statsmodels: Econometric and statistical modeling with python In *Proc. 9th Python Sci. Conf.*, pp. 92–96.
- [174] Shimamura AP, Janowsky JS, Squire LR (1990) Memory for the temporal order of events in patients with frontal lobe lesions and amnesic patients. *Neuropsychologia* 28:803–813.
- [175] Siapas AG, Lubenov EV, Wilson MA (2005) Prefrontal phase locking to hippocampal theta oscillations. *Neuron* 46:141–151.
- [176] Siegle JH, Wilson MA (2014) Enhancement of encoding and retrieval functions through theta phase-specific manipulation of hippocampus. *eLife* 2014:1–18.
- [177] Sigurdsson T, Stark KL, Karayiorgou M, Gogos JA, Gordon JA (2010) Impaired hippocampal-prefrontal synchrony in a genetic mouse model of schizophrenia. *Nature* 464:763–767.
- [178] Sirota A, Montgomery S, Fujisawa S, Isomura Y, Zugaro M, Buzsáki G (2008) Entrainment of neocortical neurons and gamma oscillations by the hippocampal theta rhythm. *Neuron* 60:683–697.
- [179] Skelin I, Zhang H, Zheng J, Ma S, Mander BA, McManus OK, Vadera S, Knight RT, McNaughton BL, Lin JJ (2021) Coupling between slow waves and sharp-wave ripples engages distributed neural activity during sleep in humans. *Proc. Natl. Acad. Sci. U. S. A.* 118:e2012075118.
- [180] Solomon EA, Kragel JE, Sperling MR, Sharan A, Worrell G, Kucewicz M, Inman CS, Lega B, Davis KA, Stein JM, Jobst BC, Zaghloul KA, Sheth SA, Rizzuto DS, Kahana MJ (2017) Widespread theta synchrony and high-frequency desynchronization underlies enhanced cognition. *Nat. Commun.* 8:1704.
- [181] Solomon EA, Stein JM, Das S, Gorniak R, Sperling MR, Worrell G, Inman CS, Tan RJ, Jobst BC, Rizzuto DS, Kahana MJ (2019) Dynamic theta networks in the human medial temporal lobe support episodic memory. *Curr. Biol.* 29:1100–1111.

- [182] Squire LR (2011) Memory: Neural organization and behavior In *Comprehensive Physiology*, pp. 295–371. John Wiley and Sons, Ltd.
- [183] Stangl M, Topalovic U, Inman CS, Hiller S, Villaroman D, Aghajan ZM, Christov-Moore L, Hasulak NR, Rao VR, Halpern CH, Eliashiv D, Fried I, Suthana N (2021) Boundary-anchored neural mechanisms of location-encoding for self and others. *Nature* 589:420–425.
- [184] Stefanini F, Kushnir L, Jimenez JC, Jennings JH, Woods NI, Stuber GD, Kheirbek MA, Hen R, Fusi S (2020) A distributed neural code in the dentate gyrus and in CA1. *Neuron* 107:703–716.e4.
- [185] Strange BA, Witter MP, Lein ES, Moser EI (2014) Functional organization of the hippocampal longitudinal axis. *Nat. Rev. Neurosci.* 15:655–669.
- [186] Sugar J, Moser MB (2019) Episodic memory: Neuronal codes for what, where, and when. *Hippocampus* 29:1190–1205.
- [187] Suh J, Rivest AJ, Nakashiba T, Tominaga T, Tonegawa S (2011) Entorhinal cortex layer III input to the hippocampus is crucial for temporal association memory. *Science* 334:1415–1420.
- [188] Tambini A, Ketz N, Davachi L (2010) Enhanced brain correlations during rest are related to memory for recent experiences. *Neuron* 65:280–290.
- [189] Taxidis J, Pnevmatikakis EA, Dorian CC, Mylavarapu AL, Arora JS, Samadian KD, Hoffberg EA, Golshani P (2020) Differential emergence and stability of sensory and temporal representations in context-specific hippocampal sequences. *Neuron* 108:984–988.e9.
- [190] Tiganj Z, Jung MW, Kim J, Howard MW (2017) Sequential firing codes for time in rodent medial prefrontal cortex. *Cereb. Cortex* 27:5663–5671.
- [191] Tranel D, Jones RD (2006) Knowing "what" and knowing "when". *J. Clin. Exp. Neuropsychol.* 28:43–66.
- [192] Treisman M (1963) Temporal discrimination and the indifference interval: Implications for a model of the "internal clock". *Psychol. Monogr. Gen. Appl.* 77:1–31.
- [193] Trimper JB, Colgin LL (2018) Spike time synchrony in the absence of continuous oscillations. *Neuron* 100:527–529.
- [194] Tsao A, Sugar J, Lu L, Wang C, Knierim JJ, Moser MB, Moser EI (2018) Integrating time from experience in the lateral entorhinal cortex. *Nature* 561:57–62.
- [195] Tubridy S, Davachi L (2011) Medial temporal lobe contributions to episodic sequence

encoding. *Cereb. Cortex* 21:272–280.

- [196] Tulving E (1972) Episodic and semantic memory In *Organization of memory*, pp. 381–403. Academic Press, New York, NY.
- [197] Tulving E (1983) *Elements of episodic memory* Oxford University Press, New York, NY.
- [198] Uitvlugt MG, Healey MK (2019) Temporal proximity links unrelated news events in memory. *Psychol. Sci.* 30:92–104.
- [199] Umbach G, Kantak P, Jacobs J, Kahana M, Pfeiffer BE, Sperling M, Lega B (2020) Time cells in the human hippocampus and entorhinal cortex support episodic memory. *Proc. Natl. Acad. Sci. U. S. A.* 117:28463–28474.
- [200] Vass LK, Copara MS, Seyal M, Shahlaie K, Farias ST, Shen PY, Ekstrom AD (2016) Oscillations go the distance: Low-frequency human hippocampal oscillations code spatial distance in the absence of sensory cues during teleportation. *Neuron* 89:1180–1186.
- [201] Virtanen P, Gommers R, Oliphant TE, Haberland M, Reddy T, Cournapeau D, Burovski E, Peterson P, Weckesser W, Bright J, van der Walt SJ, Brett M, Wilson J, Millman KJ, Mayorov N, Nelson AR, Jones E, Kern R, Larson E, Carey CJ, Polat Feng Y, Moore EW, VanderPlas J, Laxalde D, Perktold J, Cimrman R, Henriksen I, Quintero EA, Harris CR, Archibald AM, Ribeiro AH, Pedregosa F, van Mulbregt P, Vijaykumar A, Bardelli AP, Rothberg A, Hilboll A, Kloekner A, Scopatz A, Lee A, Rokem A, Woods CN, Fulton C, Masson C, Häggström C, Fitzgerald C, Nicholson DA, Hagen DR, Pasechnik DV, Olivetti E, Martin E, Wieser E, Silva F, Lenders F, Wilhelm F, Young G, Price GA, Ingold GL, Allen GE, Lee GR, Audren H, Probst I, Dietrich JP, Silterra J, Webber JT, Slavič J, Nothman J, Buchner J, Kulick J, Schönberger JL, de Miranda Cardoso JV, Reimer J, Harrington J, Rodríguez JLC, Nunez-Iglesias J, Kuczynski J, Tritz K, Thoma M, Newville M, Kümmeler M, Bolingbroke M, Tartre M, Pak M, Smith NJ, Nowaczyk N, Shebanov N, Pavlyk O, Brodtkorb PA, Lee P, McGibbon RT, Feldbauer R, Lewis S, Tygier S, Sievert S, Vigna S, Peterson S, More S, Pudlik T, Oshima T, Pingel TJ, Robitaille TP, Spura T, Jones TR, Cera T, Leslie T, Zito T, Krauss T, Upadhyay U, Halchenko YO, Vázquez-Baeza Y (2020) SciPy 1.0: Fundamental algorithms for scientific computing in python. *Nat. Methods* 17:261–272.
- [202] Waskom M (2021) Seaborn: Statistical data visualization. *J. Open Source Softw.* 6:3021.
- [203] Watrous AJ, Fried I, Ekstrom AD (2011) Behavioral correlates of human hippocampal delta and theta oscillations during navigation. *J Neurophysiol* 105:1747–1755.
- [204] Watrous AJ, Lee DJ, Izadi A, Gurkoff GG, Shahlaie K, Ekstrom AD (2013) A comparative study of human and rat hippocampal low-frequency oscillations during spatial

navigation. *Hippocampus* 23:656–661.

- [205] Watrous AJ, Miller J, Qasim SE, Fried I, Jacobs J (2018) Phase-tuned neuronal firing encodes human contextual representations for navigational goals. *eLife* 7:e32554.
- [206] Watrous AJ, Tandon N, Conner CR, Pieters T, Ekstrom AD (2013) Frequency-specific network connectivity increases underlie accurate spatiotemporal memory retrieval. *Nat. Neurosci.* 16:349–356.
- [207] Whitten TA, Hughes AM, Dickson CT, Caplan JB (2011) A better oscillation detection method robustly extracts EEG rhythms across brain state changes: The human alpha rhythm as a test case. *Neuroimage* 54:860–874.
- [208] Wills TJ, Lever C, Cacucci F, Burgess N, O’Keefe J (2005) Attractor dynamics in the hippocampal representation of the local environment. *Science* 308:873–876.
- [209] Wood ER, Dudchenko PA, Robitsek RJ, Eichenbaum H (2000) Hippocampal neurons encode information about different types of memory episodes occurring in the same location. *Neuron* 27:623–633.
- [210] Yadav N, Noble C, Niemeyer JE, Terceros A, Victor J, Liston C, Rajasethupathy P (2022) Prefrontal feature representations drive memory recall. *Nature* 608:153–160.
- [211] Yassa MA, Mattfeld AT, Stark SM, Stark CEL (2011) Age-related memory deficits linked to circuit-specific disruptions in the hippocampus. *Proc. Natl. Acad. Sci. U. S. A.* 108:8873–8878.
- [212] Yntema DB, Trask FP (1963) Recall as a search process. *J. Verbal Learning Verbal Behav.* 2:65–74.
- [213] Zhang H, Jacobs J (2015) Traveling theta waves in the human hippocampus. *J. Neurosci.* 35:12477–12487.
- [214] Zheng J, Stevenson RF, Mander BA, Mnatsakanyan L, Hsu FPK, Vadera S, Knight RT, Yassa MA, Lin JJ (2019) Multiplexing of theta and alpha rhythms in the amygdala-hippocampal circuit supports pattern separation of emotional information. *Neuron* 102:887–898.e5.
- [215] Zhou Y, Shu N, Liu Y, Song M, Hao Y, Liu H, Yu C, Liu Z, Jiang T (2008) Altered resting-state functional connectivity and anatomical connectivity of hippocampus in schizophrenia. *Schizophr. Res.* 100:120–32.